MICROCOPY RESOLUTION TEST CHART

AD-A185 989

David W. Taylor Naval Ship Research and Development Center

DTNSRDC-87/027   September 1987

Ship Materials Engineering Department
Research and Development Report

Reaction Mechanism of Sulfur Dioxide with Single Crystal Cobalt and Chromium and CoCrAlY Coatings
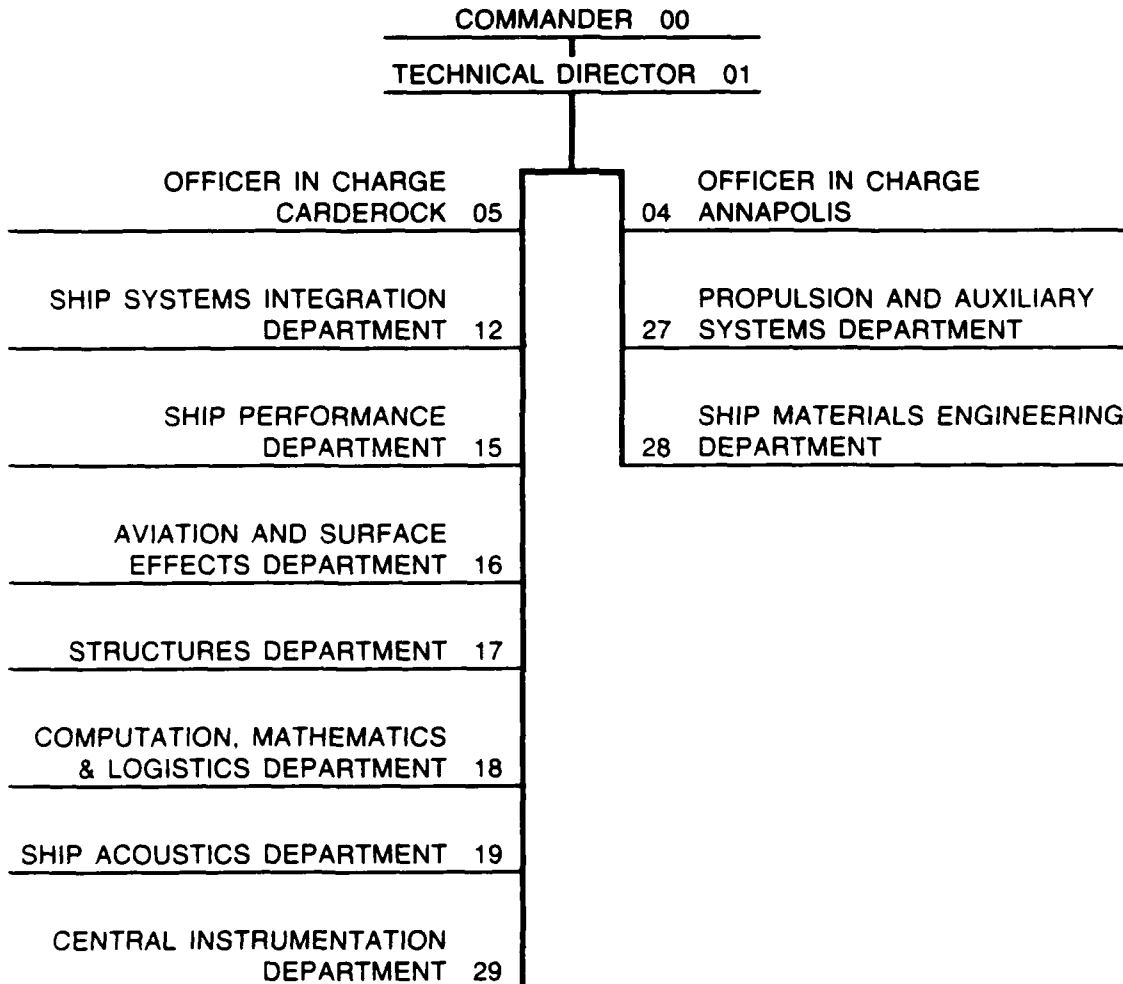
by
Louis F. Aprigliano

DTIC
ELECTE
NOV 2 0 1987
S D
D

DTNSRDC-87/027   Reaction Mechanisms of Sulfur Dioxide with Single Crystal Cobalt and Chromium and CoCrAlY Coatings

87   500

MAJOR DTNSRDC TECHNICAL COMPONENTS

COMMANDER   00

TECHNICAL DIRECTOR   01

OFFICER IN CHARGE CARDEROCK 05	04 OFFICER IN CHARGE ANNAPOLIS
SHIP SYSTEMS INTEGRATION DEPARTMENT 12	27 PROPULSION AND AUXILIARY SYSTEMS DEPARTMENT
SHIP PERFORMANCE DEPARTMENT 15	28 SHIP MATERIALS ENGINEERING DEPARTMENT
AVIATION AND SURFACE EFFECTS DEPARTMENT 16	
STRUCTURES DEPARTMENT 17	
COMPUTATION, MATHEMATICS & LOGISTICS DEPARTMENT 18	
SHIP ACOUSTICS DEPARTMENT 19	
CENTRAL INSTRUMENTATION DEPARTMENT 29	

REPORT DOCUMENTATION PAGE

AD-A185 989

1a REPORT SECURITY CLASSIFICATION	1b RESTRICTIVE MARKINGS
UNCLASSIFIED	

2a SECURITY CLASSIFICATION AUTHORITY	3 DISTRIBUTION AVAILABILITY OF REPORT
2b DECLASSIFICATION DOWNGRADING SCHEDULE	Approved for Public Release; Distribution is Unlimited.

4 PERFORMING ORGANIZATION REPORT NUMBER(S)	5 MONITORING ORGANIZATION REPORT NUMBER(S)
DTNSRDC-87/027	

6a NAME OF PERFORMING ORGANIZATION	6b OFFICE SYMBOL (If applicable)	7a NAME OF MONITORING ORGANIZATION
David Taylor Naval Ship R&D Center	Code 2812	

6c ADDRESS (City, State, and ZIP Code)	7b ADDRESS (City, State, and ZIP Code)
Bethesda, MD 20084-5000	

8a NAME OF FUNDING/SPONSORING ORGANIZATION David Taylor Naval Ship R&D Center	8b OFFICE SYMBOL (If applicable) Code 012	9 PROCUREMENT INSTRUMENT IDENTIFICATION NUMBER

8c ADDRESS (City, State, and ZIP Code)	10 SOURCE OF FUNDING NUMBERS			
	PROGRAM ELEMENT NO	PROJECT NO	TASK NO	WORK UNIT ACCESSION NO
Bethesda, MD 20084-5000	61152N	ZR00001	ZR00001	DN505513

11 TITLE (Include Security Classification)
Reaction Mechanism of Sulfur Dioxide with Single Crystal Cobalt and Chromium and CoCrAlY Coatings

12 PERSONAL AUTHOR(S)
Louis F. Aprigliano

13a TYPE OF REPORT	13b TIME COVERED FROM 851001 TO 870301	14 DATE OF REPORT (Year, Month, Day) September 1987	15 PAGE COUNT 139
Final			

16 SUPPLEMENTARY NOTATION
Note that this is also a doctoral dissertation for George Washington University.

17	COSATI CODES		18 SUBJECT TERMS (Continue on reverse if necessary and identify by block number)
FIELD	GROUP	SUB-GROUP	High temperature metallic coatings Sulfur dioxide
			X-ray photoelectron spectroscopy Cobalt
			Chromium

19 ABSTRACT (Continue on reverse if necessary and identify by block number)

When gas turbine engines are used in a marine environment, the blades and vanes in the hot section of the engine suffer a form of material degradation known as hot corrosion. An important part of the hot corrosion process involves the formation of cobalt sulfate by the interaction of the metal blade and vane surfaces with the sulfur dioxide present in the combustion gas. The cobalt sulfate can form a molten mixed-salt with the sodium sulfate present in the sea salt ingested by the engine. This molten salt can corrode the blades and vanes. Metallic coatings that contain cobalt, chromium, aluminum, and yttrium (CoCrAlY) are used to extend the service life of these parts. Cobalt is the base element in these coatings; chromium is the primary elemental constitutent used to enhance corrosion resistance; and aluminum provides oxidation resistance.

(Continued)

20 DISTRIBUTION/AVAILABILITY OF ABSTRACT	21 ABSTRACT SECURITY CLASSIFICATION
☒ UNCLASSIFIED-UNLIMITED ☐ SAME AS RPT ☐ DTIC USERS	Unclassified

22a NAME OF RESPONSIBLE INDIVIDUAL	22b TELEPHONE (Include Area Code)	22c OFFICE SYMBOL
Louis F. Aprigliano	(301) 267-2484	Code 2812

DD FORM 1473, 84 MAR

83 APR edition may be used until exhausted
All other editions are obsolete

SECURITY CLASSIFICATION OF THIS PAGE

★ U.S. Government Printing Office 1985-639-012

0102-LF-014-6602

The objective of this research was to obtain a basic understanding of the reaction mechanism of sulfur dioxide with cobalt and chromium and to use this understanding to analyze the more complex reaction mechanism of sulfur dioxide with CoCrAlY coatings. A basic premise in achieving the objective was that the reaction mechanisms of sulfur dioxide with cobalt and chromium are similar and can be described in two basic steps:

1. $SO_2 \xrightarrow{\ \ \ } 2(O) + (S)$ on the surface
2. $2(O) + SO_2 \xrightarrow{\ \ \ } SO_4$ on the surface.

Using x-ray photoelectron spectroscopy (XPS), it was found that sulfur dioxide reacted with the oxide-free surfaces of single crystal Co(0001) and Cr(110) as described above. The rates of these reactions were found to be similar for the two metals. No appreciable difference in activation energies could be determined with the exposures used of $75\mu mHg$ and 1 atm pressure sulfur dioxide at 100°, 230°, and $300^\circ C$ for times of 1, 5, and 15 min.

Quantitative depth profiling by XPS of the CoCrAlY coatings showed that at each of three chromium contents (20, 29, and 35 weight percent) the initial oxide films on the coatings were all basically aluminum oxide with an yttrium-rich phase. The yttrium-rich phase was tentatively identified as yttrium aluminum garnet. This similarity in all of the initial oxide films indicated that the hot corrosion benefit derived by increasing the chromium content of these coatings must be in improving the hot corrosion resistance of the coating under the oxide film. For this reason oxide-free surfaces of the CoCrAlY coatings with 20 and 35 wt % chromium were exposed to 1 atm pressure sulfur dioxide for 1, 5, 15, 30, and 60 min at $230^\circ C$. Both coatings formed "cobalt-sulfate" and "chromium-sulfate" in a manner similar to that described above for the elemental cobalt and chromium. In addition, increasing the chromium content of the coatings reduced the amount of cobalt sulfate formed. This in turn was related to the formation of sigma phase in the high chromium coating. The sigma phase was theorized to be a more difficult surface on which to form cobalt or chromium sulfate as compared to the alpha and beta phases present in the lower chromium coating. The formation of the sigma phase is believed to retard the overall corrosion process.

A cluster of ten cobalt and two oxygen atoms was used to model the second part of the reaction mechanism described above. The approximate energies of the electrons in the cluster were calculated with the SCF-Xα-SW method and the electron levels most likely involved in the sulfate formation identified. This information could provide a means to analyze the second part of the reaction mechanism as it occurs on other metals whose sulfates are not as detrimental as that of cobalt or to devise an alloying scheme that would impede this reaction step.

CONTENTS

CONTENTS (Continued)

CONTENTS (Continued)

FIGURES

FIGURES (Continued)

FIGURES (Continued)

TABLES

TABLES (Continued)

ABBREVIATIONS

A	Angstrom
ACIL	Aberration-compensated input lense
ads	Adsorbed
AES	Auger electron spectroscopy
at %	Atomic percent
BCC	Body centered cubic
CoCrAlY	Class of coatings containing cobalt, chromium, aluminum, and yttrium
FCC	Face centered cubic
HCP	Hexagonally close packed
HOMO	Highest occupied molecular orbital
LUMO	Lowest unoccupied molecular orbital
MO	Molecular orbital
mtorr	10^{-3} torr
PVD	Physical vapor deposition
SCF-Xα-SW	Self-consistent field x alpha scattered wave
UHV	Ultra-high vacuum
UPS	Ultra-violet photoelectron spectroscopy
wt %	Weight percent
XPS	X-ray photoelectron spectroscopy

ABSTRACT

When gas turbine engines are used in a marine environment, the blades and vanes in the hot section of the engine suffer a form of material degradation known as hot corrosion. An important part of the hot corrosion process involves the formation of cobalt sulfate by the interaction of the metal blade and vane surfaces with the sulfur dioxide present in the combustion gas. The cobalt sulfate can form a molten mixed-salt with the sodium sulfate present in the sea salt ingested by the engine. This molten salt can corrode the blades and vanes. Metallic coatings that contain cobalt, chromium, aluminum, and yttrium (CoCrAlY) are used to extend the service life of these parts. Cobalt is the base element in these coatings; chromium is the primary elemental constitutent used to enhance corrosion resistance; and aluminum provides oxidation resistance.

The objective of this research was to obtain a basic understanding of the reaction mechanism of sulfur dioxide with cobalt and chromium and to use this understanding to analyze the more complex reaction mechanism of sulfur dioxide with CoCrAlY coatings. A basic premise in achieving the objective was that the reaction mechanisms of sulfur dioxide with cobalt and chromium are similar and can be described in two basic steps:

1. $SO_2 \longrightarrow 2(O) + (S)$ on the surface
2. $2(O) + SO_2 \longrightarrow SO_4$ on the surface.

Using x-ray photoelectron spectroscopy (XPS), it was found that sulfur dioxide reacted with the oxide-free surfaces of single crystal Co(0001) and Cr(110) as described above. The rates of these reactions were found to be similar for the two metals. No appreciable difference in activation energies could be determined with the exposures used of 75μ mHg and 1 atm pressure sulfur dioxide at $100°$, $230°$, and $300°C$ for times of 1, 5, and 15 min.

Quantitative depth profiling by XPS of the CoCrAlY coatings showed that at each of three chromium contents (20, 29, and 35 weight percent) the initial oxide films on the coatings were all basically aluminum oxide with an

1

yttrium-rich phase. The yttrium-rich phase was tentatively identified as yttrium aluminum garnet. This similarity in all of the initial oxide films indicated that the hot corrosion benefit derived by increasing the chromium content of these coatings must be in improving the hot corrosion resistance of the coating under the oxide film. For this reason oxide-free surfaces of the CoCrAlY coatings with 20 and 35 wt % chromium were exposed to 1 atm pressure sulfur dioxide for 1, 5, 15, 30, and 60 min at 230°C. Both coatings formed "cobalt-sulfate" and "chromium-sulfate" in a manner similar to that described above for the elemental cobalt and chromium. In addition, increasing the chromium content of the coatings reduced the amount of cobalt sulfate formed. This in turn was related to the formation of sigma phase in the high chromium coating. The sigma phase was theorized to be a more difficult surface on which to form cobalt or chromium sulfate as compared to the alpha and beta phases present in the lower chromium coating. The formation of the sigma phase is believed to retard the overall corrosion process.

A cluster of ten cobalt and two oxygen atoms was used to model the second part of the reaction mechanism described above. The approximate energies of the electrons in the cluster were calculated with the SCF-Xα-SW method and the electron levels most likely involved in the sulfate formation identified. This information could provide a means to analyze the second part of the reaction mechanism as it occurs on other metals whose sulfates are not as detrimental as that of cobalt or to devise an alloying scheme that would impede this reaction step.

ADMINISTRATIVE INFORMATION

ZR-000-01-01 under DTNSRDC Work Unit 1-2812-017. This report satisfies milestone 1-2812-017-60.

INTRODUCTION

PROBLEM SYNOPSIS

When gas turbine engines are used for power generation in a marine environment, the blades and vanes in the hot section of the engine suffer a form of material degradation known as hot corrosion. In brief, the hot corrosion process involves the interaction of the metal blade and vane surfaces with the sulfur dioxide and sea salt present in the combustion gases. The engineering solution to this problem has been to develop special metallic coatings to extend the service life of these parts. The base element in these coatings is cobalt, and the primary elemental constituent used to enhance their corrosion resistance is chromium. This use of chromium was developed empirically, by test and evaluation. The purpose of this research is to obtain a basic understanding of the reaction mechanism of sulfur dioxide with cobalt and chromium and to use this understanding as a means to analyze the more complex reaction mechanism of sulfur dioxide with metallic coatings containing these elements.

A reasonable starting point from which to approach a problem such as this is to reduce it to an analysis of the most critical aspects involved. One such aspect would be a detailed understanding of the composition of the coating surface as presented to the environment. This composition need not be the same as that of the bulk coating composition. The nature of the surface composition will

3

provide useful information as to how important the initiation stage of the corrosion process is to the problem being studied. Another important part of this problem is to understand the interaction of the most significant corrodent gas in the environment (in this instance sulfur dioxide) with the material surface that is under attack. The last aspect of this problem is to understand how the elements in the coatings (primarily cobalt and chromium) affect the corrosion process. This will provide information on how important the propagation phase of the corrosion process is to the problem. In summary, this research effort was aimed at elucidating the interaction of sulfur dioxide with the metallic surfaces of cobalt and chromium as a means to understanding the more complex problem of how sulfur dioxide interacts with CoCrAlY coatings.

HOT CORROSION

Hot corrosion is the broad term applied to the high temperature corrosion of the blade and vane components of gas turbine engines when operated in a marine environment. The parts most severely attacked are the metallic coatings used to protect the turbine blades. These coatings are often a mixture of cobalt, chromium, aluminum and yttrium and as a class are identified by the acronym CoCrAlY. Hot corrosion can take several forms and the form that is of special concern in a marine environment has been designated type 2 or low-temperature hot corrosion (Grisik et al.[1]). The major

aspects of this corrosion process can be described as follows:

- Sulfur in the fuel forms sulfur dioxide during combustion.

- Sulfur dioxide reacts with the cobalt in the turbine blade coating and forms cobalt sulfate.

- Sodium sulfate from the sea salt ingested by the engine deposits in solid form on the turbine blades.

- In the temperature range of 677° to 732°C (1250° to 1350°F) the sodium sulfate and the cobalt sulfate form a mixed salt that has a lower melting point then either of the pure salts. This results in the degradation of the coating.

One way to stop the corrosion process would be to prevent the formation of cobalt sulfate. In several research efforts (Goward[2] and unpublished work of tne author) it has been found that increasing the chromium content of the CoCrAlY coating to 30 or 40 weight percent (wt%) from the originally used 20 wt% dramatically improved the hot corrosion resistance of these coatings. During the open discussions of both the Fourth and Fifth Conferences on Gas Turbine Materials in a Marine Environment, it had been speculated that in the 20 wt% chromium coatings the oxide scales that form on these coatings are a mixture of cobalt oxide, chromium oxide and aluminum oxide, while in the 40 wt% chromium coatings the oxide scale is predominantly chromium oxide. This continous layer of chromium oxide then would serve as a barrier to the formation of cobalt sulfate. This same situation had been postulated by Luthra and Wood[3] to occur for binary CoCr alloys as the Cr content increases.

An important part of the objective of this work was to study the validity of this hypothesis by examining the initial protective

5

oxide scales that form on actual coatings. While the specifics of that phase of the experimental efforts are properly discussed in more detail below, it is helpful to the discussion at this point to note that the protective oxide scales for CoCrAlY coatings containing nominal levels of 20, 29, and 35 wt% chromium were essentially the same. They were predominately alumina with an yttrium-rich phase. The surface oxides also contained small amounts of cobalt and chromium. Preferential segregation of elements to the surface of an alloy, such as has occurred with the yttrium, has been found to occur in other systems, such as CuNi (Sinfelt et al.[4]).

Sprague et al.[5] and Hwang et al.[6] have shown that in drop castings of CoCrAlY with low chromium contents (20 to 23 wt%) the yttrium-rich phase in the oxide scale on these castings can provide initiation sites for the hot corrosion process. The corrosion or sulfation of the yttrium-rich phase serves to mechanically disrupt the remaining alumina and thereby expose the metallic coating to the hot corrosion process. Due to the similarity of the starting scale in all of the coatings in this study, a logical proposal is that the chromium provides its hot corrosion benefit in slowing the propagation phase of corrosion attack through the metallic CoCrAlY coating.

A means by which varying the chromium content of these coatings might slow the propagation of hot corrosion can be envisioned by considering the works of Luthra[7,8] on the sulfation of the alloys of cobalt-chromium, cobalt-aluminum, and cobalt-chromium-aluminum. It has been found that it takes lower levels of sulfur dioxide to result in a mixed low melting point salt of cobalt sulfate in sodium sulfate

6

than it does for chromium sulfate (or aluminum sulfate) and that the levels of sulfur dioxide that are present in typical marine gas turbines are sufficient to support the formation of liquid mixed sulfates with cobalt sulfate but not chromium sulfate (or aluminum sulfate). This solution of the one sulfate in the other is necessary in order to promote and stabilize the formations of low melting point mixed sulfates, which when liquid result in the rapid dissolution of the coatings. Thus as more chromium is added to these types of coatings, it is possible that the formation of cobalt sulfate is suppressed in favor of chromium sulfate. (The mechanism by which this occurs was a major topic of this research effort.) If this is the case, then the formation of low melting point mixed salts that are needed for hot corrosion propagation are also suppressed. This suppression of cobalt sulfate formation is crucial to the design of coatings with improved hot corrosion resistance in a marine environment. What needs to be known is how the sulfur dioxide reacts with the surfaces of a coating. In the research work reported here, we determined that these reactions can be related to the interaction of sulfur dioxide with cobalt or chromium in their unalloyed (elemental) forms.

REACTION MECHANISMS OF SULFUR DIOXIDE WITH METALS (GENERAL)

The reaction mechanisms of sulfur dioxide with several metals have been described in the literature, and are summarized here. These studies involved exposing clean, oxide-free metals in ultra-high vacuum (UHV) conditions to sulfur dioxide gas and then examining the

7

reaction products that form on these surfaces with surface-sensitive analytical techniques such as x-ray photoelectron spectroscopy (XPS), Auger electron spectroscopy (AES), and ultra-violet photoelectron spectroscopy (UPS).

Furuyama et al.[9], using XPS, found that a two stage reaction occurs at 300 K when oxide-free surfaces of polycrystalline iron are exposed to sulfur dioxide at pressures of 10^{-5} torr for 0.1 to 5 seconds. In the first stage of the reaction the sulfur dioxide gas molecule dissociates on the iron and forms a sulfide and an oxide. With further exposure to sulfur dioxide the adsorbed oxygen reacts with the sulfur dioxide to form a sulfate. They described the reactions as:

1. $SO_2(gas) \longrightarrow S(ads) + 2O(ads)$

2. $SO_2(gas) + 2O(ads) \longrightarrow SO_4(ads)$
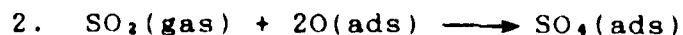
It was also found that pre-adsorbed oxygen on iron tended to inhibit the first stage of the decomposition reaction of the sulfur dioxide compared to that on a clean surface. It did not inhibit the second stage of the reaction.

Brundle and Carley,[10] using UPS and XPS, observed a dissociation reaction when nickel was exposed to sulfur dioxide. They exposed the nickel surface at 77 K and found the initial dissociation to be to either SO+O or a strongly chemisorbed SO_2 molecular species. On heating to 300 K they found evidence of sulfide and sulfate formation on the surface. Further reaction at 10^{-3} torr resulted in continued formation of the sulfide and sulfate species. They described the reaction as one of disproportionation:

$$2SO_2 + 4e^- \longrightarrow S^2 + SO_4{}^2$$

Nebesny and Armstrong,[11] using AES, studied the reaction of sulfur dioxide with lithium. They found the sulfur dioxide at pressures less than 1 mtorr to completely dissociate on a clean lithium surface and to form a monolayer of 2:1 Li_2O and Li_2S at an activation energy of 2-5 kcal/mole. The first stage of this reaction seems to be limited to one monolayer. At sulfur dioxide pressures higher than 1 mtorr an overlayer of $Li_2S_2O_4/Li_2S_2O_3$ formed on top of the Li_2O and Li_2S layer. The dissociation reaction proceeded with full retention of all parts of the original sulfur dioxide molecule and, no matter what the starting sulfur dioxide pressure, the S_2O_3/S_2O_4 overlayer was always preceded by the S^{-2}/O^{-2} layer. However, exposure of a pre-oxidized lithium surface to sulfur dioxide produced the outerlayer of $Li_2S_2O_4/Li_2S_2O_4$ but not the innerlayer of Li_2O and Li_2S. As in the case of the iron, the reaction seems to proceed by the interaction of sulfur dioxide with the oxide species formed from the initial dissociation.

Kohler and Wassmuth,[12] using AES, studied the reaction of single crystal platinum in the (111) orientation with sulfur dioxide. For the first part of this reaction they proposed a reaction similar to that described above by Furuyama et al.[9] but added more detail as to the steps involved in the first stage of the reaction. Namely,

$$(SO_2)_{gas} \longrightarrow (SO_2)_{ads} \longrightarrow (SO)_{ads} + (O)_{ads} \longrightarrow (S)_{ads} + 2(O)_{ads}$$
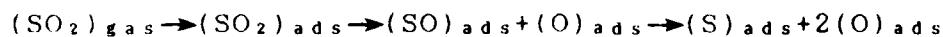
Not all metals dissociate sulfur dioxide. One that does not is silver. Outka and Madix,[13] using UPS, found that single crystal silver in a (110) orientation did not dissociate sulfur dioxide under

9

UHV conditions at ambient temperatures. The sulfur dioxide did adsorb
on the silver and Outka and Madix believed that this adsorption was
accomplished by the formation of a metal-SO_2 charge transfer complex.
In a second study, Outka et al.[14] reacted low pressure (10^{-6} torr for
1 s) sulfur dioxide with pre-oxidized Ag(110) at 241 K and it formed a
sulfur trioxide intermediate. At 500 K the sulfur trioxide species
disproportionates to give sulfur dioxide, adsorbed SO_4 and subsurface
oxygen. The SO_4 was proposed to form bidentate oxygen bonds to the
surface spanning adjacent long twofold bridge sites (Fig. 1).

REACTION MECHANISM OF SULFUR DIOXIDE WITH COBALT AND
CHROMIUM (PROPOSED)
        To begin to explain the significance of increasing the
chromium content in CoCrAlY coatings, studies that provide information
on the reaction steps involved in the formation of sulfate layers on
cobalt and chromium when they are exposed to sulfur dioxide were
useful. By comparison to the above described reactions of sulfur
dioxide with metal surfaces one can speculate on the reaction
mechanisms that should lead to the formation of sulfates on cobalt and
chromium. Sulfur dioxide is a bent molecule with each of the atoms at
the corner of an isosceles triangle with an apex angle of 119°
(Fig. 2a). It is possible that the sulfur atom could bond directly to
the metal surface (Fig. 2b) and if the bond is of a dissociative
nature will result in the freeing of the two oxygen atoms (Fig. 2c).
These two oxygen atoms will then bond to the surface (Fig. 2d) and in
so doing can become preferred sites for the formation of a sulfate by
the addition of another sulfur dioxide molecule (Fig. 2e). The extent
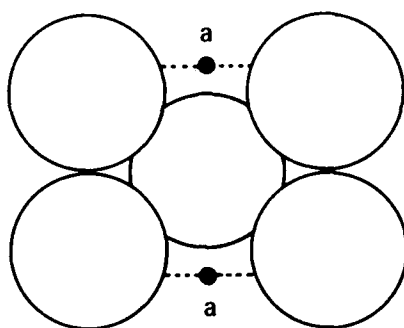
Fig. 1. FCC (110) crystallographic plane where "a" marks the long
twofold bridge sites.

STEP 1

119
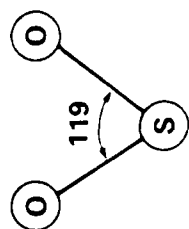
Fig. 2a. Sulfur dioxide.

STEP 2
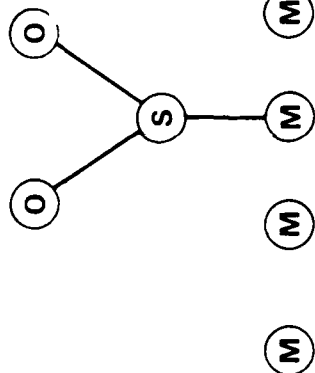
Fig. 2b. Chemisorption.

STEP 3

M   Cr or Co
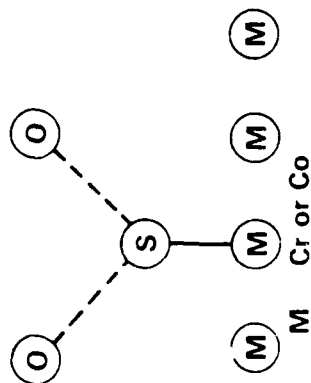
Fig. 2c. Dissociation.

STEP 4
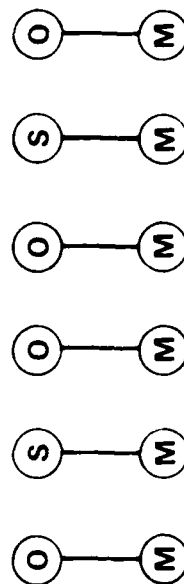
Fig. 2d. Oxides and sulfides exist on surface.

STEP 5

NOTE: THE PLANE OF THESE TWO OXYGEN ATOMS IS AT 90 TO PLANE OF OPPOSING TWO OXYGEN ATOMS IN THE TETRAHEDRAL STRUCTURE OF SO4
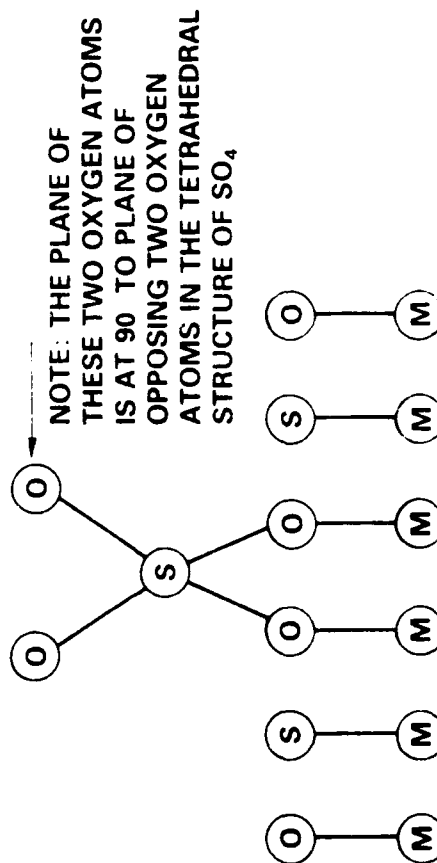
Fig. 2e. Sulfate formation.

Fig. 2. Model of SO_2 surface reaction with cobalt and chromium.

12

and rate of this reaction can vary with different metals and can provide a means to analyze the reactions that take place on the surfaces of mixed alloy systems such as coatings. Determining the variability of this reaction for cobalt and chromium was a part of this research program.

As cobalt and chromium are first series transition metal elements, it is proposed that the reactions proceed in two basic steps which are equivalent to those found for the the first series transition metals of iron and nickel as described above. For both cobalt and chromium these steps are:

1. $SO_2 \longrightarrow 2(O) + (S)$

2. $2(O) + SO_2 \longrightarrow SO_4$
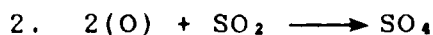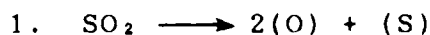
The overall reactions can be balanced as:

3. $5Cr + 6SO_2 \longrightarrow Cr_2(SO_4)_3 + 3CrS$

4. $2Co + 2SO_2 \longrightarrow CoSO_4 + CoS$
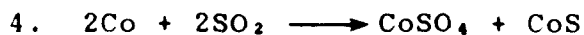
The free energies of reactions 3 and 4 can be calculated (Appendix A) and at 230°C they are -234 kcal/mole of product for reaction 3 and -47 kcal/mole of product for reaction 4. The negative values of the free energies for these reactions mean that both reactions are thermodynamically possible and that the products of reaction 3 are more stable. However, it does not mean that they have to occur nor does it provide any information as to what is happening from an atomistic viewpoint or if a minimum configuration of atoms at a surface is needed to form a given type of sulfate. To study this aspect of the problem, molecular orbital theory and cluster calculations of electron energy levels can be helpful.

13

MOLECULAR ORBITAL THEORY AND CLUSTER MODEL OF
CHEMISORPTION (GENERAL THEORY)

The first stages of most of the reactions described above are ones of adsorption and dissociative chemisorption. They typically involve the transfer of electrons from the metal surface to the lowest unoccupied molecular orbital (LUMO) of the molecule being adsorbed. This electron transfer creates the bond of the molecule to the metal surface and in so doing it can destabilize the molecule or dissociate it. The ease with which this electron transfer takes place can be thought of as an indication of the activation energy needed for the reaction to take place and is related to the rate of the initial reactions. Molecular orbital (MO) theory can be described as a modeling of the electron bonding that holds the atoms in molecules together and may be extended to modeling the electron bonding that holds molecules to metal surfaces. The theory usually handles the latter situation by modeling it as a finite cluster of atoms with some atoms from the metal and some from the molecule being held to the metal surface. For example, the chemisorption of sulfur to nickel has been modeled as one sulfur atom on top of a five-atom cluster of nickel (Shropshire). This use of a finite cluster is somewhat different from band theory, which requires the use of an infinite lattice. Band theory results in all valence electrons being delocalized over the entire crystal. However, this might not be a good model for all interactions, according to Gates et al.[16]. At least partial retention of localized electrons is believed to occur in the case of bonding orbitals with surface metal atoms (Gates et al.[16]).

14

of relocalization of electrons in the surface metal atom (Gates[16]).
For strong bonding, as in corrosive chemisorption, the localization of
electrons in the surface metal atom is almost complete and the surface
metal atom probably contributes little to the band structure of the
bulk metal (Gates et al.[16]). The electrons involved in the bonding
are then probably localized in orbitals between the added (adsorbate)
atom(s) involved in the surface compound formation and the surface
metal atom(s)   immediately associated with the adsorbate
(Gates et al.[16]). Consequently, the bonding envisioned by molecular
orbital theory involves the formation of electron orbitals that are
mutual to the bound atoms and the surface. Molecular orbital theory
involves the idea that all orbitals in a molecule or cluster can
extend (but do not necessarily have to) over the entire cluster and as
such can be delocalized over the entire cluster (Cotton[17]). However,
the theory allows (and this is a key point) the molecular orbitals to
have very large values of the wave function amplitude in certain parts
of the cluster (Cotton[17]). Surface compounds, such as oxygen
chemisorbed to a metal surface, can therefore be handled with this
theory. Thus the bonding modeled by MO theory involves the formation
of electron orbitals that are mutual to the bound atoms. These bonds
have been found to be similar to the bonds formed in the bulk oxide
(Tanaka and Tamaru[18]). A study of hydrogen adsorption on nickel found
that the nature of the chemisoption bond formed was determined more by
the structure of the surface molecule than by the properties of the
bulk metal or by the characteristics of the clean surface (Fassaert
and van der Avoird[19]).

When solving the Schrodinger equation for the situation of an electron in the complex potential field of a molecule or a cluster, the one electron orbitals can be modeled by making a linear combination of atomic orbitals (LCAO) corresponding to the atoms involved. The atomic orbitals are the wave functions that are the solution of Schrodinger's equation for an isolated atom. The existence of symmetry in most molecules and clusters makes solutions to this problem easier to obtain. These symmetry considerations lead one to model metal surfaces as symmetric assemblies of atoms. The size of the clusters used is necessarily finite so the problem can be solved. Fortunately, the calculated electron energy levels begin to approach those of band theory (i.e. the case of an infinite cluster) for relatively small clusters (from 1 to 25 atoms) (Messmer et al.[20] and Salahub and Messmer[21]). It has been found that 25 atoms accomplish this with a metal that is modeled fairly well by free electron theory (such as aluminum) where the valence electrons are more delocalized in nature (Salahub and Messmer[21]). Probably smaller clusters will work for transition metals where the electrons are more localized in nature (Salahub and Messmer[21]).

One of the simplest cases involves the adsorption and eventual dissociation of hydrogen on a nickel surface. A diagrammatic representation of the atomic orbitals involved in the bonding and their shape is shown in Fig. 3 (Deuss and van der Avoird[22]). The shapes of the orbitals shown in the figure are intended to show surfaces enclosing a certain percentage (say 90%) of the electron density. In the work of Deuss and van der Avoird,[22] MO theory was

16
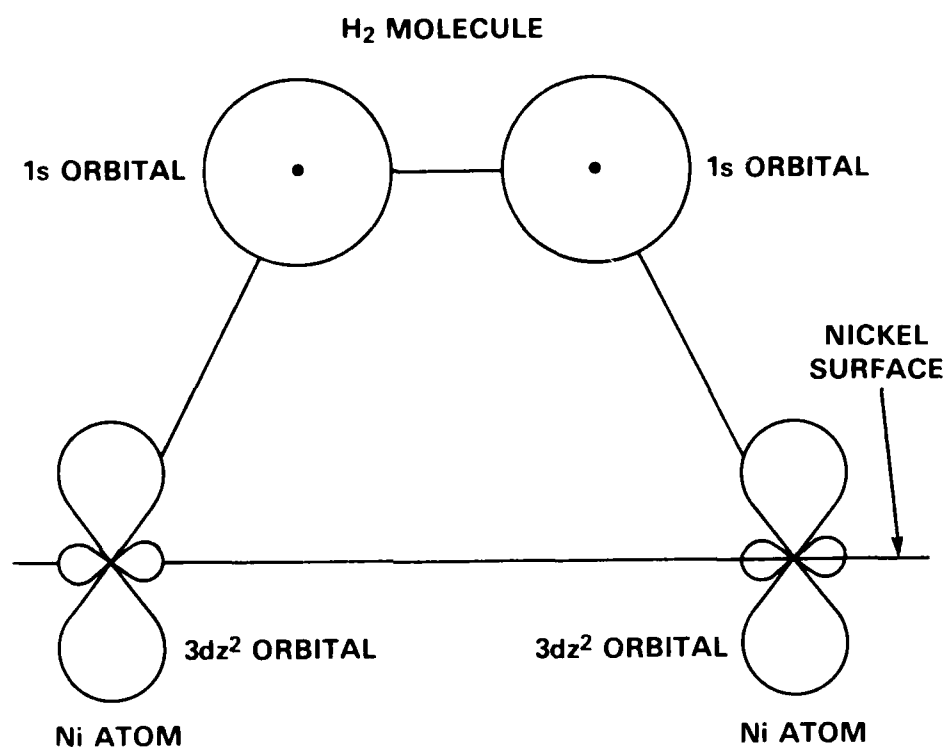
Fig. 3. Model of H_2 absorption on a nickel surface.[22]

used to show that as the hydrogen molecule approaches the surface of the nickel, " ...the $3d_{z^2}$ electrons of the two nickel atoms...attract the molecule and, on coming closer to the metal atoms, it will be dissociated.... This process of adsorption and dissociation requires no activation energy. The 4s electrons of nickel or copper cause very different behavior. The hydrogen molecule is repelled and can only be chemisorbed and dissociated if an activation barrier of approximately 50 kcal/mole for nickel or 45 kcal/mole for copper can surmounted." These same principles can be used to study the rates of SO_2 chemisorption on various metals.

A somewhat more involved cluster, which has been studied by MO theory by Harris and Painter,[23] is shown in Fig. 4. This cluster models the (100) surface of aluminum with an adsorbed oxygen atom. This MO theory approach emphasizes the local nature of the bonding. It allows for a consistent treatment of the atomic nature of the bond formed between the substrate and the absorbate (Harris and Painter[23]). The disadvantage of this approach is that the coupling of the surface cluster and the adsorbate to the bulk of the material is poorly described. However, as mentioned above, proper selection of the structure of the surface cluster can be more important to modeling the nature of the chemisorption bond than a detailed consideration of the bulk properties (Fassaert and van der Avoird[19]). This method of using a surface cluster or molecule to study chemisorption has been applied by Johnson[24] to various size clusters of platinum (13 atoms), iron (9 atoms), and nickel (13 atoms). The electron energy levels that result from these clusters were then compared to the energy

18
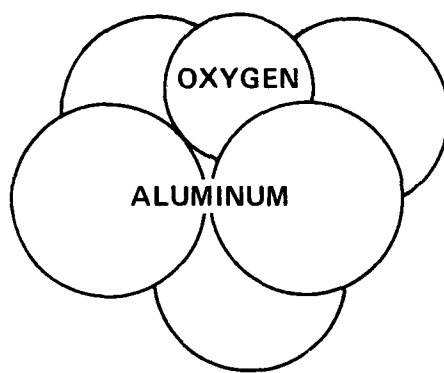
Fig. 4. Six atom cluster of aluminum and oxygen.[23]

levels of nitrogen, carbon monoxide, and oxygen. Matching of electron

orbital energies in the clusters and the gas molecules was then used

to explain why some metal surfaces absorb certain molecules more

easily than others. The π_g orbital of oxygen was found to match the

d-band of iron but not that of platinum, and this was suggested as an

explanation of the easier oxidation of iron versus platinum. The

distance or degree of mismatch of available molecular orbitals on the

adsorbate from the absorbant can possibly be correlated to activation

energy differences and enhanced kinetics of reaction on one metal

surface versus those of another.

MOLECULAR ORBITAL THEORY AND CLUSTER CALCULATIONS
(APPLICATION TO THIS PROBLEM)

On a surface of cobalt the second step of the reaction

proposed above would result in the formation of cobalt sulfate. Since

cobalt sulfate degrades the hot corrosion resistance of the coatings,

it would be interesting to use molecular orbital theory to model the

electron interactions involved in the formation of this sulfate. If

this could be done, such a model might provide a means to analyze

this step of the reaction as it occurs on other metals whose sulfates

are not as detrimental as that of cobalt or to devise an alloying

scheme to impede this reaction step. The electron energy levels of

such a cluster can be calculated by using the SCF-Xα-SW method as

described in Appendix B.

Several types of bond formation can be envisioned for sulfur

dioxide chemisorbed on transition metals. They involve sigma-type

bonds (the wave function of a sigma-type bond has rotational symmetry

20

around the axis of the bond) or pi-type bonds (the wave fuction of a pi-type bond does not have rotational symmetry around the axis of the bond). The orbitals before bonding can be described as having plus and minus lobes where the plus or minus relates to the sign of the wave function. Symmetry requirements of MO bonding require that the symmetry of the metal cluster's orbital (e.g. a d-orbital) match the symmetry of the bond to the ligand or adsorbed species. Transition metals can have as many as five d-orbitals which in the atomic case are all degenerate. These orbitals are labeled $d_{x^2-y^2}, d_{z^2}, d_{xz}, d_{yz},$ and d_{xy}, and when they are all together they total 18 lobes of equal distance from the origin. A representation of each is given in Fig. 5. Ligand field theory provides an understanding of what happens to these orbitals when a crystal forms. As a grouping of atoms forms, such as that in a crystal, the degeneracy of the d-orbitals is lifted with the energy of some raised more than others (Sanderson[25]). A six coordination number complex (an octahedron) is common for transition metals. The six ligands produced by the six atoms surrounding the acceptor atom will split two orbitals to a level called e_g and three orbitals to a level called t_{2g}. This splitting is a result of six atoms at the corners of the octahedron being able to approach six of the eighteen lobes more closely than the other twelve (Sanderson[25]). Different coordination will result in different splitting of the levels. If the coordination is four, as in the case of a tetrahedron, the t_{2g} level is higher than the e_g since four atoms approach twelve of the eighteen lobes more closely than the other six. At a surface where coordination is incomplete, orbitals should be available for
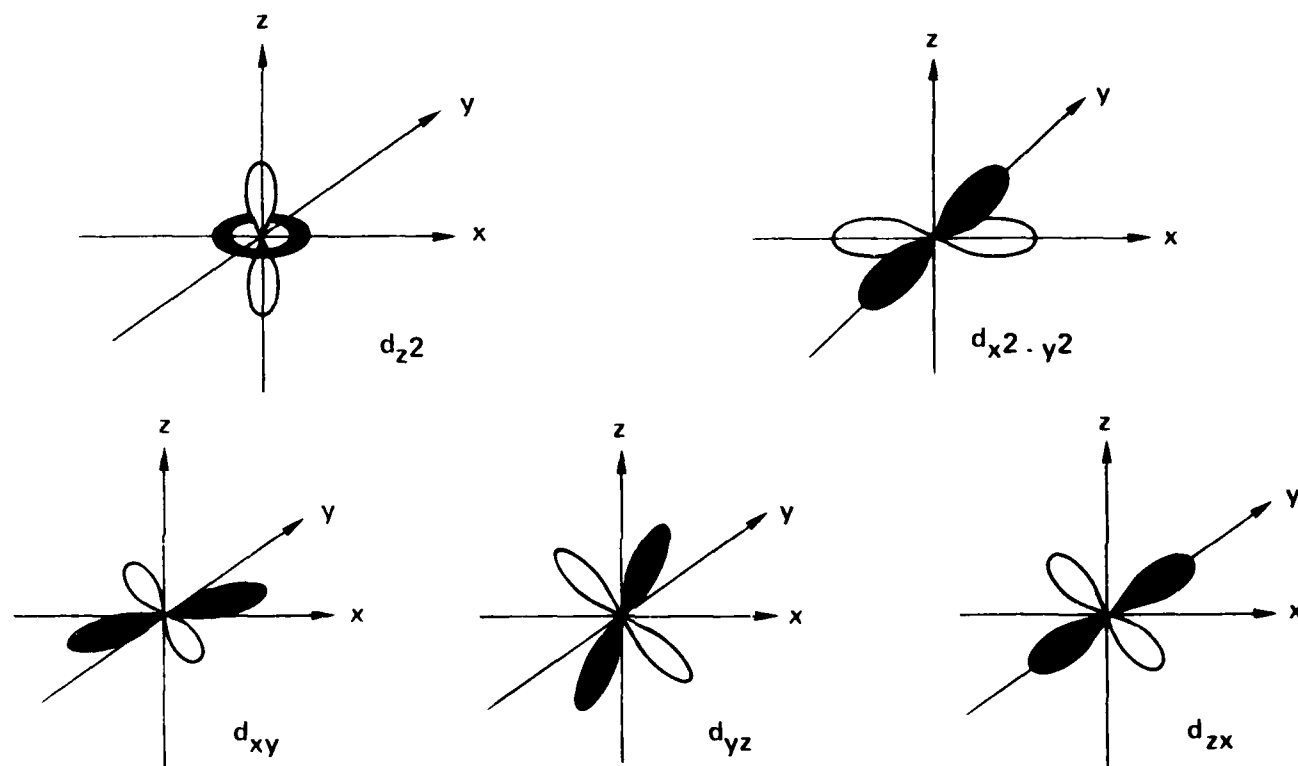
Fig. 5. Electron density distribution in the five atomic d-orbitals.

bonding with an adsorbate such as sulfur dioxide. The molecular orbitals of sulfur dioxide have been studied and described by Outka and Madix,[13] Mingos,[26] and Anderson and Debnath.[27] A diagram of the three highest occupied molecular orbitals (HOMO) and the lowest unoccupied molecular orbital (LUMO) is given in Fig. 6. In the case of silver, Outka and Madix[13] found that bonding of sulfur dioxide to the surface occurred by transfer of an electron from the metal to the LUMO in Fig. 6. Mingos[26] pointed out that sulfur dioxide can undergo electron transfers in both directions, i.e. from the metal to the LUMO or from the HOMO to an empty orbital in the metal.

THEORY AND OBJECTIVE OF THIS RESEARCH

The basic premise of this work is that the reaction mechanisms of SO_2 with cobalt and chromium are similar and are as described above. The objective was to prove this premise experimentally and then to apply what was learned to modeling the initiation stage of the SO_2 interaction with CoCrAlY coatings. The results were then used to propose a mechanism by which increasing the chromium content of these coatings improves their hot corrosion resistance.

23

b₁
LUMO

a₁
BENT π

b₂
LONE PAIR

a₂
LONE PAIR
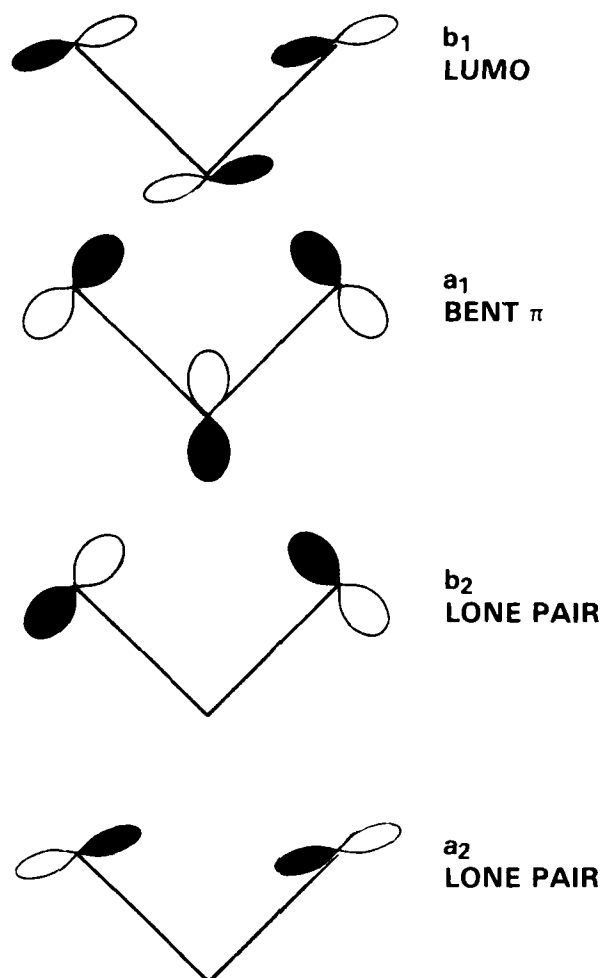
LEGEND:

A p-TYPE ATOMIC ORBITAL: BLACK = POSITIVE LOBE,
WHITE = NEGATIVE LOBE.

Fig. 6. Molecular orbitals of sulfur dioxide.[13]

EXPERIMENTAL PROCEDURE

X-RAY PHOTOELECTRON SPECTROSCOPY

Theory and Equipment

X-ray photoelectron spectroscopy (XPS) was used to examine the nature of the surface reactions that were the subject of this research effort. It was also used to study the nature of the initial oxides formed on the CoCrAlY coatings. XPS involves exposing the surface of interest to x-rays of a discrete energy. In the Kratos model XSAM 800 surface analyzer used in these experiments, Al Kα (1486.6 eV) was the radiation source. This radiation interacts with the specimen, causing the material to emit electrons whose energy is characteristic of the atoms from which they were emitted. (This process is diagrammatically represented in Fig. 7.) The XPS equipment has an electron energy analyzer, which measures the kinetic energy of the emitted electrons. This measurement is made with a hemispherical analyser having an aberration-compensated input lens (ACIL). The analyzer (shown in Fig. 8) superimposes different voltages on the the inner and outer hemispheres, which then allow only electrons with energies between these two values to pass through to the detector at the opposite end of the analyzer. The equipment scans the voltages on the two hemispheres through an energy range in steps, and during its dwell time at each step it keeps track of the counts per second, or intensity of electrons. This information can then be graphed as

25

**ATOMIC
ELECTRON
ENERGY
SHELLS OR
ORBITALS**

● ● ● ● ● ● $L_{2,3}$ OR 2p

●   ● L_1 OR 2s

INCOMING X-RAY (A PHOTON)

EMITTED PHOTOELECTRON

○   ●   K OR 1s

● ELECTRONS

○ VACANCY LEFT BEHIND BY
THE EMITTED PHOTOELECTRON
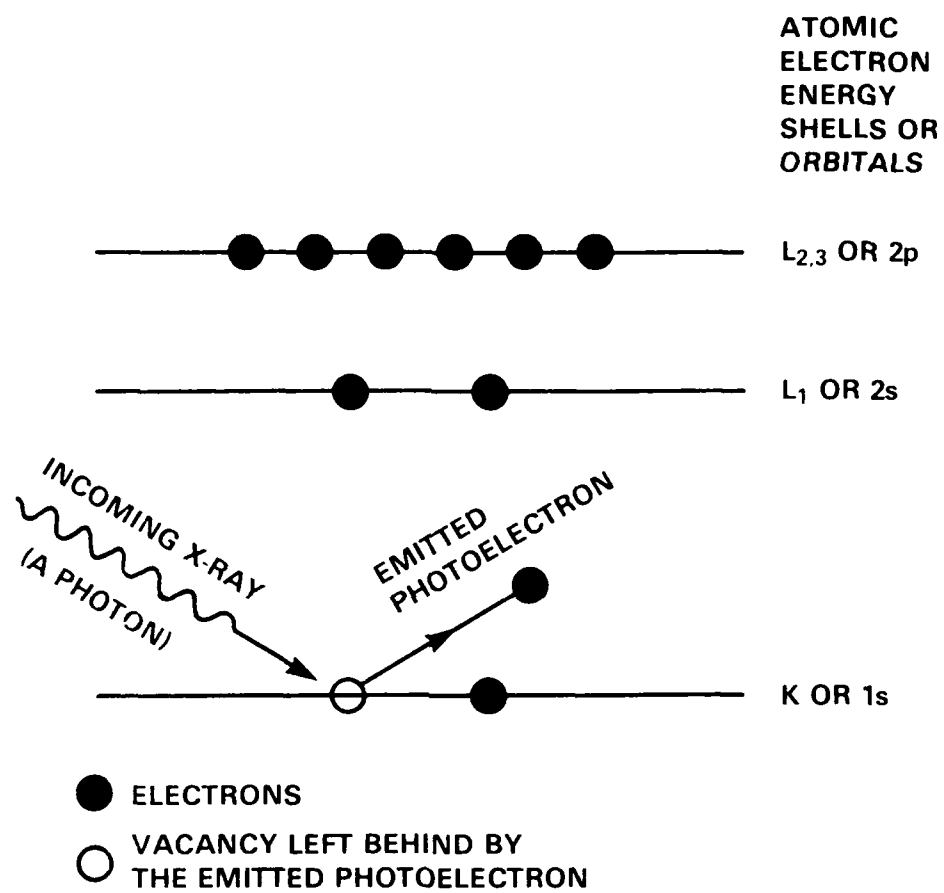
Fig. 7.   Schematic representation of x-ray photoelectron emission.

MAGNETIC SHIELD

OUTER HEMISPHERE

INNER HEMISPHERE

EXIT SLITS

FRINGE FiELD CORRECTOR

ANGLE SLIT

ACIL LENS ASSEMBLY
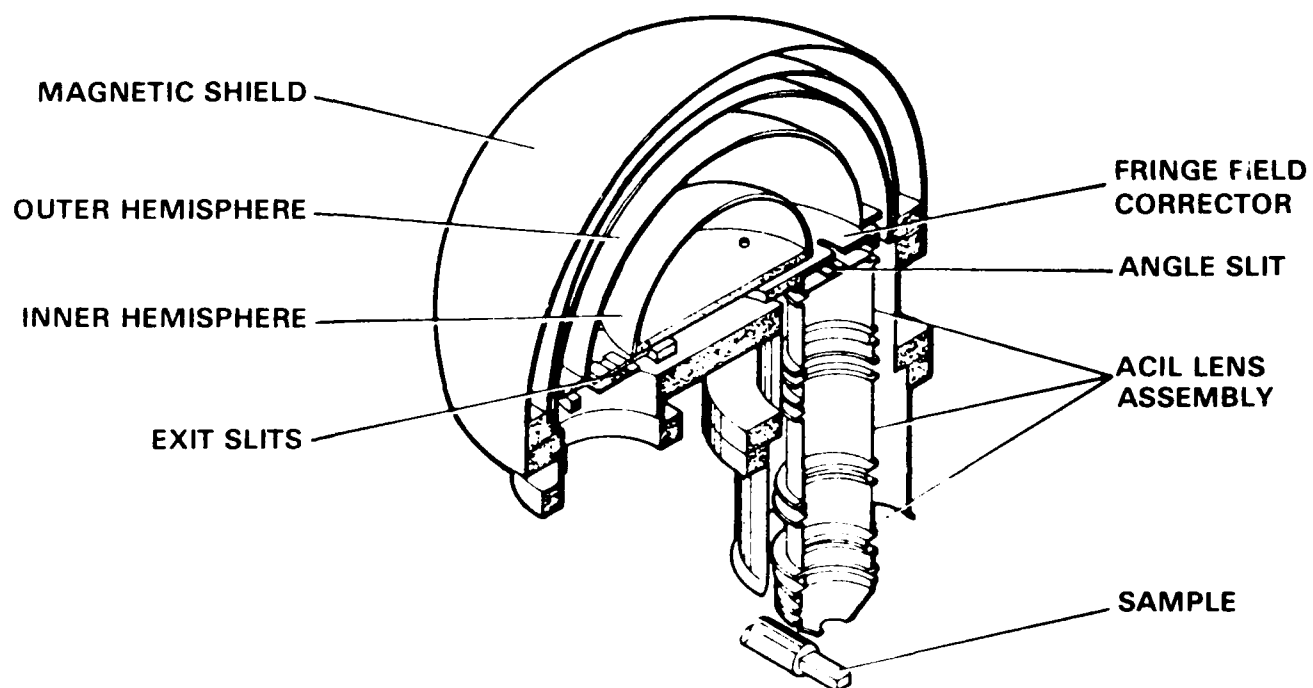
SAMPLE

Fig. 8. Lens-analyzer assembly.

electron energy versus intensity; an example of such a graph is shown
in Fig. 9. The kinetic energy of the electrons can be related to
their binding energy by the relation

$$E_b = E_{x-ray} - E_{kin} - \phi_a ,$$

where: E_{kin} = kinetic energy of electrons as passed by the
spectrometer;

ϕ_a = work function of entrance to the spectrometer lens;

E_b = binding energy of the emitted electron.

The major limit on the energy-resolving capabilities of the instrument
is the width of the exciting radiation, e.g. 1.0 eV at full-width half
maximum for Al Kα.

The XPS spectrometer and specimen are contained within an
ultra-high vacuum. This prevents the electrons from being scattered
by gas molecules before they reach the analyzer and allows experiments
to be conducted and data acquired in reasonable times before the
specimen surfaces are contaminated with unwanted gases and carbon from
the atmosphere. This latter point is important since the the XPS
method analyzes for elements on the surface and within only several
atomic layers of the surface. The surface sensitivity of the XPS
method arises from its ability to measure the energy of emitted
electrons. These electrons have a very short mean free path in solid
matter. Typically, this distance is on the order of 5 to 10 angstroms
(Fig. 10). Therefore, the emitted electrons represent elements
present in the outer layer or several atomic layers below the surface.
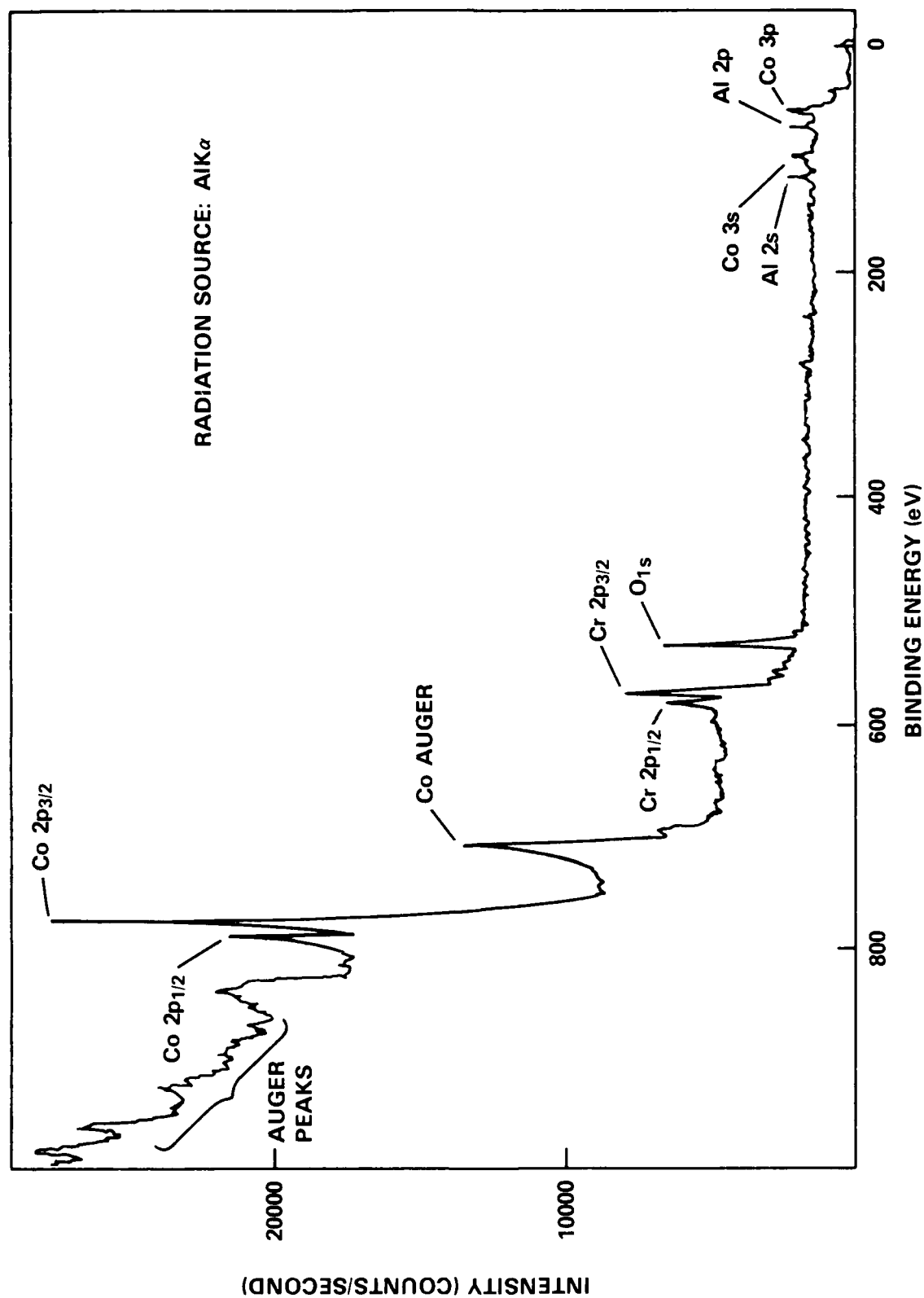
Fig. 9. Typical CoCrAlY XPS spectra after sputtering through initial oxide layer.
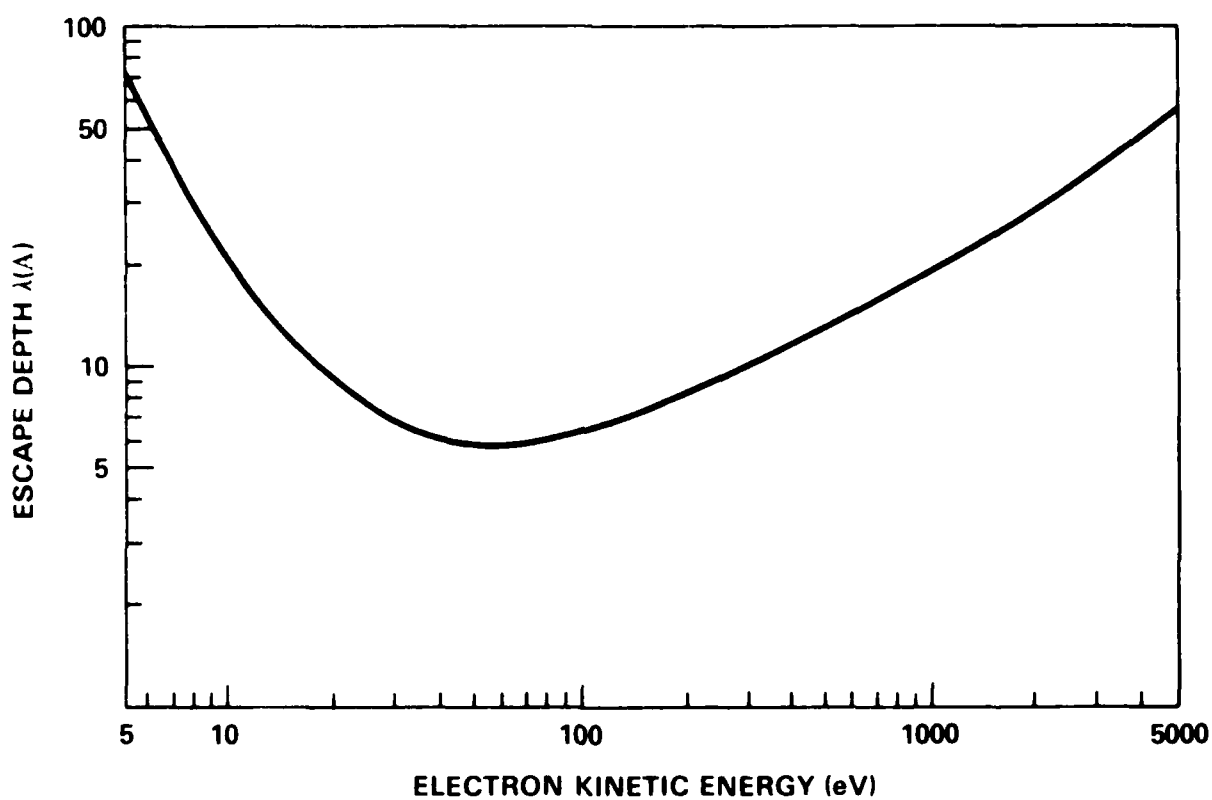
Fig. 10. Sampling depth in XPS as represented by a plot of escape depth against kinetic energy of the escaping electron.

Quantification

The concentration of a given element in the surface is represented by the intensity of electrons (counts per second) emitted at a given characteristic energy. The area under these peaks in the XPS spectrum is used as a measure of the intensity. Computer-aided routines are used to perform the necessary background subtraction around the peak of interest and to calculate the area under the peak. If peaks partially overlap, a peak synthesis routine is used to extract the peak of interest. For example, the peak synthesis routine was used to separate the yttrium $3d_{5/2}$ and $3d_{3/2}$ peaks. All intensities are then corrected by a multiplication factor which represents the spectrometer efficiency and the probability of emission from a particular electron energy level in a given atom. These correction factors were determined by the analyzer's manufacturer. The equation used to calculate the results in atomic percent is given below (David[25] and Briggs and Seah[29]):

$$C_x = \frac{I_x}{Q_x} \sum \frac{I_i}{Q_i}$$

where: Q_x = quantification factor for a given element and electron orbital;

I_x = peak intensity for a given element and a particular electron orbital;

C_x = concentration in at % of element x.

The details of the analysis parameters used to acquire the XPS data
are:

- Al excitation (1486.6 eV)
- Fixed analyzer transmission
- True time averaging

- Low magnification
- Start energy of scan, 1000 eV
- Step size, 0.25 eV

- Low resolution
- Channels, 4000
- Dwell, 0.4 s.

All XPS peaks were referenced to the adventitious carbon 1s peak at
284.6 eV. The approximate binding energy of the XPS peaks used in the
quantitative analysis are given in Table 1. To assist in identifying
the chemical state of the yttrium, XPS spectra were made of pure
standards of yttrium oxide (Y_2O_3) and yttrium aluminum garnet
($Y_3Al_5O_{12}$). Yttrium oxide can naturally be expected in the protective
oxide films on these coatings, and the possible presence of yttrium
aluminum garnet was suggested by the work of Luthra and Hall.[30] The
yttrium oxide and the yttrium aluminum garnet had purities of 99.999%
and 99.995%, respectively. These oxides are nonconductive and charge
up during the spectra acquisition. To compensate for this, the
adventitious carbon peak in both standards was referenced to the 1s
carbon peak at 284.6 eV and all other peaks were corrected
accordingly. These locations are shown in Table 2. The peaks were
acquired by averaging five 20-eV-wide scans around each peak location.
As mentioned before, in the case of the partially overlapping peaks, a
peak synthesis routine was used to separate and identify each
contribution.

Table 1. XPS binding energy locations and Kratos quantification factors.

Element	Electron Designation	Approximate Binding Energy Location of the Peak in (eV) for Elemental and/or Oxide State	KRATOS Quantification Factor
Cobalt	$2p_{3/2}$	778 – elemental 780 – oxide	2.5
Chromium	$2p_{3/2}$	574 – elemental 576 – oxide	1.5
Aluminum	$2p_{3/2}$	73 – elemental 75 – oxide	0.12
Yttrium	$3d_{5/2}$	156 – oxide	1.05
Oxygen	1s	532 – oxide Al_2O_3	0.61

For more detail on aluminum, yttrium, and oxygen peak locations, see Table 2.

33

Table 2. Yttrium, aluminum, and oxygen XPS peak identification.

Material		Binding Energy (eV) of XPS Peaks*					
		Yttrium		Oxygen		Aluminum	
		$3d_{5/2}$	$3d_{3/2}$	1s		2p	
Yttrium Oxide (Y_2O_3)		156.35	160.7	529.25		--	
Yttrium Aluminum Garnet $(Y_2Al_5O_{12})$		157.1	160.6	530.8		73.7	
Aluminum Oxide+ (Al_2O_3)		--	--	531.6		74.7	
CoCrAlY# Coatings	20Cr	158.1	160.1	531.35 Minor	532.1 Major	74.35 Minor	75.1 Major
	29Cr	157.8	158.5	530.8 Minor	532.1 Major	73.85 Minor	74.85 Major
	35Cr	158.35	160.35	531.1 Minor	531.85 Major	73.85 Minor	74.6 Major

* All peaks calibrated to 284.6 eV, all values ±0.25 eV.
+ Values obtained from Riggs et al.[31]
# All CoCrAlY coatings are in the heat treated condition followed by 1 min of argon sputter cleaning.

DEPTH PROFILING

To measure the changes in composition of the elements as they vary through the protective oxide film on the coatings, the original surface was sputtered off in successive layers while the specimen was in the UHV chamber of the analyzer. This was done with the ion sputter gun attached to the analyzer chamber. The ion sputter gun allows an accelerated ionized beam of argon atoms to impinge on the specimen surface. By a collision process this strips off the surface layers. Typical ion sputter gun parameters used were:

- Beam voltage, 4.5 kV
- Emission, 25 mA
- Pressure, 2.0×10^{-2} Pa
- Beam rastered to cover the entire surface area

By using a tantalum dioxide standard, these parameters represent a sputter rate of 30.0×10^{-8} cm/min for this standard. The standard preparation procedures used are given in Appendix C. After the desired thickness is removed, an XPS spectrum is acquired and quantified. The process is continued to the total depth desired. This procedure allows a plot of composition versus depth. Accumulated sputter times at which analyses were made were 0, 1, 3, 15, 47, 79, 159, 191, 231, 247, 263, 287, 303, 319, 343, 351, 367, 391, 407, 455, and 480 minutes.

SAMPLE PREPARATION
CoCrAlY

The specimen configuration used is as shown in Fig. 11. The specimen shown was made of cast Rene 80, a nickel-base alloy that is

35

CoCrAlY COATING 5 mils THICK

9mm DIAMETER

THIS FACE OF STUB EXPOSED TO X-RAYS

STUB MATERIAL: RENE 80

6mm

SIDE VIEW
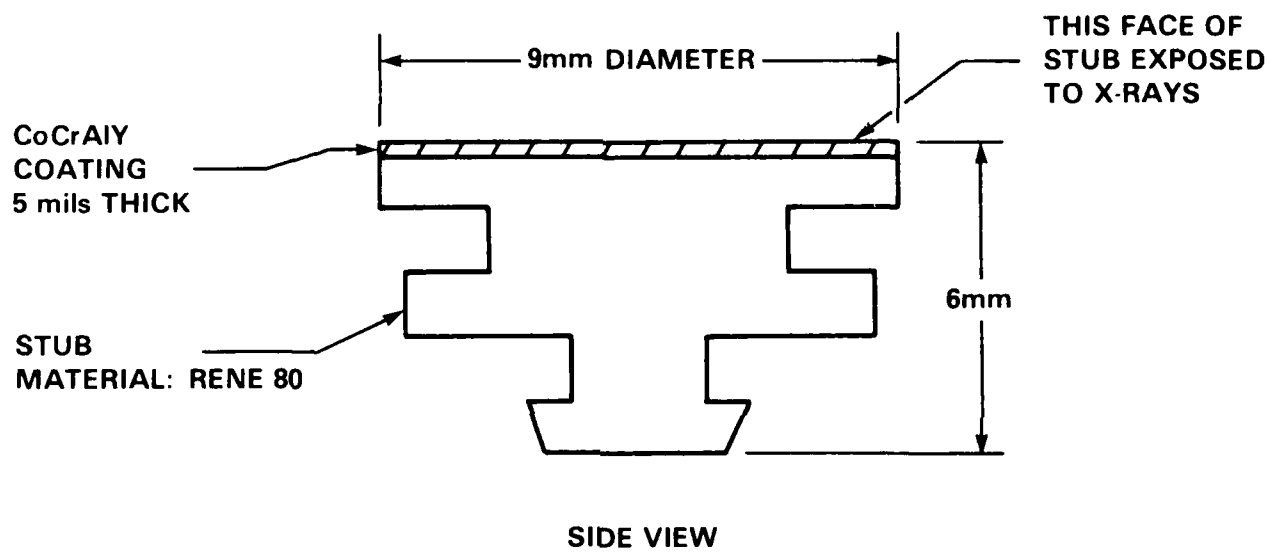
Fig. 11. Specimen configuration.

frequently used for the first stage hot-section turbine blades of marine gas turbine engines. Prior to machining, the alloy was given a solution heat treatment:

> 2225°F (1220°C)--2 h in air--air cooled,
> 2000°F (1095°C)--4 h in air--air cooled.

The machining process removed any oxides formed during the heat treatment. The specimens were then coated by using actual production coating procedures. The coating was applied by physical vapor deposition to a thickness of 0.126 mm (5 mils). Coatings with the compositions shown in Table 3 were produced. These compositions were selected to allow investigation of what effect varying the chromium content in the bulk coating has on the oxide film composition. After the application of the coating, the specimens were given the following heat treatment:

> 1925°F (1051°C)--4 h in vacuum (10^{-4} torr)
> --vacuum cooled,
> 1550°F (845°C)--16 h in argon--argon cooled.

This heat treatment is similar to that given to production coatings. Production parts allow for the final step to be done in a vacuum or argon environment. After heat treatment, the coatings represented actual production blade coatings and were in a configuration that is suitable for direct insertion into the XPS analysis chamber.

Table 3. CoCrAlY Coating composition.

Identification Letter	Coating Composition* (wt%)			
	Co+	Cr	Al	Y
A	65.77	20.64	13.35	0.24
B	60.15	28.89	10.72	0.23
C	54.03	35.25	10.32	0.40

* Composition supplied by the manufacturer.
+ Cobalt composition was done by difference.

Cobalt and Chromium

Elemental, oxide-free cobalt and chromium single crystals were exposed to sulfur dioxide. The crystallographic orientation of the exposed face of the hexagonally close packed (HCP) cobalt was (0001) and of the body centered cubic (BCC) chromium was (110). These two orientations result in the surfaces exposed to the sulfur dioxide being the closest packed orientations for the respective crystal types. The purities of the cobalt and the chromium were 99.999% and 99.996%, respectively. The main impurities were oxides.

Between the various exposures to sulfur dioxide the specimen surfaces had to be cleaned of the reaction products. The surfaces were ion-bombardment cleaned with 500 eV argon at 10 μA/cm^2. Under these conditions it took approximately 30 min of sputtering to clean one or two layers of reaction product from the surface. These

conditions were selected to avoid microfaceting of the Cr(110) surface that more energetic conditions can cause, as described by Shinn and Madey[32] and Grant and Haas.[33]

SULFUR DIOXIDE EXPOSURES

Reaction Cell

In order to expose oxide-free surfaces of the materials in this research effort to sulfur dioxide gas, a reaction cell was attached to the side of the main XPS chamber (Fig. 12). Specimens are transferred from the reaction cell to the main chamber through a ball valve. A turbomolecular pump is attached to the side of the reaction cell to allow pumping the cell down to pressures in the range of 10^{-9} torr. In this pressure range it should take 5 to 10 min to form a monolayer of contaminant gas molecules on an otherwise clean surface.[34] In all of the experiments in the reaction cell the specimens were brought to temperature and exposed to the sulfur dioxide within 5 min as a means to minimize the build-up of contaminants on the clean surfaces before the surfaces could react with the sulfur dioxide. To test the integrity of the reaction cell to air leaks, test specimens were first sputter cleaned in the main chamber and an XPS spectrum of the clean surface was acquired. If there was no carbon on the surface, and if the oxygen level was not greater than that due to oxide particles normally present in the materials, the specimen was then transferred to the reaction cell through the ball valve. These specimens were then run through a typical exposure cycle and then transferred back into the main

39
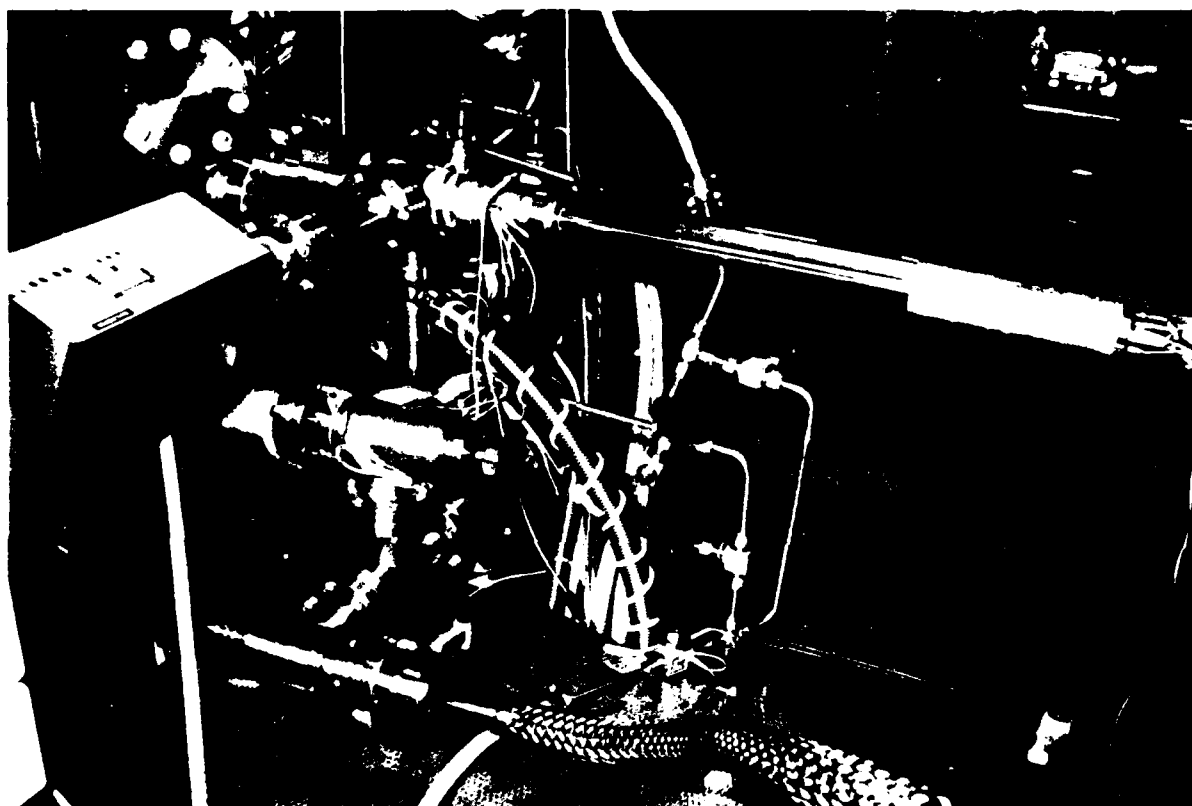
REACTION CELL

Fig. 12. Reaction cell.

40

chamber. An XPS spectrum was acquired and there was no detectable carbon on the specimens nor was there an appreciable increase in the amount of oxygen on the surface. This indicated that the reaction cell was capable of holding an acceptable vacuum during the period needed to start the test exposures to sulfur dioxide.

Procedure

Cobalt and chromium were exposed to sulfur dioxide at two pressures. These were 10^{-4} atm (75 μmHg) and 1 atm (750,000 μmHg). The 1-atm pressure was used because the work of Luthra[35] indicated that this pressure can be reached at the bottom of a corrosion pit on a CoCrAlY coating where the accompanying oxygen partial pressures are very low. The 75-μm pressure was selected because Furuyama et al.[9], Brundle and Carley[10], and Nebesney and Armstrong[11] indicate that a low pressure of sulfur dioxide is needed to investigate the first stages of sulfur dioxide reaction with a metal surface. Pressures in the range of 10^{-6} atm would have been more desirable for this aspect of the study but such low pressures were not achievable with this apparatus. Tests were run at 100°, 230°, and 300°C. The temperature of 230°C was selected because it was the highest temperature that could be achieved with this apparatus at 1 atm pressure. The other temperatures were selected to study their effect on the reaction rate.

Sulfate and Sulfide Identification

During the course of the experiments it become necessary to distinguish between the formation of sulfate or sulfide species on the

41

metal surfaces. The position of the sulfur 2p peak is useful in identifying the formation of sulfate and sulfides. The sulfur 2p peak is typically found at a binding energy of approximately 161 eV when present in a sulfide, and at 169 eV when present in a sulfate. To verify these values, XPS spectra of pure powder standards of $CoSO_4$, CoS, $Cr_2(SO_4)_3$, and Cr_2S_3 were acquired. These spectra were obtained by averaging five 20-eV-wide scans around the XPS peak of interest and correcting for the effects of charging by referencing to the adventitious carbon peak of 284.6 eV. The sulfur 2p peak locations were as follows: 169.35 eV in $CoSO_4$; 161.1 eV in CoS; 169.1 eV in $Cr_2(SO_4)_3$; and 161.6 eV in Cr_2S_3. These values have an accuracy of ± 0.25 eV. In the work involving the pure single crystals, the sulfur 2p peaks can naturally be associated with the respective sulfide or sulfate form of the metal involved. This convenience is no longer available when dealing with coatings that contain both cobalt and chromium. While still useful in determining that sulfate or sulfide species have formed, the sulfur 2p peaks as present in the sulfides and sulfates of cobalt and chromium are too close to be easily discriminated. In coatings containing these two metals, we were able to identify the formation of the respective sulfates by using the $2p_{3/2}$ peaks of cobalt and chromium. In the multiscan spectra acquisitions described above, the $2p_{3/2}$ peaks of cobalt and chromium were also obtained. The results are given in Table 4, along with values for cobalt and chromium in their elemental and oxide forms.

Table 4. Locations of $2p_{3/2}$ XPS peaks for cobalt
and chromium.

Chemical State	$2p_{3/2}$ Peak Location (eV)
Co-elemental	777.9*
CoO	780.0*
CoSO$_4$	782.6
Cr-elemental	574.1*
Cr$_2$O$_3$	576.6*
Cr$_2$(SO$_4$)$_3$	578.6

* Values obtained from Riggs et al.[31]

It can be seen that the $2p_{3/2}$ peak differentiates the presence of these three chemical states of these two elements. When extracting quantitative information from the spectra in the test runs, the problem of any peak overlap was handled by using a peak synthesis routine to separate the peaks. The peak synthesis routine was more complicated than usual due to both the cobalt and chromium peaks being asymmetric (Fig. 13). This asymmetry has been described by Doniach and Sunjic[36] as being the result of the escaping electron in the XPS process losing kinetic energy by interacting with electrons near the Fermi level. In an XPS spectra plot of binding energy this results in a "spreading out" of the high binding energy side of a peak. This effect is most prevalent in metals that have a high density of states near the Fermi level, such as found in the transition metals of cobalt and chromium. Since the peak synthesis routine used works with only gaussian curves that are symmetric, more than one gaussian had to be combined to arrive at a computer simulation of the elemental cobalt

43
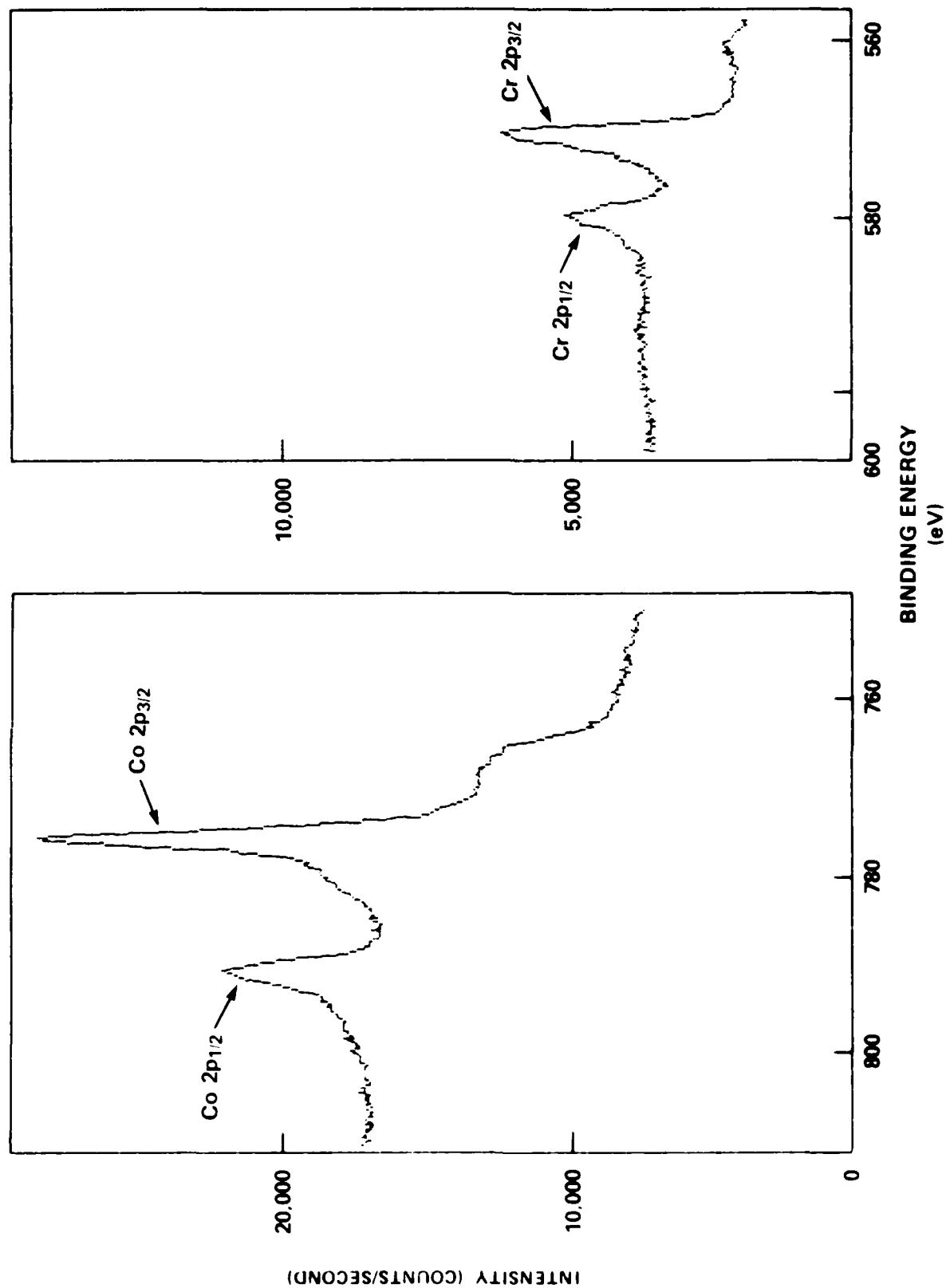
Figure 38. XPS spectra for Co and Cr 2p3/2 and 2p1/2 peaks in a CoCrAlY coating.

and chromium peaks shown in Fig. 13. In the case of cobalt, five gaussians were used. Several combinations of five gaussians can be used to model the shape of the cobalt spectra, but for the purposes of this effort the locations of the peaks were made to correspond to various features that might be found in or near a Co $2p_{3/2}$ peak. The major peak was made to correspond to the location of elemental cobalt (778 eV) with minor peaks located to correspond to the oxide peak (780 eV), the sulfate peak (782.5 eV), the oxide-shakeup peak (787 eV), and the Co $2p_{3/2}$ satellite peak (785 eV). The shakeup peak is the result of a multielectron excitation. When it occurs in cobalt oxide, the emitted electron (the cobalt 2p electron) loses kinetic energy when an oxygen 2p electron transfers into an unoccupied cobalt 3d orbital. An autofit routine was used to fit these peaks to the elemental Co $2p_{3/2}$ spectra (Fig. 14). This "standard" set of gaussians was then fit to the Co $2p_{3/2}$ spectra from the sulfur dioxide runs. By adding an additional (sixth) peak (Fig. 15) at the location where sulfur is present in $CoSO_4$ (782.5 eV) and by varying its intensity, it was possible to extract quantitative information regarding the formation of cobalt sulfate. A similar procedure was used to analyze the spectra from chromium. However, the oxide-shakeup peak was located at a higher binding energy for the oxide of chromium.

In general, the methods and procedures used for the purposes of this effort were able to adequately account for the cobalt and chromium spectra. One difficulty was the location of the major peaks of

BINDING ENERGY (eV)

Fig. 14b. "Standard" spectra composed of 5 gaussians.

BINDING ENERGY (eV)

GAUSSIAN SPECIFICS		
ENERGY	PEAK HEIGHT	FWHH
1·778	94.1	2.5
2·780	22.9	3.5
3·782.5	11.2	4.2
4·785	4.8	3.5
5·787	2.9	4.2

Fig. 14d. "Standard" spectra plus the 5 gaussians used to form the "standard" spectra.

RELATIVE INTENSITY

BINDING ENERGY (eV)
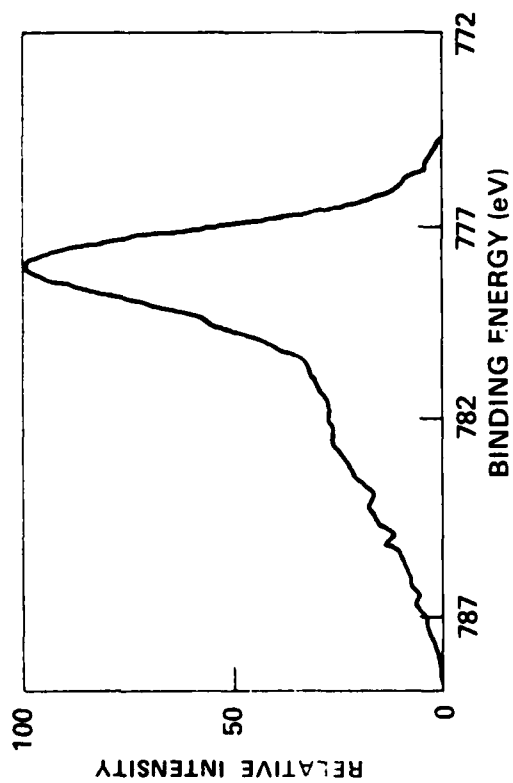
Fig. 14a. Actual cobalt $2p_{3/2}$ peak.

RELATIVE INTENSITY

BINDING ENERGY (eV)
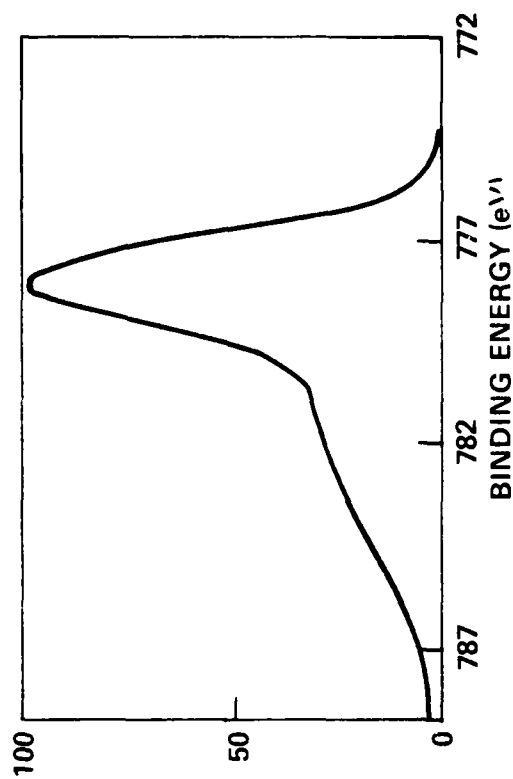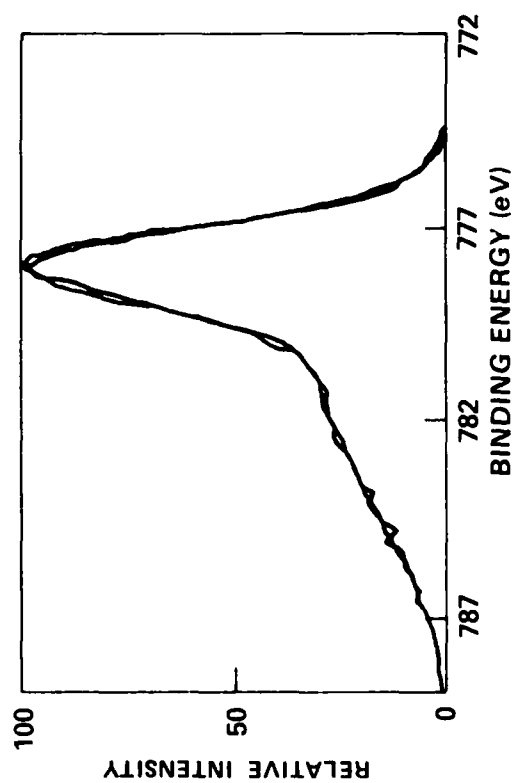
Fig. 14c. Actual cobalt $2p_{3/2}$ peak with "standard" spectra superimposed.

Fig. 14. Co $2p_{3/2}$ peak synthesis using superposition of 5 gaussians.

Fig. 15b. Top right plot — axes: BINDING ENERGY (eV), with values 777, 782, 787; intensity axis 0, 50, 100.

Fig. 15b. "Standard" spectra composed of 5 gaussians.

Fig. 15d. axes: BINDING ENERGY (eV) 777, 782, 787; intensity 0, 50, 100.

GAUSSIAN SPECIFICS		
ENERGY	PEAK HEIGHT	FWHH
1-778	94.1	2.5
2-780	22.9	3.5
3-782.5	11.2	4.2
4-785	4.8	3.5
5-787	2.9	4.2
6-782.5	20.0	5.0

Fig. 15d. "Standard" spectra plus sixth gaussian for sulfate.

Fig. 15a. Bottom left plot — "STANDARD" SPECTRA, SO₂ EXPOSED COBALT. Axes: RELATIVE INTENSITY (100, 50, 0), BINDING ENERGY (eV) (777, 782, 787).

Fig. 15a. Spectra of Co exposed to SO₂ compared to "standard" spectra.

Fig. 15c. Axes: RELATIVE INTENSITY (100, 50, 0), BINDING ENERGY (eV) (777, 782, 787).
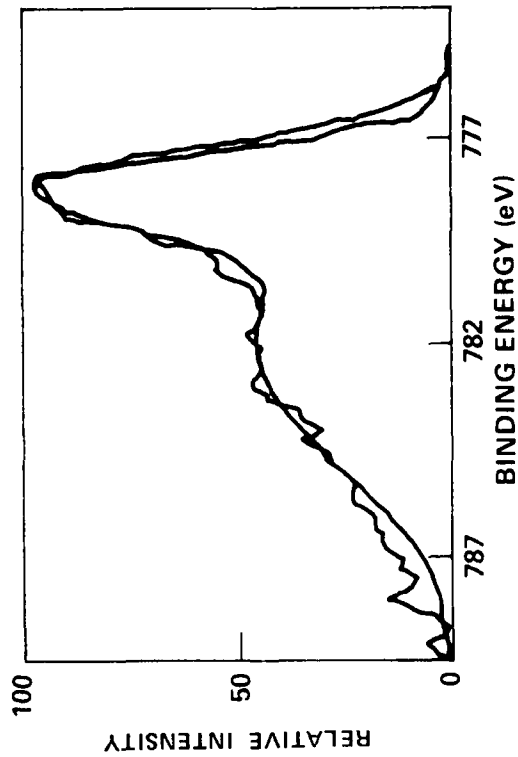
Fig. 15c. Spectra of Co exposed to SO₂ compared to "standard" spectra plus sixth gaussian for sulfate.
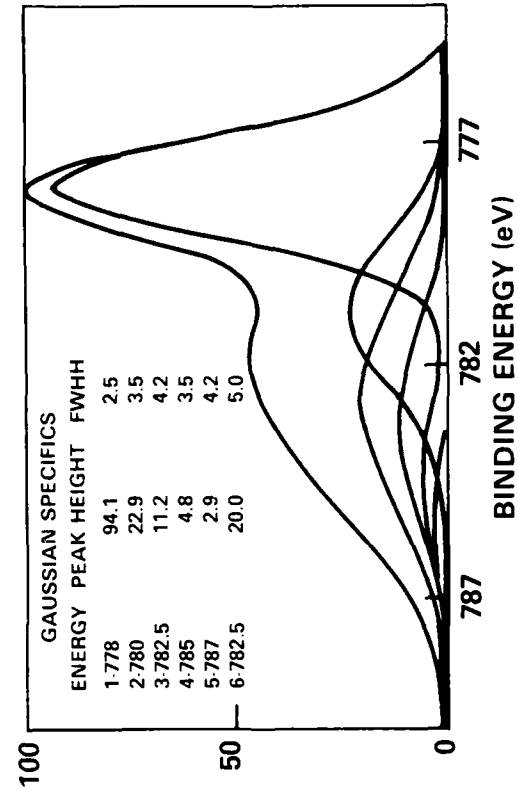
Fig. 15. Co 2p3/2 peak synthesis using superposition of 5 gaussians plus sixth gaussian for sulfate identification.

47

both elements in their sulfide state are difficult to distinguish from their oxide state. Knowing that sulfides had formed based on the position of the sulfur 2p peak was sufficient.

CLUSTER CALCULATIONS

To calculate the energies of one-electron orbitals for the various clusters of atoms to be described below, a set of computer programs was used that employ the SCF-Xα-SW method. The SCF-Xα-SW method is described in detail in Appendix B. The computer programs were obtained from the Quantum Chemistry Program Exchange located at Indiana University. This software was developed by Cook and Case.[37] A typical calculation begins with a run of the program XASYMFN to determine the symmetry of the cluster. This is followed by a run of the program XAINPOT to determine the starting potential of the cluster. One or more runs are made in the ESEARCH mode of the XASCF program to find the one-electron energies to go along with the original starting potential. These one-electron energies are then used in another run of XASCF in the SCF mode in order to converge the starting potentials and the energies in a self-consistent manner.

RESULTS AND DISCUSSION

QUANTITATIVE ANALYSIS OF OXIDE LAYER ON CoCrAlY

The results of the quantitative analysis are shown in Figs. 16, 17, and 18 and are listed on Tables 5, 6, and 7. The data plots show the quantitative analysis in weight percent on the coordinate axis. For reference, the approximate depth of sputtering related to a given sputtering time is also shown. This approximation represents the depth of sputtering as derived from a Ta_2O_5 standard and should serve as an adequate guide to the depth of sputtering on the coatings. These sputter/quantitative runs were made for the coatings containing 20, 29, and 35 wt% chromium. They show that the initial oxide scales in all cases are essentially rich in aluminum, yttrium, and oxygen with only minor amounts of chromium or cobalt.

The significant yttrium in the outer layers of the coatings is interesting; only 0.2 wt % yttrium is added to the bulk coating, but approximately 5 to 6 wt% is found in the outer protective oxide scale. Preferential segregation of elements to the surface of an alloy has been found to occur in other alloy systems, such as Cu-Ni (Sinfelt et al.[4]). With time of sputtering, the composition of the coatings, particularly for the 35 wt% chromium-containing coating, begin to approach the bulk coating composition. Accordingly, the oxygen levels drop from that of the initial layer, but they are not yet zero after the total sputtering time of 180 min or approximately 1.2 μm in depth. This oxygen probably represents coating defects called leaders) that are common in PVD CoCrAlY coatings. These leaders are typically alumina.

Table 5. Surface composition of 20Cr CoCrAlY as determined by XPS as a function of accumulated sputter time.

Accumulated Sputter Time (min)	20Cr CoCrAlY Coating Composition									
	Weight %					Atomic %				
	Co	Cr	Al	Y	O	Co	Cr	Al	Y	O
0	5.0	3.8	47.8	5.4	38.0	1.9	1.7	40.5	1.4	54.5
1	5.4	3.4	48.4	6.0	36.8	2.1	1.5	41.6	1.6	53.2
3	5.3	3.1	48.9	5.9	36.8	2.1	1.4	41.9	1.5	53.1
15	4.0	2.4	49.8	2.8	41.0	1.5	1.0	40.5	0.7	56.3
47	4.7	2.0	52.6	1.6	39.1	1.8	0.8	43.0	0.4	54.0
79	4.3	3.4	52.3	1.3	38.7	1.6	1.5	43.0	0.3	53.6
159	7.8	3.9	49.0	0.4	38.9	3.0	1.7	40.8	0.2	54.3
191	12.0	5.7	47.0	0.2	35.1	4.9	2.6	41.0	0.1	51.4
231	22.0	10.0	39.0	0.3	28.7	9.8	5.0	38.0	0.1	47.1
247	27.0	9.5	35.0	---	28.5	12.4	4.9	34.8	---	47.9
263	29.2	15.3	35.1	---	20.4	14.8	8.7	38.7	---	37.8
287	38.0	18.3	24.3	---	19.4	20.8	11.3	28.9	---	39.0
303	32.7	18.8	33.9	---	14.9	18.0	11.7	40.3	---	30.0
319	38.9	25.3	24.6	---	11.2	23.9	17.6	33.0	---	25.5
343	41.7	19.5	23.0	---	15.8	24.2	12.8	29.2	---	33.8
351	41.3	21.5	24.7	---	12.5	25.0	14.7	32.6	---	27.7
367	40.7	25.1	23.0	---	11.2	25.3	17.7	31.4	---	25.6
383	41.3	21.2	27.0	---	10.5	25.4	14.7	36.2	---	23.7
399	44.1	23.3	23.2	---	9.4	28.3	17.0	32.5	---	22.3
447	45.0	24.5	22.9	---	7.5	30.0	18.4	33.3	---	18.3

50

Table 6. Surface composition of 29 Cr CoCrAlY as determined by XFS as a function of accumulated sputter time.

Accumulated Sputter Time (min)	29 Cr CoCrAlY Coating Composition									
	Weight %					Atomic %				
	Co	Cr	Al	Y	O	Co	Cr	Al	Y	O
0	6.8	5.5	43.4	6.0	38.3	2.7	2.5	37.5	1.6	55.7
1	7.3	7.4	37.7	5.8	41.8	2.9	3.3	32.2	1.5	60.1
3	6.2	5.5	43.5	6.0	38.8	2.4	2.5	37.4	1.6	56.1
15	2.3	6.4	51.1	3.4	36.8	0.9	2.8	43.0	0.9	52.4
47	6.4	3.3	49.9	2.2	38.2	2.4	1.4	41.8	0.6	53.8
79	5.3	1.0	51.4	1.1	41.2	2.0	0.4	41.4	0.3	55.9
159	5.1	4.3	50.0	0.9	39.7	1.9	1.8	41.0	0.2	55.1
191	6.9	6.5	46.9	0.7	39.0	2.7	2.8	39.2	0.2	55.1
231	14.5	6.5	44.9	0.7	33.3	6.0	3.1	40.3	0.2	50.4
247	18.0	8.4	41.9	0.5	31.2	7.7	4.1	39.1	0.1	49.0
263	24.5	10.6	41.5	---	23.4	11.5	5.6	42.5	---	40.4
287	26.8	13.7	42.5	---	17.0	13.6	7.8	46.8	---	31.8
303	36.6	11.9	31.3	---	20.2	19.2	7.0	35.6	---	38.2
319	39.7	20.7	21.1	---	18.5	22.4	13.2	26.0	---	38.4
343	32.5	19.7	32.0	---	15.6	18.6	8.3	40.2	---	32.9
351	42.1	14.7	28.2	---	15.0	24.0	9.5	35.1	---	31.4
367	43.6	15.2	27.1	---	14.1	25.4	10.0	34.4	---	30.2
391	49.5	19.2	19.6	---	11.7	31.6	13.8	27.2	---	27.4
407	48.8	23.2	17.4	---	10.6	32.1	17.3	25.0	---	25.6
455	49.8	17.9	23.1	---	9.2	32.3	13.1	32.6	---	22.0

Table 7. Surface composition of 35Cr CoCrAlY as determined by XPS as a function of accumulated sputter time.

Accumulated Sputter Time (min.)	35Cr CoCrAlY Coating Composition									
	Weight %					Atomic %				
	Co	Cr	Al	Y	O	Co	Cr	Al	Y	O
0	8.7	5.8	40.2	5.0	40.3	3.4	2.6	34.5	1.3	58.2
1	6.7	3.6	46.1	4.1	39.1	2.6	1.6	39.0	1.0	55.8
3	7.2	4.4	46.7	3.4	38.3	2.8	1.9	39.7	0.9	54.7
7	5.2	5.8	47.0	3.3	38.7	2.0	2.5	39.6	0.8	55.1
15	2.7	6.3	46.3	2.7	42.0	1.0	2.7	37.8	0.7	57.8
31	6.6	3.7	50.6	2.2	36.9	2.6	1.6	42.7	0.6	52.5
63	3.7	4.9	50.7	0.5	40.2	1.4	2.1	41.3	0.1	55.1
169	5.1	4.5	47.5	0	42.9	1.9	1.9	38.2	0	58.0
247	15.3	15.2	42.3	0	27.2	6.9	7.6	41.0	0	44.6
303	22.9	24.7	30.8	0	21.6	11.6	14.2	34.0	0	40.2
351	32.9	23.7	25.5	0	17.9	18.1	14.8	30.7	0	36.4
407	32.2	31.6	23.3	0	12.9	19.3	21.6	30.6	0	28.5
455	34.1	37.6	18.4	0	9.9	22.2	27.7	26.2	0	23.9
480	37.6	30.5	20.6	0	11.3	23.6	21.8	28.3	0	26.3
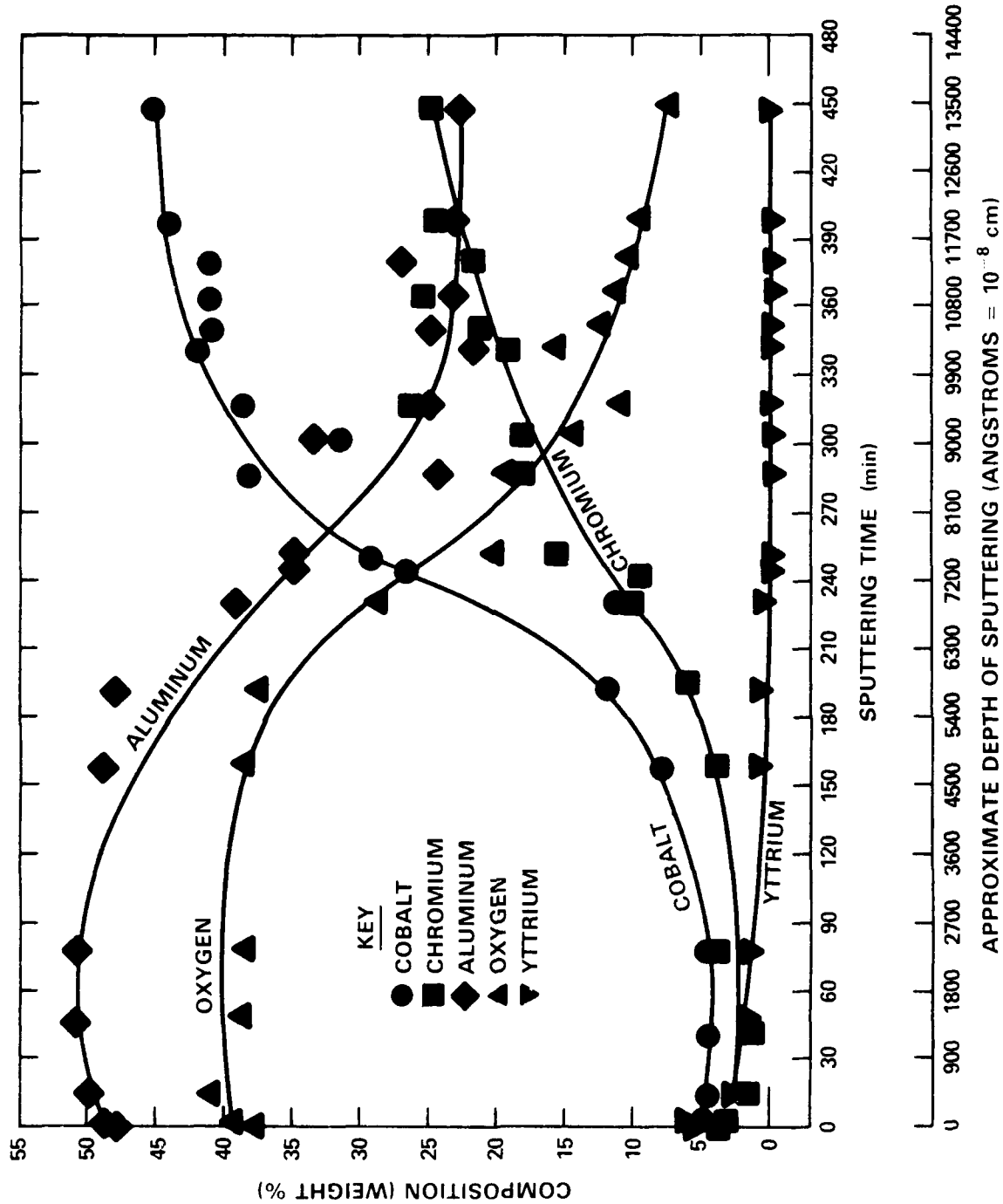
Fig. 16. Surface composition of 20Cr CoCrAlY as determined by XPS as a function of depth of sputtering.

53
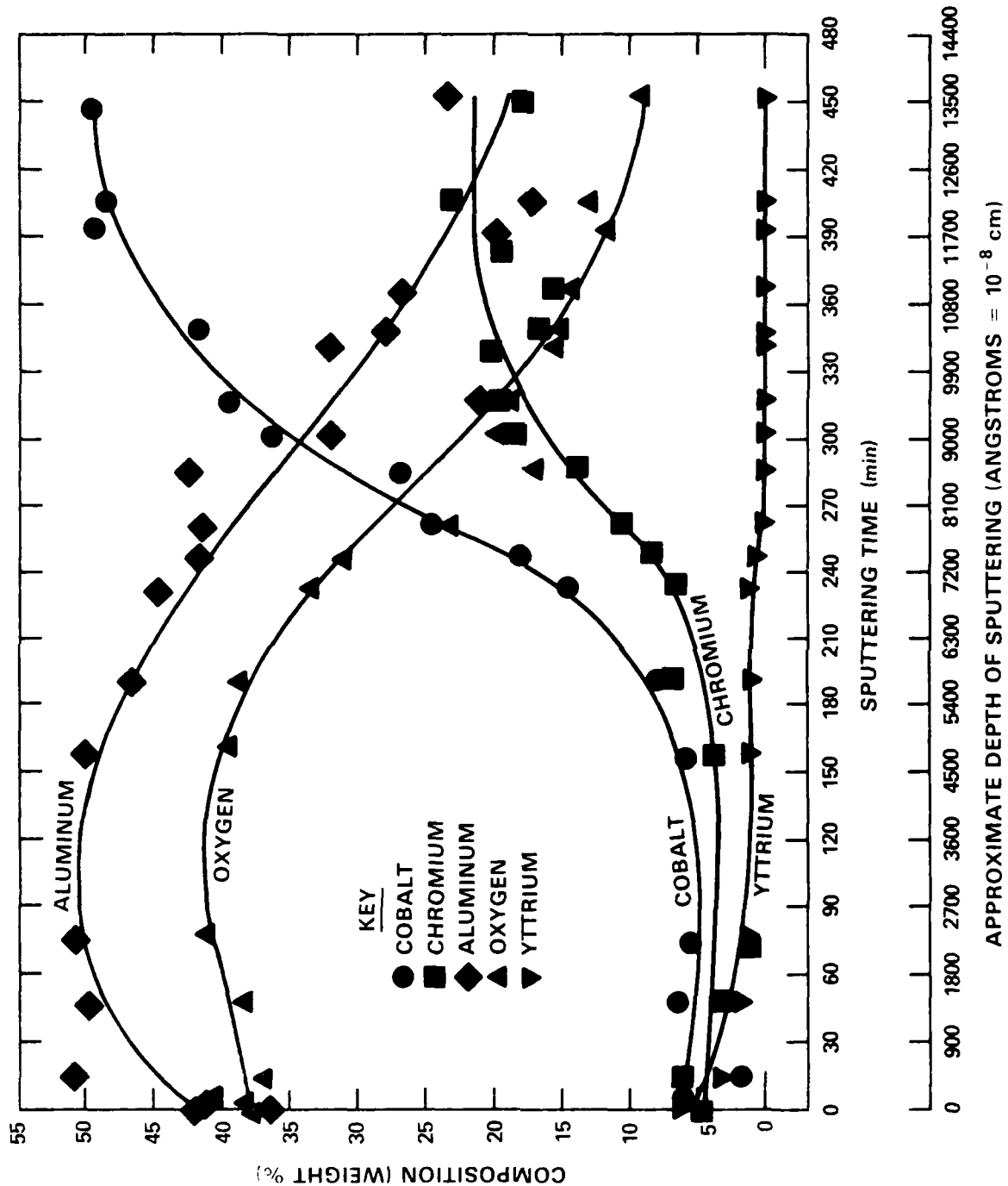
Fig. 17. Surface composition of 29Cr CoCrAlY as determined by XPS as a function of depth of sputtering.

54
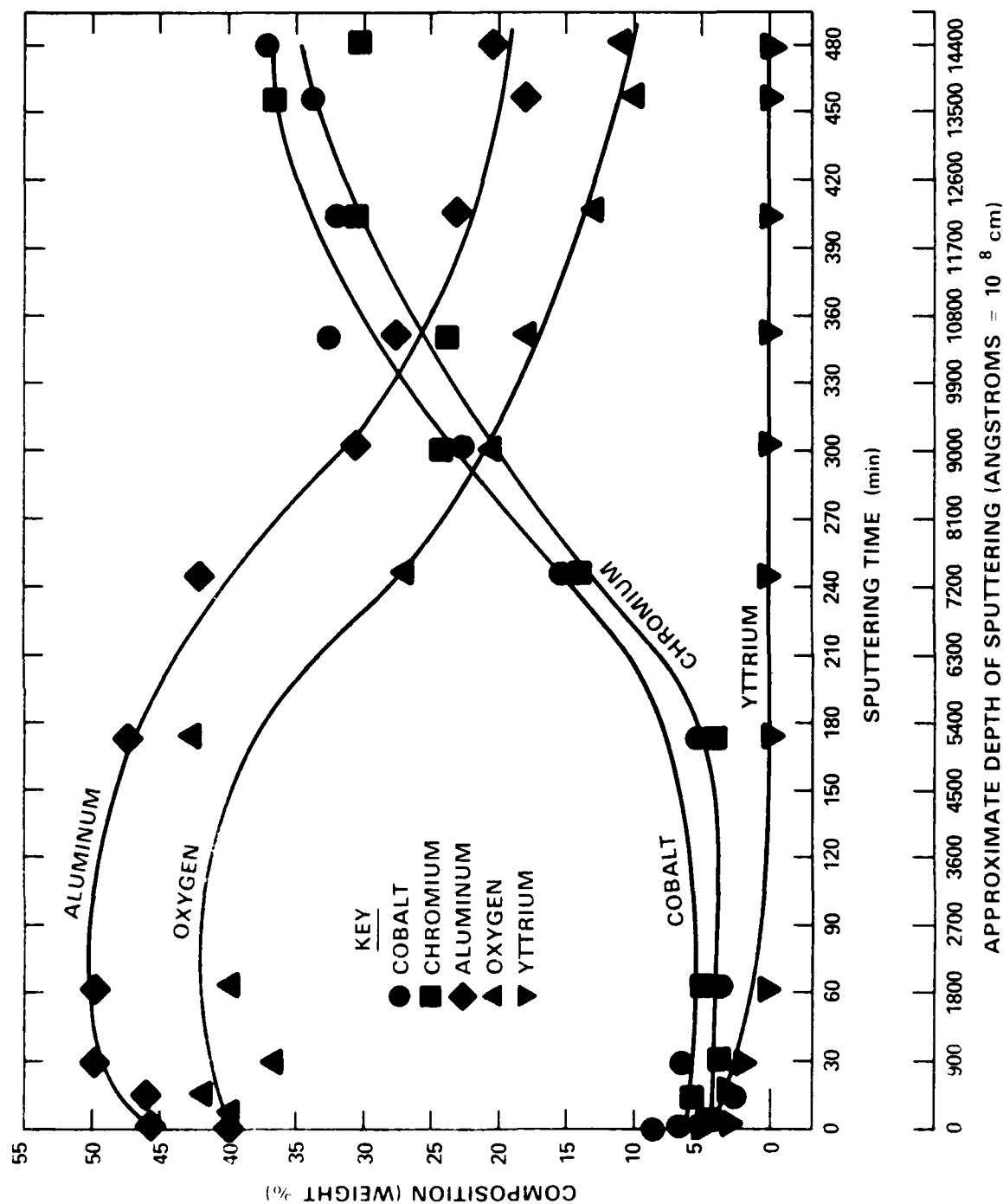
Fig. 15. Surface composition of 35Cr CoCrAlY as determined by XPS as a function of depth of sputtering.

The discovery of the high concentration of aluminum and yttrium in the outer layers of these coatings, even when the chromium content is at 35 wt%, is an important result of this research. Several studies (Goward[2] and unpublished work of the author) have shown that increasing the chromium content of the coatings to 30 or 40 wt% from the originally used 20 wt% dramatically improved the hot corrosion resistance of these coatings. During the open discussions of both the Fourth and the Fifth Conferences on Gas Turbine Materials in a Marine Environment, it was speculated that in the 20 wt% chromium coatings the oxide scales which form on these coatings are a mixture of cobalt oxide, chromium oxide, and aluminum oxide, while in the 40 wt% chromium containing coatings the oxide scale is predominantly chromium oxide. Thus, it had been hypothesized that in high-chromium coatings the formation of cobalt sulfate would be impeded by the continuous nature of the chromium oxide. The results reported here, however, show that the scales are predominantly aluminum and oxygen with a relatively high amount of yttrium, even at the 35 wt% chromiun level.

The aluminum and yttrium on the surface of these coatings can be present in their separate oxide forms or, as indicated in the work of Ramanarayanan,[38] as yttrium aluminum garnet. Consequently, we attempted to determine the oxide form of aluminum and yttrium in the outer surface of the CoCrAlY coatings. XPS spectra were acquired of yttrium oxide and yttrium aluminum garnet for comparison with the XPS spectra of the CoCrAlY's. The peak locations given by Riggs et al.[31] for aluminum and oxygen as found in aluminum oxide were also used for

comparison. These peak locations are shown in Table 2. The oxygen and aluminum peaks on the CoCrAlY specimens were each found to be made up of two overlapping peaks, one major and one minor. A computerized peak synthesis routine allowed the separate identification of these peaks, and these data are shown in Table 2. Within the experimental accuracy (±0.25 eV) of locating the peak positions, the major aluminum and oxygen peaks seemed most closely correlated to the aluminum and oxygen peaks of aluminum oxide, whereas the minor peaks of these two elements correlate to aluminum and oxygen as in yttrium aluminum garnet. The yttrium $3d_{5/2}$ peak in the CoCrAlY coatings is closer to yttrium, as in yttrium aluminum garnet, than it is to yttrium oxide, i.e., 0.7 to 1.2 eV vs. 1.5 to 2 eV respectively. If these values were less than 0.5 eV, the confidence in the comparison would be higher. For this reason the yttrium in the CoCrAlY's is tentatively identified as being present in the form of yttrium aluminum garnet. Consequently, the protective oxide on these CoCrAlY's seems to be predominantly aluminum oxide with yttrium possibly present as yttrium aluminum garnet. Some cobalt and chromium were also present in the analysis of the surface of these CoCrAlY coatings; however, the amounts were low relative to the bulk coating composition and it was no possible to determine from these data if the cobalt and chromium were present as discrete oxides or were simply contained within the aluminum oxide.

The significance of this high amount of yttrium in the surface oxide layers can be appreciated by considering the work of Sprague et al.[5] and Hwang et al.[6] They showed that the yttrium-rich

particles in the oxide scale can provide initiation sites common to all of these coatings at which the hot corrosion process can begin. The corrosion of the yttrium-rich particles serves to mechanically disrupt the remaining alumina scale and thereby expose the bulk of the coating to the hot corrosion process.

Due to the similarity of the starting scale in all of these coatings, a logical proposal is that the chromium provides its hot corrosion benefit in slowing the propagation phase of the bulk coating attack. A means by which varying the chromium content of these coatings might slow the propagation of hot corrosion can be envisioned by considering the works of Luthra[7,9] on the sulfation of elemental salt and chromium. It has been found that it takes lower levels of sulfur dioxide to stabilize a mixed low melting point salt of cobalt sulfate in sodium sulfate than it does for chromium sulfate (or aluminum sulfate). This solution of the one sulfate in the other is necessary in order to promote and stabilize the formation of low melting point mixed sulfates which result in the rapid dissolution and fluxing of the coatings. Thus as more chromium is added to these types of coatings, the formation of cobalt sulfate is probably suppressed in favor of chromium sulfate. If so, then the formation of low melting point mixed salts needed for hot corrosion propagation are not significant. The suppression of the formation of cobalt sulfate could thus result in coatings with improved resistance to hot corrosion attack. The remainder of this research was an investigation to determine the kinetics and of cobalt sulfate formation so that the rate and mechanism of the reactions can

be correlated to the properties of cobalt or chromium in their unalloyed (elemental) forms.

REACTION OF COBALT AND CHROMIUM WITH SULFUR DIOXIDE

To understand how CoCrAlY coatings react with sulfur dioxide, we studied how two of the more predominant elements in the coatings, cobalt and chromium, react with sulfur dioxide. After sputter cleaning from the surface all oxides and carbon contamination, Co(0001) and Cr(110) were exposed to sulfur dioxide at pressures of 75 mHg at 230°C for various times. The amounts (in atomic percent) of sulfate and sulfide formed on the surfaces were calculated using the sulfur 2p XPS peaks as described above. These results were plotted versus time in the Figs. 19a and 19b. The straight lines through the data points in these plots were arrived at by a linear regression analysis. For Cr(110), sulfide was the predominant species. Some sulfate was present, even for the 1-min exposure. With time the amount of sulfate began to approach the amount of sulfide. The Co(0001), in contrast, had a much higher amount of sulfide relative to sulfate at the 1-min point. This could indicate that Co(0001) had less of an activation energy than Cr(110) to dissociate the sulfur dioxide to sulfide. Efforts to determine this activation energy are described below. With time of exposure for the Co(0001), the amount of sulfate increased, as it did for the Cr(110).

Sputter clean surfaces of Co(0001) and Cr(110) were also exposed to sulfur dioxide at 1 atm pressure. Plots of at % sulfide and sulfate produced on these surfaces are shown in Figs. 20 and 21
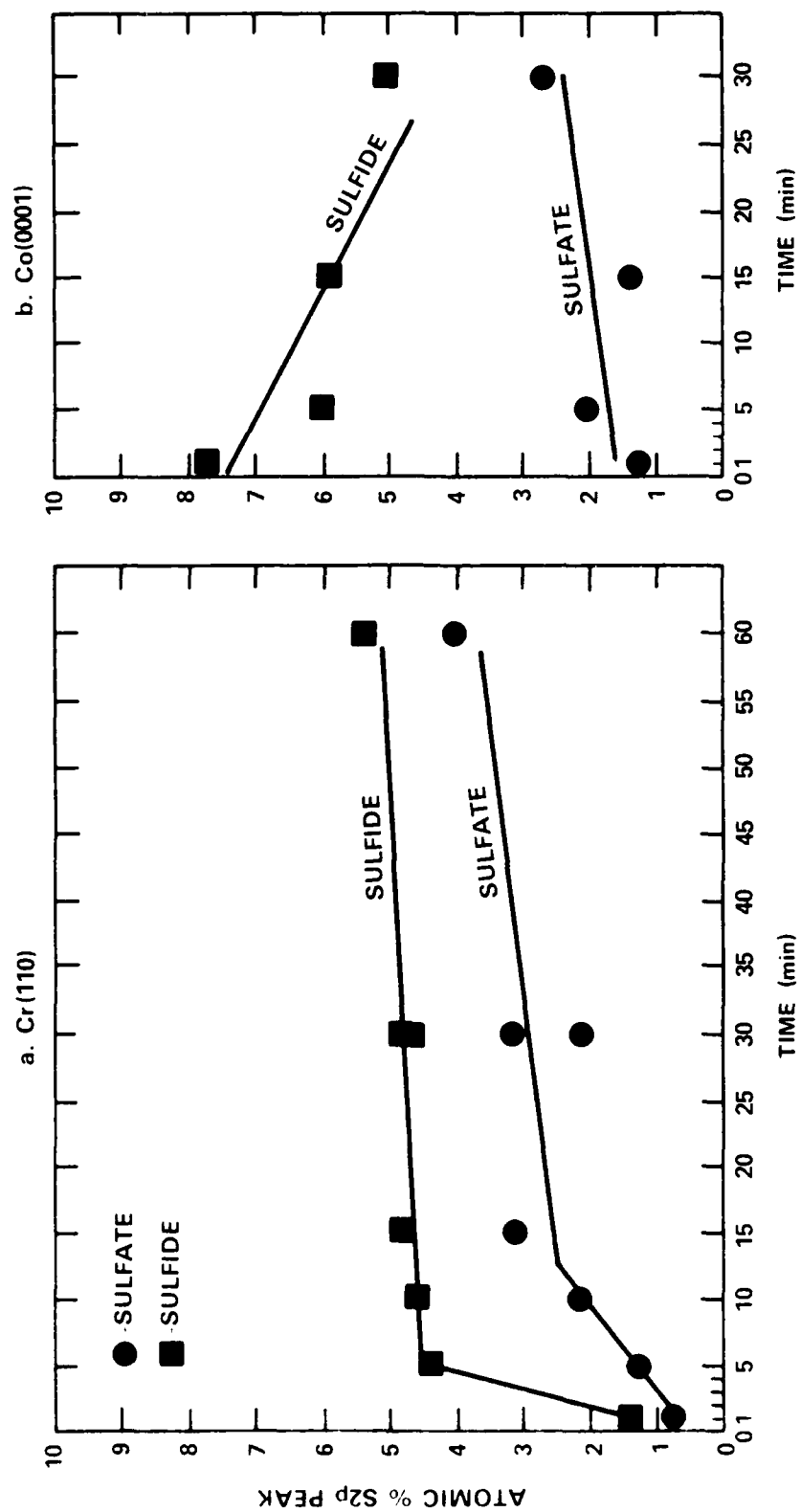
Fig. 14. Atomic % sulfide and sulfate vs. time for sulfur dioxide exposures of Cr(110) and Co(0001) at 75 μm Hg pressure and 230°C.

for time of exposure at 230°C. The major difference between these exposures and the 75-μm exposures was the the occurrence of sulfate as the predominant species on the surface. On Cr(110) after 1 min exposure to 1 atm sulfur dioxide there was slightly more sulfide than sulfate, but very quickly the sulfate exceeded the sulfide. The Co(0001) had more sulfate than sulfide even at the 1 min mark.

To plot the 75-μm and 1-atm data on the same graph, a modified time line was used. The number of collisons of sulfur dioxide per unit area per unit time can be calculated from the equation:

$$\# \text{ of collisions} = P_{so} / \sqrt{2 \ mkT}$$

Other than time, the only variable in these experiments was the pressure of sulfur dioxide. The use of 10^{-4} atm of sulfur dioxide in one set of experiments versus 1 atm in the other set means that 10,000 more gas collisions occurred per unit time in the 1-atm tests. Therefore, to create a common time scale, all of the exposure times for the 1-atm tests were multiplied by 10,000 and then plotted (Fig. 22) on a log scale with the unmodified times from the 75-μm tests. As pointed out before, the Co(0001) showed an initial high value of sulfide after 1 min at 75-μm and a steady decline from that point in favor of the sulfate. For the Cr(110), the amount of sulfide started to level off after 5 to 15 min at 75 μm, and after about 30 min started to decrease.
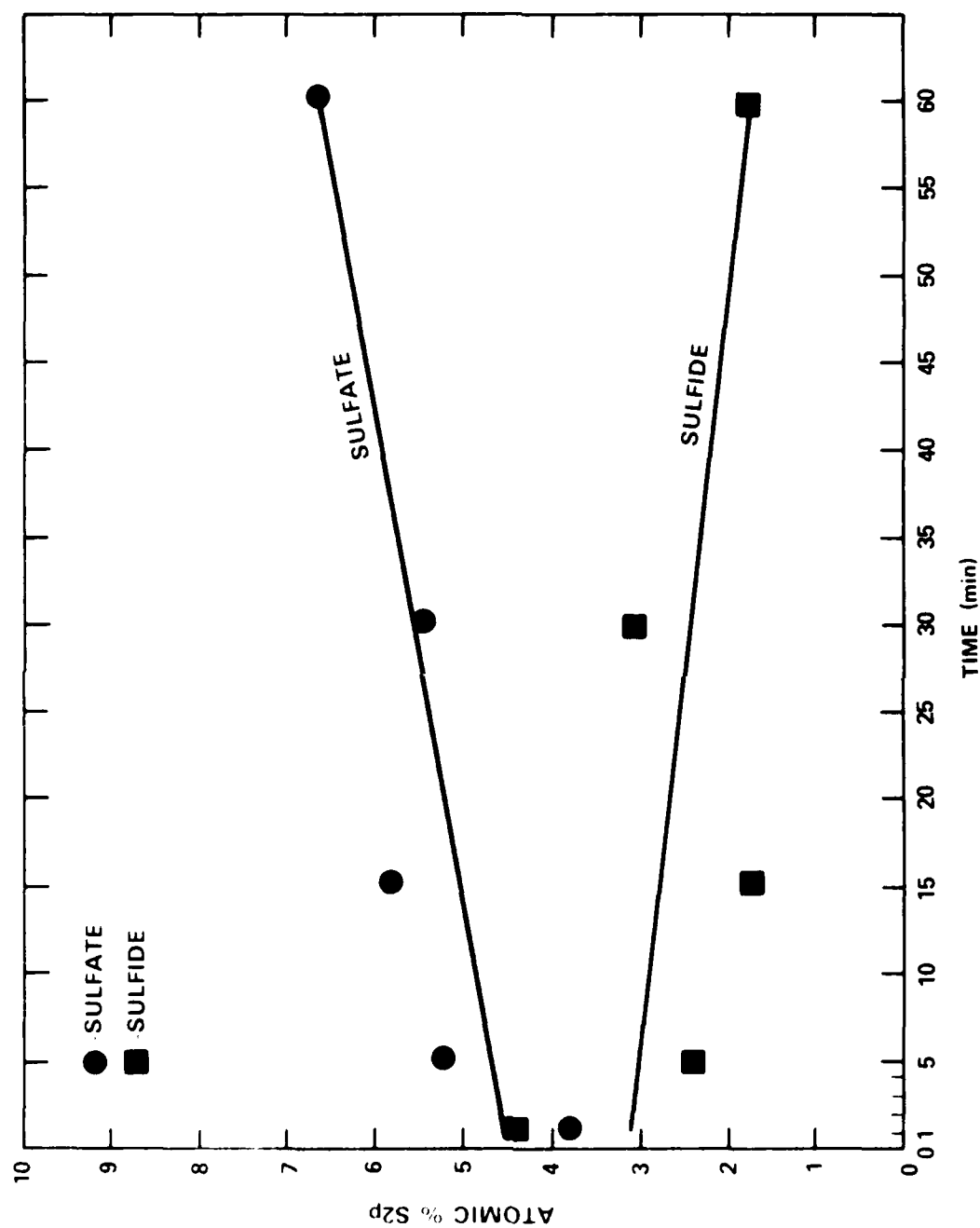
Fig. 20. Atomic % sulfide and sulfate vs. time for sulfur dioxide exposures of Cr(110) at 1 atm pressure at 230°C.
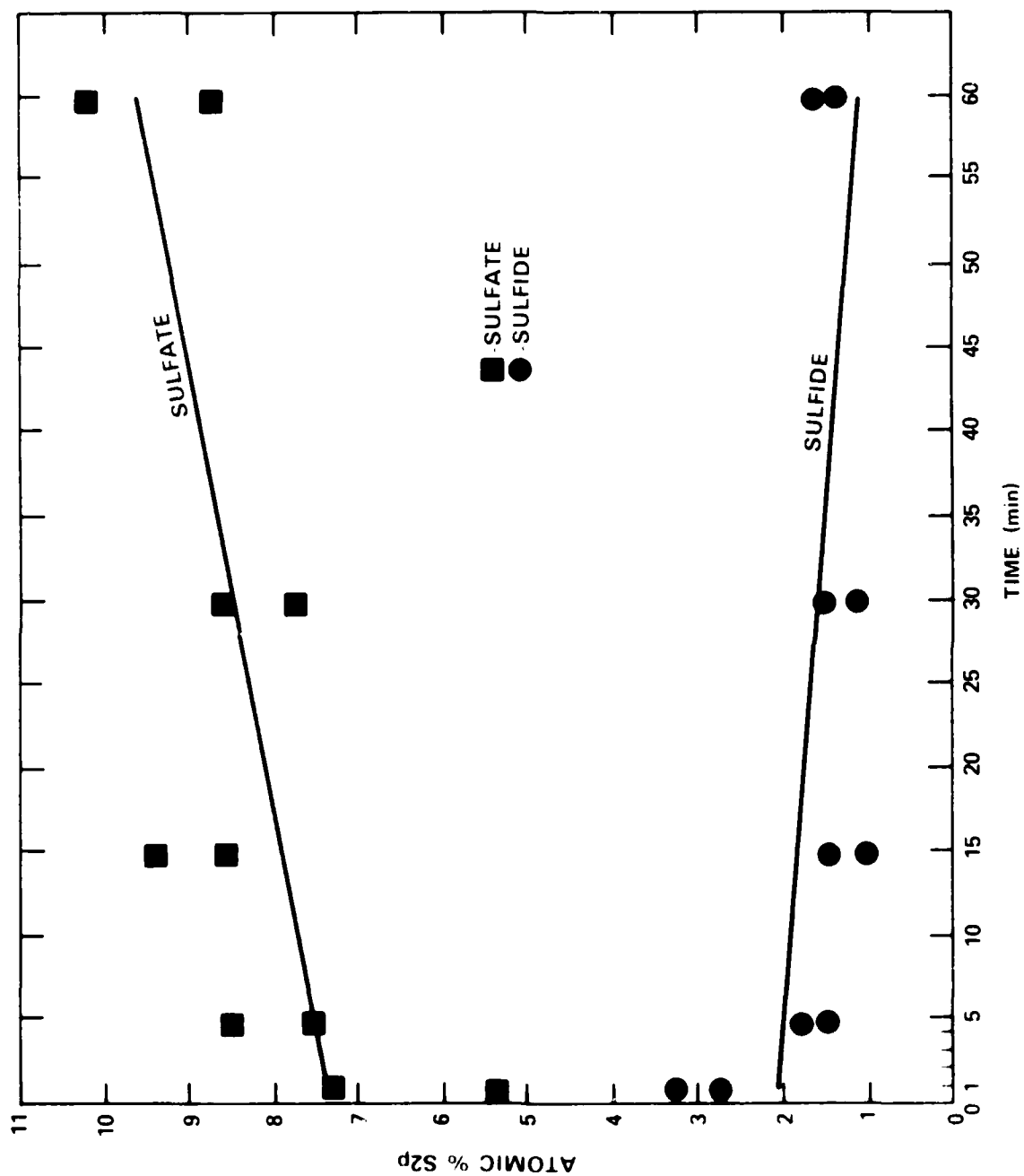
Atomic sulfide and sulfate vs. time for sulfur dioxide exposure of Co(0001) at 1 atm pressure at 230°C.

TIME (min)
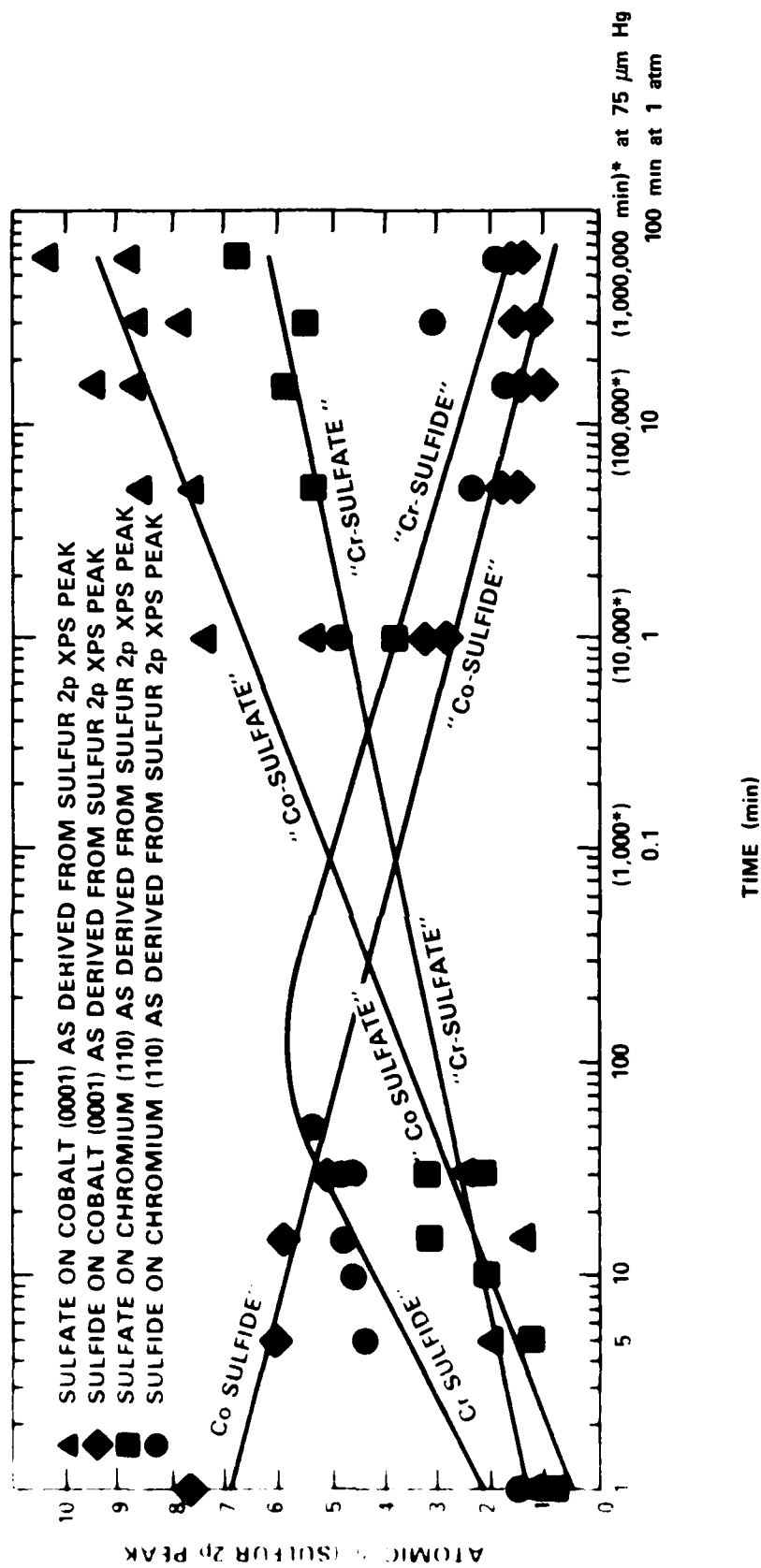
*THESE VALUES IN PARENTHESES ARE GIVEN TO SHOW ADJUSTMENT FOR PRESSURE WITH TIME

100 min at 1 atm

(1,000,000 min)* at 75 μm Hg

ATOMIC % (SULFUR 2p PEAK)

▲ SULFATE ON COBALT (0001) AS DERIVED FROM SULFUR 2p XPS PEAK
◆ SULFIDE ON COBALT (0001) AS DERIVED FROM SULFUR 2p XPS PEAK
■ SULFATE ON CHROMIUM (110) AS DERIVED FROM SULFUR 2p XPS PEAK
● SULFIDE ON CHROMIUM (110) AS DERIVED FROM SULFUR 2p XPS PEAK

"Cr-SULFATE"
"Cr-SULFIDE"
"Co-SULFATE"
"Co-SULFIDE"
Co SULFIDE
Cr SULFIDE

... sulfide and sulfate vs. adjusted time scale for sulfur
... ide exposures of Cr(110) and Co(0001) at 75 μm Hg and 1 atm
... at 300°C.

These results are in keeping with the proposed reaction mechanism, which was:

$$Co + SO_2 \longrightarrow CoS + CoO_2*$$
$$CoO_2 + SO_2 \longrightarrow CoSO_4$$
and
$$Cr + SO_2 \longrightarrow CrS + CrO_2*$$
$$CrO_2 + SO_2 \longrightarrow CrSO_4*$$
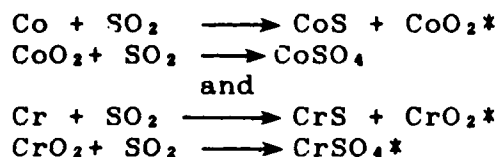
where * indicates nonstiochiometry.

To determine if the sulfur dioxide forms from the oxide species, pre-oxidized Co(0001) and Cr(110) were exposed to sulfur dioxide at a pressure of 1 atm and at 230°C for 15 min. The XPS spectra showed a sulfur 2p peak in both cases that was characteristic of sulfate. The conclusion is that the sulfate developed from the interaction of sulfur dioxide with the oxide species. This result will be useful in analyzing the reaction of sulfur dioxide with CoCrAlY coatings. A similar result was obtained by Furuyama et al.[9] for the reaction of sulfur dioxide with pre-oxidized iron and by Outka et al.[14] for the reaction of sulfur dioxide with pre-oxidized Ag(110) when heated to 500 K. The fact that the sulfate forms by a reaction of sulfur dioxide with the adsorbed oxygen indicates that the decreases with time of the sulfide concentration in the various plots were probably due to an attenuation of the sulfide peak intensity by the overgrowing sulfate layer.

KINETICS STUDY OF SULFUR DIOXIDE REACTION WITH COBALT AND CHROMIUM

The initial stage of reaction as described above is

$$M + SO_2 \longrightarrow MS + MO_2$$

The effect of temperature on the rate of this reaction was studied by exposing Co(0001) and Cr(110) to sulfur dioxide at a pressure of 75 μmHg for 1, 5, 10 and/or 15 min at 100° and 300°C, in addition to the data already discussed for 230°C. The results of these tests are plotted on Figs. 23 and 24 with the at % of sulfate and sulfide as calculated from the sulfur 2p peak versus time. For the Co(0001) at 230°C and 300°C (Figs. 19b and 24b) this reaction was so fast (as measured by at % of sulfide as represented by the S 2p peak) under these test conditions that the above reaction was essentially complete before the end of the 1-min exposures. This was not the case for Cr(110) (Figs. 19a, 23a, and 24a). An effort was made with the Cr(110) to calculate a rate constant by assuming a first order reaction (See Appendix D). The data show that the rate constant was about the same at 100°C and 230°C, 1.1×10^{-3} versus 1.2×10^{-3} s, but decreased at 300°C to 4.6×10^{-4} s^{-1}. When the slope of an assumed linear relation of 1/T vs. log k is calculated, a negative value of 1400 cal/mole results. Since activation energies must be positive and on the order of kilocalories to have any validity, this value has no real meaning. This result and the fact that this reaction on Co(0001) was complete within 1 min means a real difference cannot be measured in the change of the rate constants for the first stage of this reaction (as shown above) for either the Co(0001) or the Cr(110). It must be remembered that the ability to measure small differences in the rate constants was constrained by the limited temperature range and the pressure minimum of the experimental setup used.
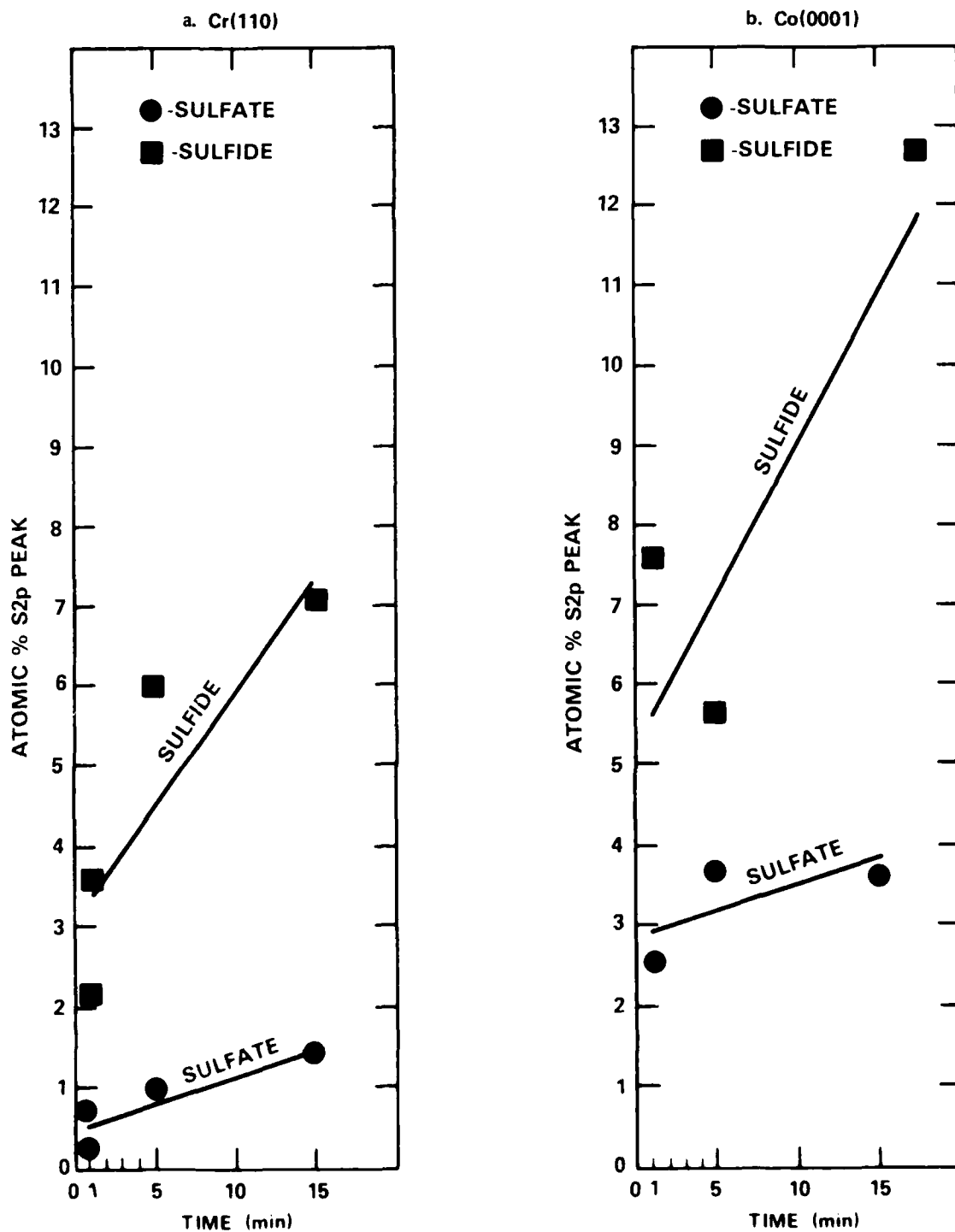
Fig. 28. Atomic % sulfide and sulfate for sulfur dioxide exposure of Cr(110) and Co(0001) at 75 m Torr pressure and 10⁻³ s.

a. Cr(110)

b. Co(0001)

The second stage of the reaction was described as

$$MO_2 + SO_2 \longrightarrow MSO_4$$

The rate constants and the activation energy for this reaction for Co(0001) and Cr(110) were derived from the data of at % of sulfate (as represented by the S 2p peak) shown in Figs. 19, 23, and 24. (See Appendix D for details.) The rate constants for the Co(0001) reaction were 3.5×10^{-4}, 2.8×10^{-4} and 6.9×10^{-4} s^{-1} and for the Cr(110) were 8×10^{-4}, 1.7×10^{-3} and 9×10^{-4} s^{-1} at 100°C, 230°C, and 300°C respectively. Using a linear regression analysis of log k vs. 1/T, activation energies for the Co(0001) and the Cr(110) of respectively 1012 and 689 cal/mole were calculated. As part of the linear regression analysis a correlation coefficient of the fit of the data points to the straight line used is also calculated. The correlation coefficients for the reactions were -0.5 for the Co(0001) and -0.4 for the Cr(110). A value close to 1 or -1 would mean that the data are highly correlated and would indicate a high degree of confidence may be placed in the fit of the straight line to the data. The values of -0.4 and -0.5 indicate low confidence in the appropriatness of the straight line fit to the data. Consequently, the confidence in the rate constants as describing straight line plots of log k vs. 1/T is

... has ... the range measured when considered in light of
... results ... for lithium. Nebesny and Armstrong[11] measured
... of energy ... 2 to 5 kcal for the initial reaction of
... with sulfur dioxide. They did this by measuring the change in
partial pressure of sulfur dioxide during the reaction while using
... pressure ... Unfortunately, changes in sulfur dioxide
pressure in this pressure range could not be measured with our
experimental set up.

REACTION OF OXIDE-FREE CoCrAlY WITH SULFUR DIOXIDE

Since the protective oxide scales on all of the CoCrAlY
coatings were the same, it was surmised that the chromium in CoCrAlY
must provide its hot corrosion benefit in slowing the propagation
phase of the bulk coating attack. This process was examined by
sputtering off the oxide on the 20Cr and 35Cr CoCrAlY's and exposing
them to sulfur dioxide. Luthra[35] showed that the environment at the
base of a corrosion pit has a very low partial pressure of oxygen and
a high pressure of sulfur dioxide (almost 1 atm). Thus as a
simplified model of the propagation phase of the hot corrosion
process, two sputter-cleaned oxide-free CoCrAlY surfaces were exposed
... 1 atm sulfur dioxide for various times from 1 min to 1 h and in the
... CoCrAlY, 1 h. These exposures were made at 230°C, the
... temperature ... stable at this gas pressure with this reaction ...

the Co $2p_{3/2}$ and Cr $2p_{3/2}$ XPS peaks from each CoCrAlY could be used to find the amount of cobalt sulfate and chromium sulfate formed on each CoCrAlY. The results of the at % of the sulfates (as represented by the Co $2p_{3/2}$ and Cr $2p_{3/2}$ peak intensities) versus time of exposure are plotted in Figs. 25 and 26 and the values are given in Table 8. As expected, the 20Cr CoCrAlY formed more cobalt sulfate than chromium sulfate while the reverse was true on the 35Cr CoCrAlY. What is interesting is the ratio of cobalt sulfate produced

Table 8. "Co-sulfate" as in the Co $2p_{3/2}$ peak and "Cr-sulfate" as in the Cr $2p_{3/2}$ peak as produced on the 20Cr and 35Cr CoCrAlY for various times of exposure at 230°C to 1 atm sulfur dioxide. Values in at %.

Time of Exposure (min)	20Cr CoCrAlY		35Cr CoCrAlY	
	"Co-sulfate"	"Cr-sulfate"	"Co-sulfate"	"Cr-sulfate"
1	3.5	1.1	1.9	2.3
5	4.7	3.3	1.7	2.8
15	7.0	4.0	1.9	4.1
30	5.8	5.0	1.8	4.4
60	5.6	4.4	2.3	6.3
240	–	–	1.2	7.9

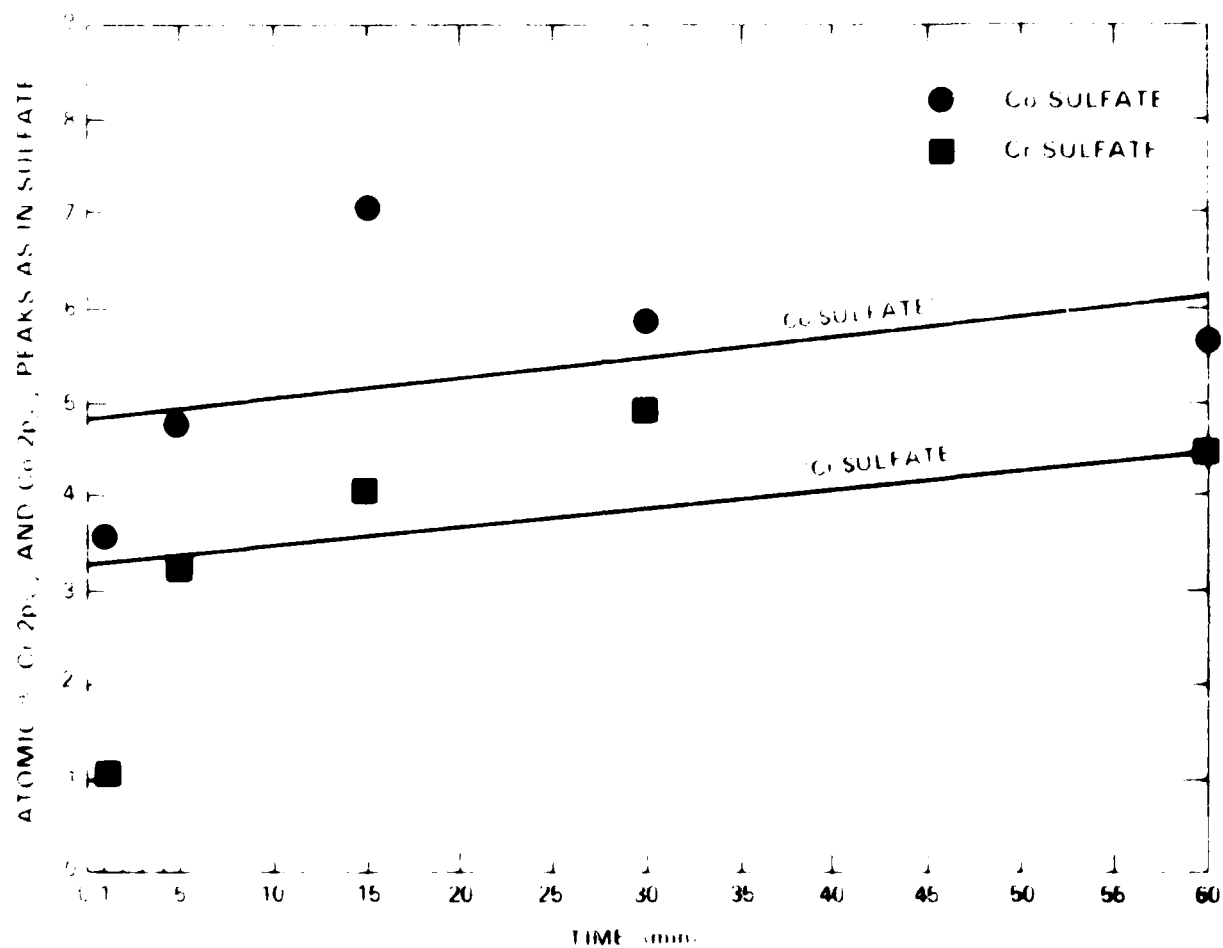on the 20Cr CoCrAlY versus that on the 35Cr CoCrAlY and the of chromium sulfate produced on the 35Cr CoCrAlY versus that on the 20Cr CoCrAlY. The ratio of cobalt sulfate produced on 20Cr to the CoCrAlY is shown in Table 9. The average value is 2.8 and the standard deviation is 0.6, indicating that between 2 to 3 times cobalt sulfate was produced on the 20Cr CoCrAlY compared to the CoCrAlY. This could mean that the 20Cr CoCrAlY had 2 to initiating sites for cobalt sulfate than did the 35Cr CoCrAlY.

71
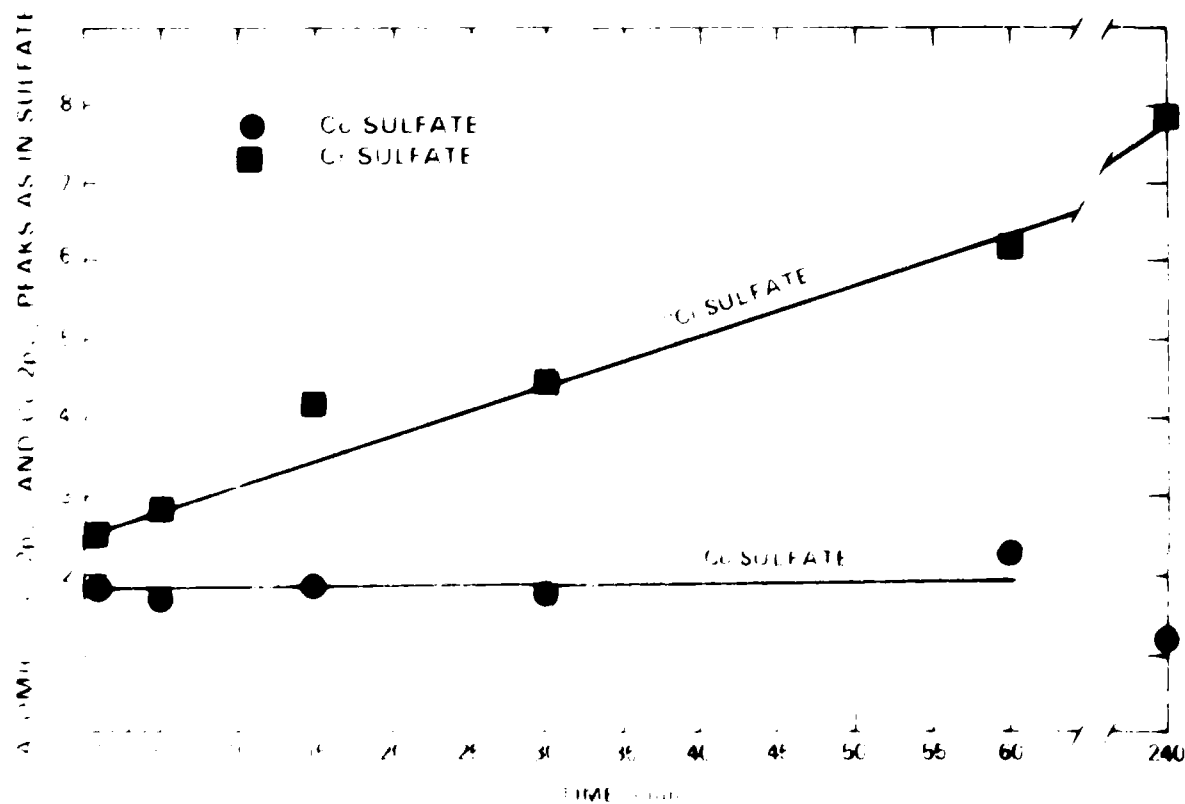
ratio of chromium sulfate produced on the 35Cr to the 20Cr CoCrAlY, also shown in Table 9, is 1.2 and the standard deviation is 0.5. These values indicate that the change in the amount of chromium sulfate was not as significant as it was for cobalt sulfate when the Cr content was increased in the two CoCrAlY's.

decrease in cobalt sulfate (See Figs. 27 and 28). This could mean that the changes in the number of cobalt sulfate initiating sites with variations in alloy composition are critical to these reactions. Such changes could result from the dilution effect of adding the

ATOMIC .... PEAKS AS IN SULFATE

240

the range

the

properties of

the

microscopic phase

chromium content varies.

chromium and cobalt for

a way that is not

CATINGS

the microstructure of the 20Cr

for the formation of phases that

of atoms in the alloy matrix. Both

appearances when viewed under the optical

have a white phase and a grey or dark phase,

properties. (See Fig. 29.) For 20Cr CoCrAlY,

described the white phase as an alpha phase

cobalt and chromium with some aluminum and the grey
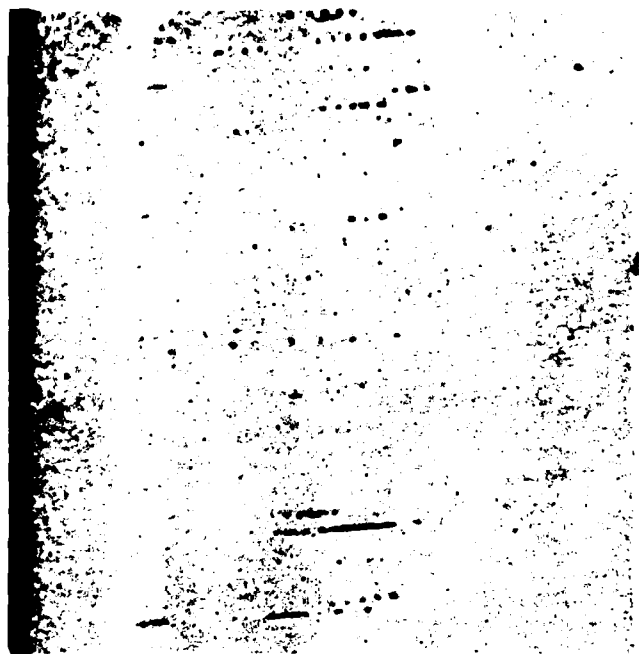
a. 20Cr CoCrAlY, 500X, UNETCHED
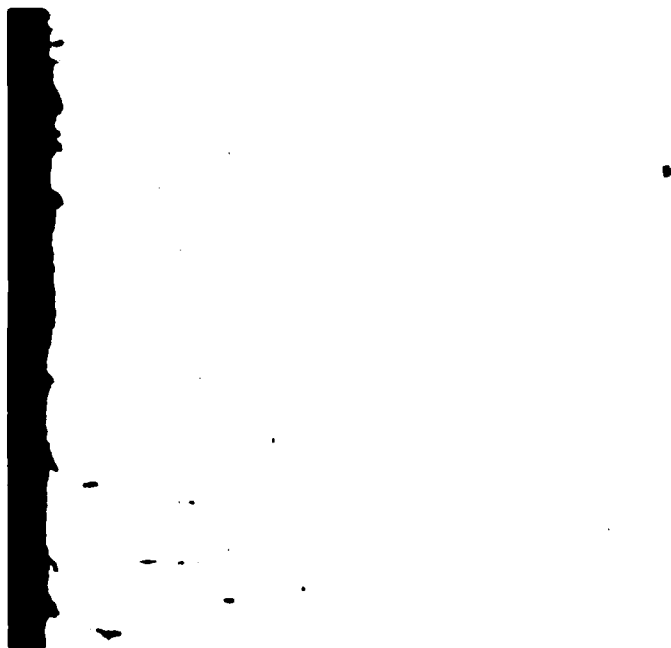
b. 35Cr CoCrAlY, 500X, UNETCHED

Fig. 29. Optical photomicrograph of 20Cr and 35Cr CoCrAlY's.

79

phase as a beta phase with predominantely cobalt and aluminum that also contains some chromium. In addition, the grey or beta phase is described as having the CsCl structure. The literature is basically silent on the 35Cr CoCrAlY.

An electron microprobe determination was made of the chemical composition of both phases in both coatings. The analyses from ten different spots were averaged for each phase. For the 20Cr CoCrAlY the white (alpha) phase was 64 at % Co, 30 at % Cr and 6 at % Al, and the dark (beta) phase was 56 at % Co, 14 at % Cr and 30 at % Al. An image analysis showed the white phase to cover 11.4% and the dark phase 88.6% of the coating surface area. For the 35Cr CoCrAlY the white phase was 46 at % Co, 48 at % Cr and 6 at % Al, and the dark phase was 51 at % Co, 20 at % Cr and 29 at % Al. The image analysis showed the white and the dark phases to cover 40.7 and 59.3%, respectively, of the coating surface area. The composition of the white phase in the 35Cr CoCrAlY indicated that a sigma phase had formed in this coating.

In the cobalt/chromium binary system the sigma phase occurs within a narrow composition range around 50 at % Co and 50 at % Cr (Am. Soc. Metals[40]). The sigma phase is an intermetallic compound, primarily involving transition metal elements, in which the elements do not occupy random locations in the lattice. This ordering of the sigma phase is described below. A literature search did not turn up a good room temperature ternary phase diagram for the CoCrAl system. However, an examination of the binary CoCr phase diagram in the Metals Handbook[40] showed that at room temperature the sigma phase exists in

80

equilibrium with a second phase of solid solution cobalt and chromium when the chromium content is between 15 and 58 at %. From 58 to 62 at % chromium the binary alloy is in the single phase sigma field. On a ternary phase diagram for CoCrAl at 1175°C (Gupta et al.[41]) a sigma phase is present in a region where the chromium varies from 50 to 60 at % and the aluminum from 0 to 5 at %. Based on this information it is not unreasonable to postulate that sigma phase may be found in CoCrAlY coatings with high chromium contents, and, if so, that it exists with a composition similar to the composition of the high chromium coating in this study.

In the case of sigma phase in the binary CoCr system, the crystal structure, as described by (Henry and Longsdale[42]) is that of a tetragonal unit cell (with a=8.81Å and c=4.56Å) containing 30 atoms. The structure of the unit cell has been described by Dickens et al.[43] as hexagonal, close-packed sheets in the planes z=0 and z=c/2, which serve as the main layers, and with 4 atoms in each of the secondary planes at z=c/4 and z=3c/4. The crystal is classified as being of the space group P4/mnm which has the arrangement of atoms detailed in Table 10. For a composition of 13 Co and 17 Cr atoms (i.e. 56.4 at % Cr), Dickens et al.[43] found the Co and Cr atoms to order themselves at the various lattice sites in regular way with the 2a and the 8i1 sites (as described in Table 10) occupied by cobalt and the 4g and 8i2 sites by chromium. The 8j sites are occupied at random by the two elements. Since the compositon described by Dickens et al.[43] is close to that of the sigma in the CoCrAlY coatings, the atom

Table 10. Positions of atoms in the ... cell of sigma ...*

Designated Plane	Lattice Site Designation	Position of the Atoms ... (Å)			
z = 0	2a	0	0		
	4g	3.51	...		
	4g	-3.51	...		
	8i1	0.58	2.29		
	8i1	-0.58	-2.29	0	
	8i1	2.29	0.58		
	8i1	-2.29	-0.58	0	
	8i2	4.73	1.11	0	
	8i2	-4.73	-1.11	0	
	8i2	1.11	4.73	0	
	8i2	-1.11	-4.73	0	
z = 1/2 c	2a	4.40	4.40	2.28	Co
	4g	7.86	7.86	2.28	Cr
	4g	0.89	0.89	2.28	Cr
	8i1	4.98	2.12	2.28	Co
	8i1	3.83	6.69	2.28	Co
	8i1	6.69	3.83	2.28	Co
	8i1	2.12	4.98	2.28	Co
	8i2	9.14	3.27	2.28	Cr
	8i2	-0.33	5.54	2.28	Cr
	8i2	5.54	-0.33	2.28	Cr
	8i2	3.27	9.14	2.28	Cr
z = 1/4 c	8j	2.80	2.80	1.14	Co or Cr
	8j	-2.80	-2.80	1.14	Co or Cr
	8j	7.20	1.61	1.14	Co or Cr
	8j	1.61	7.20	1.14	Co or Cr
z = 3/4 c	8j	7.20	1.61	3.42	Co or Cr
	8j	1.61	7.20	3.42	Co or Cr
z = -1/4 c	8j	2.80	2.80	-1.14	Co or Cr
	8j	-2.80	-2.80	-1.14	Co or Cr

* In the tetragonal unit cell the edge lengths are of the relationship a=b≠c; and the interaxial angles are $\alpha = \beta = \gamma = 90°$. CoCr sigma has 30 atoms per unit cell with a=8.81Å and c=4.56Å

Note 1: The dimension a is taken in the x-direction; b in the y-direction; and c in the z-direction.

2: Lattice site designations are as per Henry and Lonsdale[42] Lattice site occupancies are as per Dickens et al.[43]
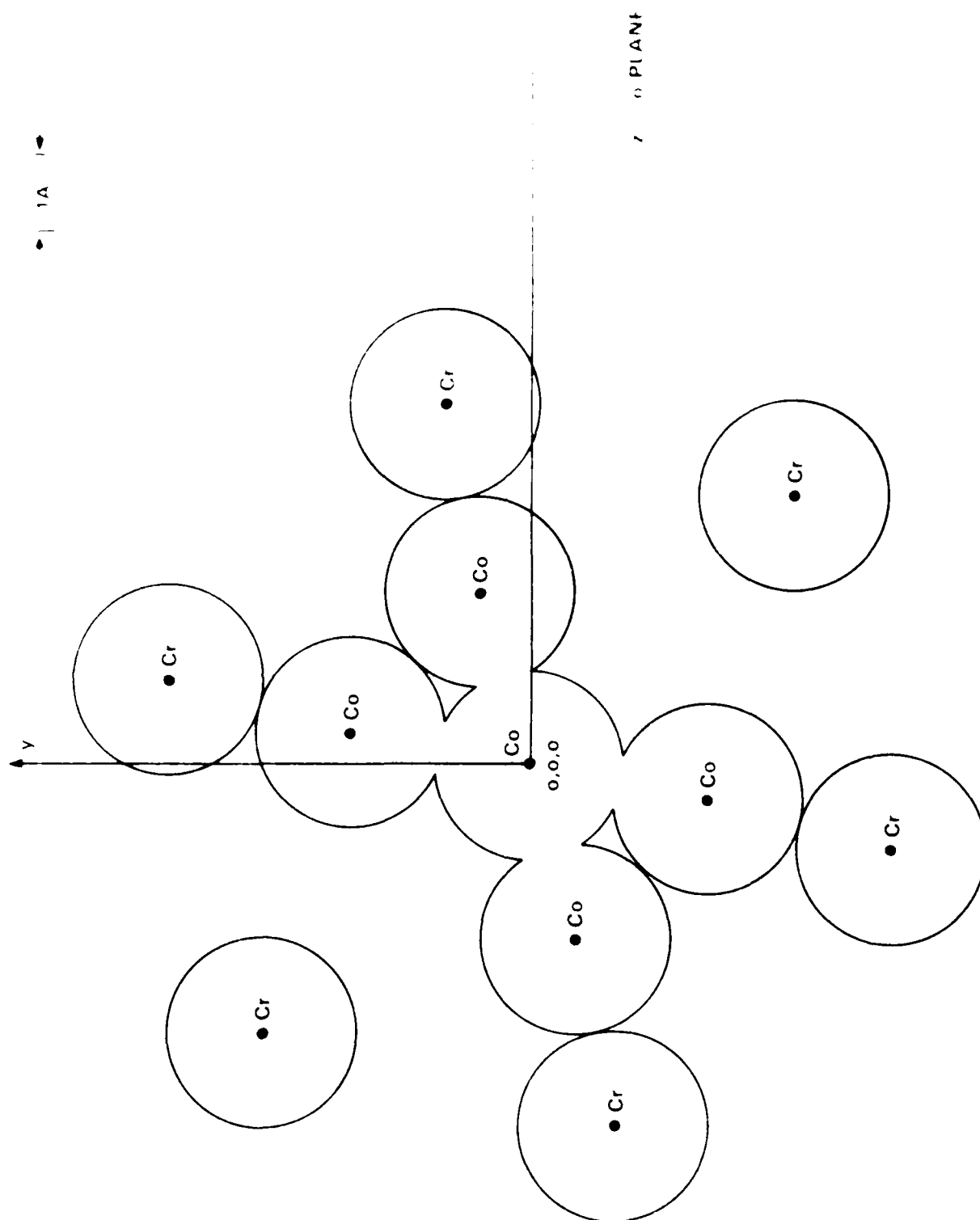
... this phase change in going from the low to the high

... the probability calculations discussed above were redone

with several new conditions and assumptions. For several reasons the

sigma phase in the higher chromium CoCrAlY was assumed to be a more

difficult starting condition for the formation of either cobalt or

chromium sulfate as compared to the alpha phase of the lower chromium

CoCrAlY. The sigma phase is an intermetallic compound while the alpha

phase is a solid solution of the alloying elements. Intermetallic

compounds frequently form bonds of a covalent nature, and these bonds

should require a higher activation energy to disrupt. As discussed

below, the majority of the chromium atoms (See Figs. 30 and 31) in the

sigma phase are not so positioned as to provide convenient sites for

83

Fig. 30. Atom positions in CoCr sigma phase on the [ ]

MICROCOPY RESOLUTION TEST CHART
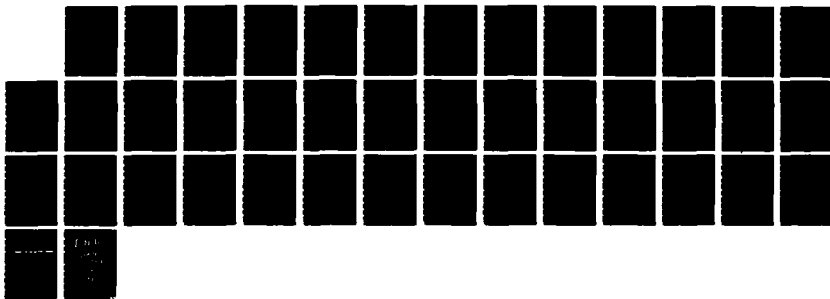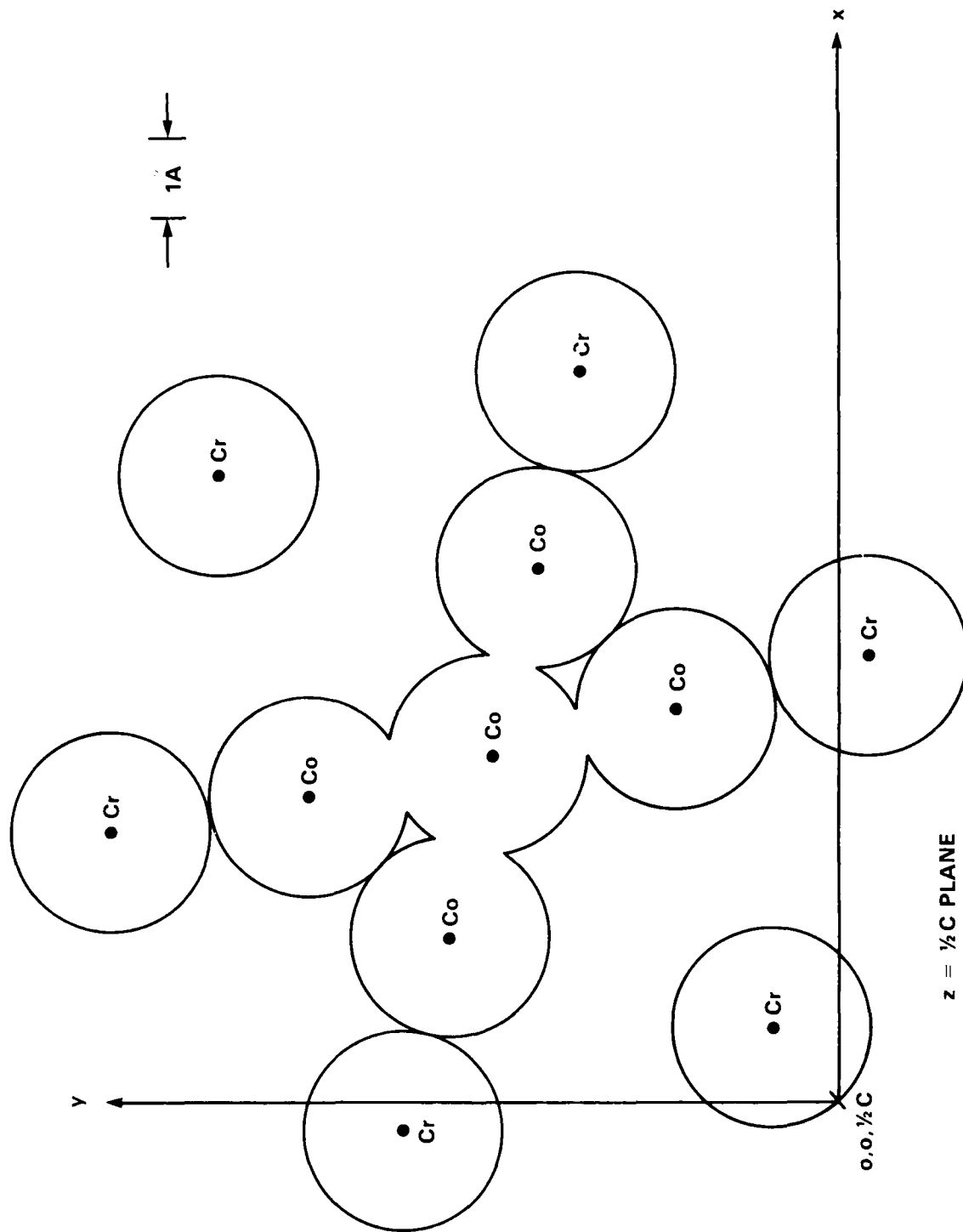
z = ½ C PLANE

Fig. 31. Atom positions in CoCr sigma phase on the z=1/2C plane.

the formation of a sulfate precursor. Reconstruction of the surface would be required to provide these sites in the case of sigma, which in turn would require some bond breaking. Although the cobalt atoms in the sigma phase are adjacent to one another in Figs. 30 and 31, most of the d-electrons that might be used for adsorption are tied up in covalent bonding with neighbors and unavailable for use in forming adsorption bonds. For these reasons, in the probability calculations discussed in Appendix F, any sigma that forms was considered to reduce the surface available for the formation of sulfates by the direct interaction with sulfur dioxide. The beta phase, being of a CsCl structure, should be alternating planes of aluminum and cobalt/chromium. For the purposes of the probability calculations, 50% of the total area of beta phase exposed at the surface was considered not to form cobalt or chromium sulfate and the other 50% was assumed to represent planes of atoms with a random arrangement of chromium and cobalt in proportion to these atoms' concentration in the beta. These assumptions were made even though the beta phase is also an intermetallic compound, because testing by Provenzano et al.[45] has shown that the beta phase can be attacked during hot corrosion.
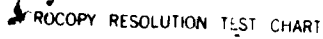
In summary, the following basic assumptions were made in the probability calculations of Appendix F: (1) the sigma phase is not capable of easily producing a precursor state of cobalt or chromium sulfate; (2) only 50% of the total area represented by the beta phase is capable of producing cobalt or chromium sulfate; and (3) the alpha phase is a random mix of the three major coating elements and is capable of producing cobalt or chromium sulfate. Based on these

86

assumptions, it was found that in going from the high chromium to the low chromium CoCrAlY, the likelihood of producing 3, 4, or 5 adjacent cobalt atoms as a precursor for cobalt sulfate changed by factors of 2.3, 2.5, and 2.7, respectively. In going from the low chromium to the high chromium CoCrAlY the likelihood of producing 3, 4, or 5 adjacent chromium atoms as a precursor to the formation of chromium sulfate changed by a factors of 1.08, 1.1, and 1.2, respectively. Thus, this is as a possible mechanism by which increasing the chromium content of the coatings can result in the suppression of cobalt sulfate formation without a change in the chromium sulfate formation, as occurred in the results presented in Figs. 27 and 28 and Table 9. One benefit of adding chromium to the coatings seems to be in the formation of the sigma phase, which results in the suppression of the cobalt sulfate that is a critical component to the low temperature hot corrosion process.

COBALT CLUSTERS AS PRECURSORS TO COBALT SULFATE FORMATION ON CoCrAlY

A five-atom cluster of adjacent cobalt atoms (Fig. 32a) could form a precusor state on the surface of CoCrAlY for the formation of cobalt sulfate. A five-atom cluster would have two sites between the five atoms to adsorb the oxygen that is released when sulfur dioxide is dissociated. These two oxygens would then have a spacing that is fairly close to the spacing between two coplanar oxygen atoms in sulfur dioxide (Fig. 32b) and a sulfate molecule (Fig. 32c). Thus the bonding of a sulfur dioxide molecule to these two oxygen atoms would form a good approximation of a sulfate molecule (Fig. 32d). The

87
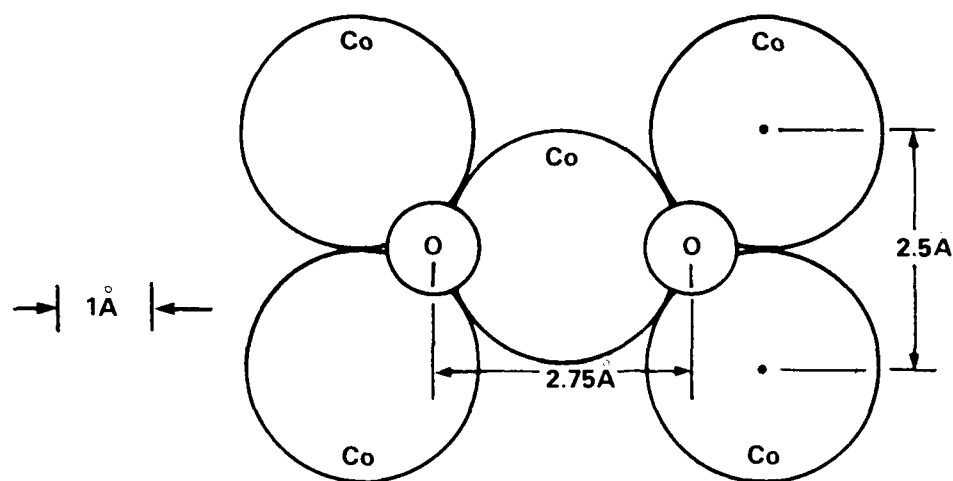
a. CLUSTER OF 5 Co AND 2 OXYGEN ATOMS

b. GEOMETRY OF SO₂

FOURTH OXYGEN BEHIND THIS THIRD OXYGEN
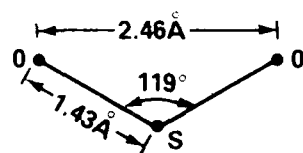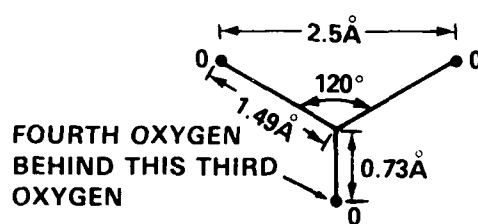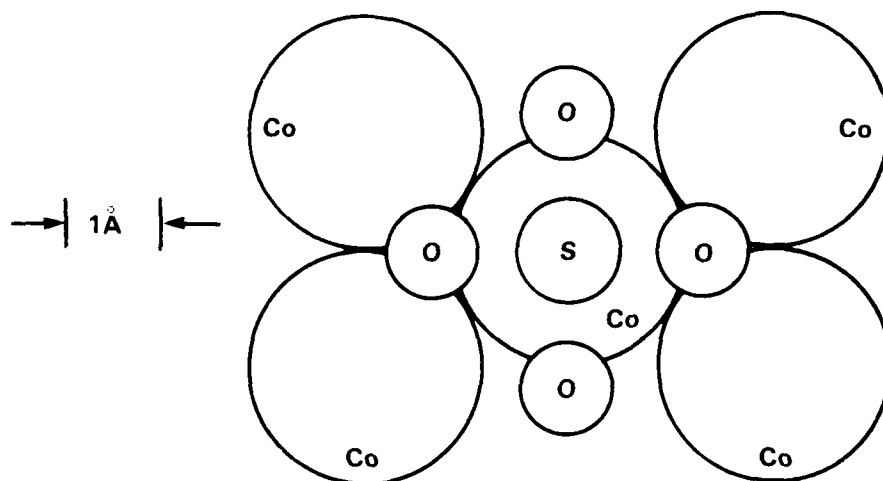
c. GEOMETRY OF SO₄

d. CLUSTER IN "a." WITH SO₂ ADDED

Fig. 32.   Geometry of "Co-oxide" cluster, SO_2, SO_4, and "Co-sulfate" cluster.

spacings and angles were obtained from Mingos[26] for sulfur dioxide, from Cruickshank[46] and Connolly and Johnson[47] for sulfate, and from Carter[48] and Anderson[49] for Co(0001). Thus this arrangement or cluster of atoms would then be ideally suited for the addition of a sulfur dioxide molecule that would then be the start of a discernable sulfate. Although it will take much more experimental work than contained herein to prove what exactly is the precusor state and how many different configurations will satisfy this requirement, a cluster calculation that builds on the arrangement of the atoms shown in Fig. 32d can prove informative and serve as a starting point for further investigations.

CLUSTER CALCULATIONS

In the experiments described above, both the Co(0001) and the Cr(110) reacted in a similar manner to sulfur dioxide adsorption and the reactions proceeded without a large difference in activation energies. This result is considered reasonable due to the close proximity of these two elements on the periodic chart and their similar band structure, as described by Varma and Wilson.[50] It was also found that the benefit in hot corrosion resistance realized by increasing the chromium content in CoCrAlY could be attributed to the onset of sigma phase formation and the likelihood of realizing minimum cluster sizes that facilitate cobalt and chromium sulfate formation. Based on these observations an activation energy difference is not considered responsible for the improvement in the hot corrosion resistance of CoCrAlY as the chromium content increases.

Consequently, it is not of paramount importance to model with a
cluster calculation the existence of an activation energy difference
to sulfur dioxide adsorption by these two metals. Instead, a more
interesting model would describe the formation of sulfate by the
chemisorption of sulfur dioxide to a cluster of cobalt and oxygen
atoms. This reaction is the second part of the mechanism proposed
above as occuring for both metals as the initiating step in sulfate
formation. The model would demonstrate the feasibility of this
reaction step based on theoretical calculations and would provide
information as to the electron orbitals involved in the bonding
process and the direction of the electron transfer involved in the
bonding. Such a model will create added confidence in the
appropriateness of the proposed reaction mechanism and will provide a
foundation on which to base theoretical studies of clusters of other
elements that might resist the formation of these sulfates.

The cluster to be modeled (*Fig. 33*) builds on the cluster of
five cobalt and two oxygen atoms (depicted in Fig. 32d) by adding five
more cobalt atoms. Two are used to complete the hexagonal pattern of
cobalt atoms as would be found on a Co(0001) surface and three are
added to make a second layer in the configuration of HCP cobalt, which
will make the cluster more representative of a true surface. The
spacings for the cobalt atoms were obtained from Brick et al.[51]; the
size of the oxygen atoms and their position in height above the row of
seven cobalt atoms were obtained from the works of Marcus et al.[52] and
Van Hove and Tong[53] on the adsorption of oxygen onto nickel. Nickel
is adjacent to cobalt on the periodic chart and the size of the two

90
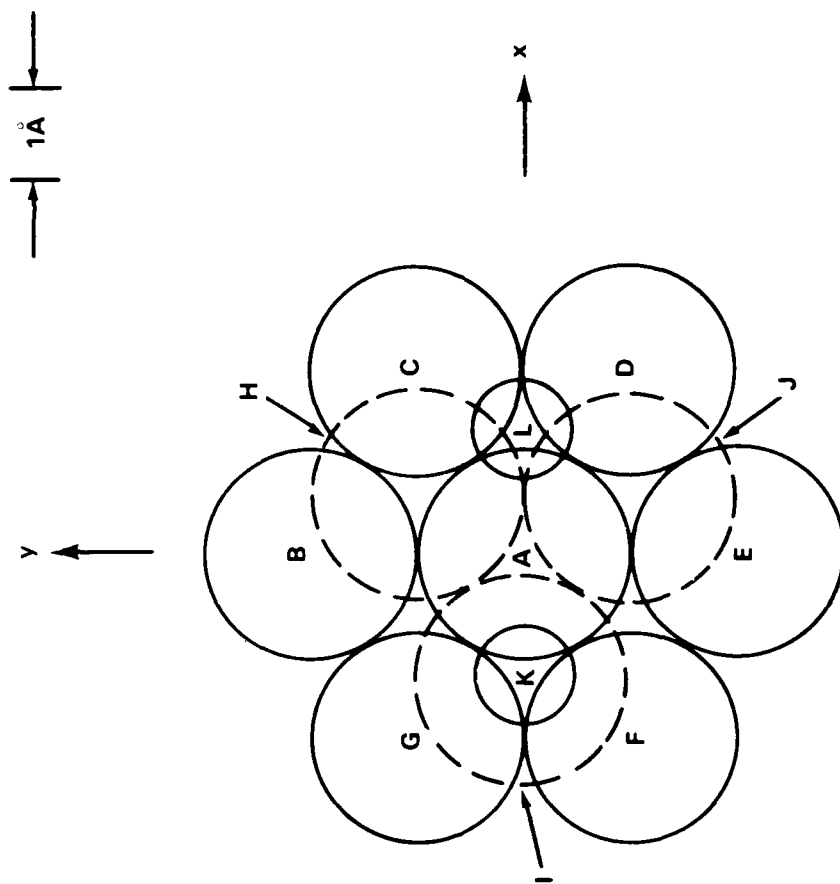
Fig. 33. Cluster of 10 cobalt and 2 oxygen atoms.

91

elements is considered near enough to use this reference data as an
approximation for the cluster under study. The positions of the atoms
in this cluster of ten cobalt and two oxygen atoms are given in
Table 11.

Table 11. Atom positions in a ten-cobalt, two-oxygen cluster.

Atom Designation	Position		
	X (Å)	Y (Å)	Z (Å)
Cobalt			
A	0	0	0
B	0	2.508	0
C	2.172	1.254	0
D	-2.172	-1.254	0
E	0	-2.508	0
F	-2.172	-1.254	0
G	-2.172	1.254	0
H	0.724	1.254	-2.034
I	-1.448	0	-2.034
J	0.724	-1.254	-2.034
Oxygen			
K	-1.448	0	2.268
L	1.448	0	2.268

The SCF-Xα-SW method (Appendix B) calculations used to arrive
at the converged self-consistent values of the one-electron energies
required extensive amounts of CPU time on a VAX 11/780 computer. It
was found that one iteration of the 85 degenerate orbitals during the
convergence part of the calculations takes 1 hour of CPU time. After
60 iterations the solution is nearing convergence. The energy values
for the valence levels at this point in the iterations to convergence
are listed in Table 12. A similar calculation was performed to
convergence for the simpler problem of a tetrahedral cluster of four
cobalt atoms, and the energy values for the valence levels of that

cluster are listed in Table 13. Comparison of the two indicates that the larger cluster is nearing convergence. Calculations will be continued until convergence is reached and the results will be published separately.

Useful information can be extracted at this point in the calculations. As part of the calculations a list is made of the amount of charge for each orbital on each atom in the cluster. The atom or pair of atoms with the most charge for a given orbital gives an indication of predominant atom or atoms with which the orbital is associated. These relationships for the valence levels are shown on Table 12. The 2p electrons of the oxygen atoms lie at approximately 9.8 to 12.7 eV. They are very near in energy to the lowest unoccupied molecular orbital of sulfur dioxide, which Anderson and Debnath[27] reported to be 9 eV. These orbitals are probably the ones involved in the electron transfer and sharing in bonding a subsequent sulfur dioxide molecule to the cluster as part of SO_4 formation. Once convergence is achieved the orbital contours can be mapped to better show this bonding.

Table 12. Approximate energies of degenerate valence level orbitals for a cluster of ten cobalt and two oxygen atoms.

Energy (eV)	Atom(s)* with the majority of charge for each level in order of predominance
26.93	O K, O L
26.60	O L, O K
13.50	Co A
13.20	Co A
13.05	Co A
12.90	Co A
12.84	Co A
12.70	O K, O L, Co A
11.40	O K, O L
10.40	O L, O K
10.36	O K, O L
9.90	O L, O K, Co A
9.80	O L, O K
9.50	Co I, Co H*
9.20	Co I, Co H
9.10	Co I, Co H
9.00	Co H, Co I
8.90	Co I, Co H
8.85	Co H, Co I
8.80	Co I, Co H
8.70	Co H, Co I
8.65	Co H
8.60	Co I, Co H, Co G
8.57	Co H, Co I
8.40	Co H, Co I
8.36	Co H
8.33	Co H
8.30	Co I, Co H
8.28	Co C, Co G
8.20	Co H, Co I
8.10	Co C, Co G
8.04	Co G, Co C
7.97	Co G, Co I
7.81	Co C, Co G
7.79	Co C, Co G
7.60	Co C, Co G
7.57	Co G, Co C
7.52	Co C, Co G
7.50	Co C
7.45	Co G, Co C
7.40	Co G

Table 12. (Continued)

Energy (eV)	Atom(s)* with the majority of charge for each level in order of predominance
7.32	Co C, Co G
7.30	Co G, Co C, Co B, Co I
7.29	Co C, Co G
7.26	Co G, Co C
7.21	Co G, Co C
7.18	Co B, Co C, Co G
7.14	Co B
7.13	Co C, Co G
7.11	Co B
7.07	Co B

* Letter designations for the atoms in the cluster are as given in Table 10 and shown on Fig. 33.
+ The following cobalt atoms are symmetry equivalent: B to E, C to D, G to F, and H to J.

Table 13. Converged energies of degenerate valence level
orbitals for a tetrahedral cluster of four cobalt atoms.

Energy (eV)	Atom(s)* with the majority of charge for each level in order of predominance
19.90	Co D+
12.20	Co D, Co A
10.90	Co D, Co A
6.00	Co A, Co D
4.70	Co A
4.20	Co A
4.10	Co A
3.71	Co A, Co D
3.39	Co A
3.37	Co A
3.27	Co A
3.03	Co A
2.97	Co A

* Letter designations for the atoms in the cluster are as shown on Fig. 34.
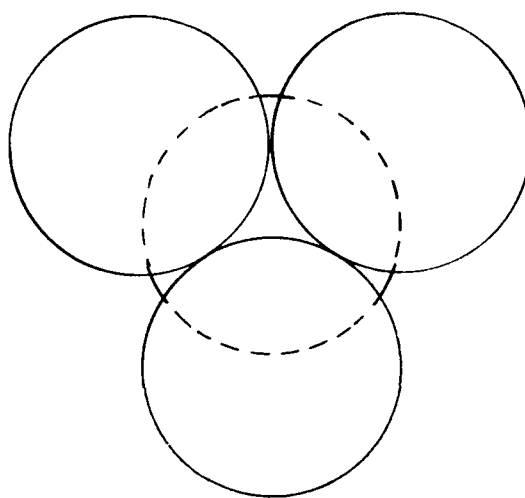+ In this cluster, atoms A, B, and C are symmetry equivalent

Fig. 34. Tetrahedral cluster of four cobalt atoms.

SUMMARY

Metallic coatings containing cobalt, chromium, aluminum, and yttrium (CoCrAlY) are used to improve the hot corrosion resistance of the hot section blades and vanes of gas turbine engines that are operated in a marine environment. Chromium is the primary element used in these coatings to improve their hot corrosion resistance; cobalt is the base element. When cobalt reacts with sulfur dioxide in the combustion gas to form cobalt sulfate, the hot corrosion performance of the coating can be degraded. By performing quantitive depth profiles with x-ray photoelectron spectroscopy (XPS), the oxides on CoCrAlY coatings with 20 to 35 weight percent chromium were all found to be alumina with an yttrium-rich phase that was probably yttrium aluminum garnet. Because of the similarity of the oxides on these coatings, it was concluded that the hot corrosion benefit derived by increasing the chromium content of these coatings must result from an improvement in the hot corrosion resistance of the coating beneath the oxide film.

To aid in understanding this process, the reactions of elemental, single crystal Co(0001) and Cr(110) were studied. It had been hypothesized that the reaction of sulfur dioxide with cobalt and chromium might proceed in two basic steps as follows:

1. $SO_2 \longrightarrow 2(O) + (S)$ (on the surface)

2. $2(O) + SO_2 \longrightarrow SO_4$ (on the surface).

The first step involves the dissociation of sulfur dioxide on the metal surfaces with the resulting formation of sulfides and oxides. In the second step, these oxides provide sites at which additional

sulfur dioxide can bond to the surface and form sulfates. By using XPS to study the reaction of sulfur dioxide with oxide-free surfaces of single crystal Co(0001) and Cr(110), these steps were shown to occur. The rates of these reactions were found to be similar for the two metals, and no appreciable difference in activation energies could be determined with the exposures to sufur dioxide used of pressures of 75 μmHg and 1 atmosphere at 100°, 230°, and 300°C for times of 1, 5, and 15 min. Cluster calculations based on the SCF-Xα-SW method were used to model the second step of the reaction above. The approximate energies of the electrons in a cluster of ten cobalt and two oxygen atoms were calculated, and the electron levels most likely involved in the sulfate formation were identified. Cluster calculations are planned to identify metals that might resist the sulfate formation of step 2.

The knowledge gained of how the Co(0001) and the Cr(110) react with sulfur dioxide was used to understand the reactions of sulfur dioxide with CoCrAlY coatings. Oxide-free surfaces of CoCrAlY with 20 and 30 wt % chromium were exposed to 1 atm sulfur dioxide at 230°C for 1, 5, 15, 30, and 60 min. The CoCrAlY coatings were shown to form sulfates of both cobalt and chromium in a manner similar to that described for Co(0001) and Cr(110). It was further demonstrated that as the chromium content increased in the coatings, the formation of cobalt sulfate was reduced. Within the range of chromium contents studied, the high-chromium content coating had formed sigma phase which was not present in the low-chromium coating. In comparison to the alpha and beta phases present in the low-chromium content CoCrAlY,

the sigma phase was hypothesized to be a more difficult surface on which to form cobalt or chromium sulfate and the onset of sigma formation was considered one way in which increasing the chromium content of the coatings improves their hot-corrosion resistance.

ACKNOWLEDGMENTS

APPENDIX A

CALCULATIONS USED FOR FREE ENERGY CHANGE OF REACTIONS

If: F_T = free energy change of reaction at temperature T

H_{298} = heat of formation for the reaction

S_{298} = entropy of formation for the reaction

$S_{298}(X)$ = standard entropy for X reactant or product

$H_{(X)}$ = standard heat of formation for X reactant or product

$C_p(X)$ = heat capacity for X reactant or product

Then for the reaction aA + bB = cC + dD, where a, b, and c are moles and A, B, C, and D are reactants or products, the relationship for the free energy change of reaction at temperature T is:

$$F_T = H_{298} + \int_{298}^{T} C_p \, dT - T \, S_{298} - T \int_{298}^{T} \frac{C_p}{T} \, dT$$

where:

$H_{298} = d(H_D) + c(H_C) - a(H_A) - b(H_B)$

$S_{298} = d[S_{298}(D)] + c[S_{298}(C)] - a[S_{298}(A)] - b[S_{298}(B)]$

$C_p = d[C_p(D)] + c[C_p(C)] - a[C_p(A)] - c[C_p(B)]$

Note: Reference source is Kubaschewski and Alcock.[55]

APPENDIX B

THE SCF-$X\alpha$-SW METHOD FOR CALCULATING
THE ONE-ELECTRON ENERGIES OF CLUSTERS

An excellent description of the SCF-$X\alpha$-SW method of cluster calculations can be obtained by referring to the works of Slater[56] and Johnson.[57] The following text is a synopsis of that work.

The true potential field of the many electrons and nuclei that make up a cluster of atoms is extremely complex. To solve Schrodinger's equation for the energy of electrons moving in such a potential field, one must develop a suitable model or approximation to this potential field that will make the solution tractable. One such approximation is to take the potential field of all the electrons and the nuclei and replace it with an averaged self-consistent field (SCF). The Schrodinger equation is then solved for the case of one electron moving in the averaged potential field of all of the other electrons and the nuclei. The solution will result in a set of eigenfunctions (wavefunctions or spin-orbitals) and eigenvalues (the one-electron energies). These spin-orbitals are then "filled" with the electrons in the cluster which then makes it possible to compute an electronic charge density. If the normalized spin-orbital is designated u_i then $u_i u_i^*$ is the charge density of an electron in this spin-orbital. If all of the charge densities of the electrons are summed and added to the charges of the nuclei, classical electrostatics can be used to find the electrostatic potential energy of an electron in this field. This is called the "coulomb potential".

Corrections must be made to this potential since it involves an electron acting electrostatically on itself as well as on all of the other electrons. Obviously, an electron does not electrostatically interact with itself and this self-interaction must be removed from the coulomb potential. This correction is referred to as the exchange correlation potential. (It is the "ex" in the word exchange from which one gets the "X" in SCF-Xα-SW). It also accounts for the effects of antisymmetry and Pauli forces. Slater[58] proposed that the exchange correlation potential is proportional by a factor "α" to the one-third power of the local electronic charge density, $\rho(r)$. (This is the "α" in SCF-Xα-SW.) With this correction to the potential, the u_i's can be varied, and Schrodinger's equation can be solved again and a new potential calculated. With the new potential field a new set of u_i's can be calculated. This iterative procedure (first used by Hartree[59]) can be continued until no appreciable change occurs in the potential. (It is from this that the term self-consistent field (SCF) arises.) The resultant potential field and the u_i's used with the Schrodinger equation will result in the final estimate of energy values for the one-electron orbitals.

The actual application of this method to a cluster of atoms involves breaking the space in and around the cluster into three regions. This has been described by Johnson[57] for a cluster of four atoms and is depicted in Fig. 35.

Region 1:

Atomic--The regions within spheres around
each atom in the cluster. These
regions can be slightly overlapping
or nonoverlapping.

Region 2:

Interatomic--The region between the spheres of the
atomic regions surrounding each atom
and the outer sphere surrounding the
entire cluster.

Region 3:

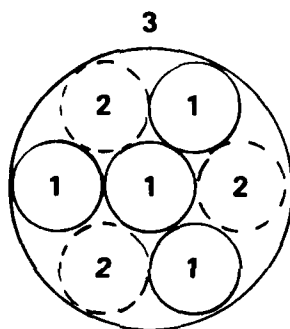Cluster Exterior--The region external to the outer
sphere.

Fig. 35. Regions of a cluster.

A further simplification involves using spherical zones (broken
circles) within the interatomic zone 2.

The one-electron Schrodinger equation (in Rydberg units) is
$[-\nabla^2 + V(\bar{r})] \, \psi(\bar{r}) = E \, \psi(\bar{r})$, which must be solved in each of the three
regions for a local potential energy function of

$V(\overline{r}) = V_c(\overline{r}) + V_{x\alpha}(\overline{r})$, where $V_c(\overline{r})$ is the coulombic contribution and $V_{x\alpha}(\overline{r}) = -6\alpha\,[(3/8\pi)\,\rho(\overline{r})]^{1/3}$ is the $X\alpha$ statistical approximation to exchange correlation. The calculation is started by expanding the potential at any arbitrary point r of the cluster as a superposition $V(\overline{r}) = \sum_j V_j\,(|\overline{r}-\overline{R}_j|)$ of free-atom SCF-$X\alpha$ potentials centered at positions R_j, where j is the index for each of the atoms in the cluster. Herman and Skillman[60] generated the original free atom potentials which have been modified to use the $X\alpha$ exchange correlation scaling parameter. The potential energy in each region 1 is expanded by superpositon of spherical harmonics. (See Johnson[57] for complete details.) In this expansion the first term includes the contribution from the atom in the region 1 of interest and the spherically averaged contribution of all the other atoms in the region. Thus, this method includes the first order effects of overlapping potentials. In region 2 the potential can be spherically averaged inside the spheres described by the broken circles in Fig. 35, or in many cases an average of the potential in region 2 is sufficient and will result in a constant interatomic potential energy. In region 3 a spherical average of the potential with respect to the center of the cluster is used. This partitioning of space into zones of spherically- and volume-averaged potentials allows for the mathematical representation of wave functions as composite partial wave representation. The wave function can then be dealt with as an expansion of terms that allow for a numerical intergration solution to Schrodinger's equation (See Johnson[57] for details). The wave functions and their first derivatives are joined continously throughout the various regions of

the cluster.   The SW term in the title of the method comes from the

fact that the wave function in the interatomic region is built up with

the scattered waves (SW) from the various atomic sites.   The solution

of Schrodinger's equation becomes a set of secular equations which are

solved numericaly for energies and wave functions.   The procedure is

repeated using the wave functions to generate a new electronic charge

density, which in turn is used to generate a new potential.   The new

potential is volume averaged in the intersphere region and is

spherically averaged inside the atomic and interatomic spheres and in

the cluster exterior.   This potential is then averaged with the

potential from the previous iteration and this average is used as the

input potential for the next iteration.   The process is continued

until the potentials and the charge density achieve self-consistency.

APPENDIX C

SPUTTER RATE STANDARD PREPARATION PROCEDURES

A 1000 Å anodized tantalum specimen may be prepared in the following manner:

a. Polish two 0.125-mm foils of tantalum by dipping them for up to 1 or 2 seconds in an acid solution (59.0% H_2SO_4, 17.0% HF, 23.5% HNO_3).

b. Pass the samples through two rinses of deionized H_2O.

c. Blow them dry with N_2.

d. Using one polished foil as an anode and another as a cathode, apply 6.66 V dc between them while they are suspended in an electrolyte (94.3% deionized H_2O, 5.7% HNO_3). One of these plates is sufficiently anodized when the current drops to zero.

e. Rinse the "gold" anodized specimen in acetone. The gold color indicates 1000 Å of Ta_2O_5.

d. Blow the specimen dry with N_2.

Note: This procedure was obtained from the operating manual for the Phi Electronics Sputter Gun.

APPENDIX D

FIRST ORDER REACTION RATE CALCULATIONS

Assuming a reaction of the form:

$$aA + bB \longrightarrow cC \ ,$$
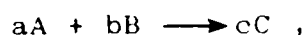
where a, b, and c are moles, and A, B, and C are products or

reactants, then for rates of reaction we have:

$$\frac{1}{c} \frac{d[C]}{dt} = \frac{-1}{a} \frac{d[A]}{dt} = \frac{-1}{b} \frac{d[B]}{dt} \ ,$$

where A, B, and C represent concentration of products ore reactants.

If we assume the reaction is first order in concentration of C and

c is 1, then:

$$\frac{d[C]}{dt} = k(C) \ ,$$

$$\frac{d[C]}{C} = k \ dt \ ,$$

where k is the rate constant, and

$$\int_{c_1}^{c} \frac{d[C]}{C} = k \int_{t_1}^{t} dt \ .$$

If t_1 = 60 seconds

$$\ln C - \ln C_1 = k(t - t_1) = k(t - 60 \ sec)$$

$$\ln \frac{C}{C_1} = k(t - 60 \ sec)$$

$$\frac{C}{C_1} = e^{k(t - 60 \ sec)}$$

$$C = C_1 e^{k(t - 60 \text{ sec})}$$

$$\log C = \frac{k(t - 60 \text{ sec})}{2.303} + \log C$$

Thus, for a plot of log C vs. (t - 60 sec), if a straight line results, its slope = k/2.303.

This slope is obtained by assuming a straight line result and performing a linear regression analysis of the data: log C vs. (t - 60 sec). This gives values of k in units of sec^{-1}. If the reaction is assumed to follow an Arrehenius type relation with temperature then:

$$k = Ae^{-E_a/RT} \quad ,$$

where E_a is the activation energy, R is the universal gas constant, and A is a constant.

If a plot of log k vs. 1/T gives a straight line, then the activation energy for the reaction = -2.303 (R) (slope).

E_a is in units of cal/mole if T is in Kelvins and k is in sec^{-1}.

Note: Reference source is Daniels and Alberty.[61]

APPENDIX E

PROBABILITY CALCULATION OF VARIOUS SIZE CLUSTERS

If one imagines a large enough pool of atoms such that for a given concentration of one type of atom the probability of drawing that atom from the pool never significantly changes, then the probability on a surface of having two adjacent sites occupied with the same type of atom is the joint probability of drawing two of the same type of atom in succession from the pool of atoms.

For a mixture of 56 atomic % Co, 20 atomic % Cr, and 24 atomic % Al the random probability of getting two adjacent Cr atoms on a surface is:

$$0.2 \times 0.2 = 0.04$$

For a mixture of 46 atomic % Co, 34 atomic % Cr, and 19 atomic % Al, the probability is:

$$0.34 \times 0.34 = 0.1156$$

The increasing likelihood of getting two adjacent Cr atoms on going from 20 to 34 atomic % Cr is:

$$\frac{0.1156}{0.04} = 2.9$$

Likewise, the respective probabilities for a cluster of three adjacent Cr atoms with these two compositions are 0.008 and 0.039. The increasing likelihood of getting three adjacent Cr atoms on going from 20 to 34 atomic % Cr is:

$$\frac{0.039}{0.008} = 4.9$$

For the case of Co with the 56 atomic % composition, the probability of getting a two-atom cluster is 0.3136; with the 46 atomic % Co composition the probability is 0.2116. Therefore, the increasing likelihood of getting two adjacent Co atoms on going from 46 to 56 atomic % Co is 1.48

Again for the case of Co, with the 56 atomic % Co composition the probability getting a three-atom cluster is 0.175; with the 46 atomic % Co composition the probability is 0.097. Therefore, the increasing likelihood of getting three adjacent Co atoms on going from 46 to 56 atomic % Co is 1.79.

APPENDIX F

EFFECT OF SIGMA, BETA, AND ALPHA PHASES IN CoCrAlY

ON PROBABILITY CALCULATIONS

Basic assumptions:

1. The sigma phase doesn't produce any sulfates.

2. The chromium in the beta phase substitutes for Co in a random manner on the CoCr phase.

3. In the beta phase there is a 50% chance of having a plane that is predominant in aluminum at the surface.

4. In the alpha phase the atoms occupy the lattice sites at random.

Given facts:

1. In the 20Cr CoCrAlY the phase distribution at the surface is 88.6% beta, 11.4% alpha, and 0% sigma. The composition of the beta phase is 56 atomic % Co, 14 atomic % Cr, and 30 atomic % Al. The composition of the alpha phase is 64 atomic % Co, 30 atomic % Cr, and 6 atomic % Al.

2. In the 35Cr CoCrAlY the phase distribution at the surface is 40.7% sigma, 59.3% beta and 0% alpha. The composition of the sigma phase is 46 atomic % Co, 48 atomic % Cr, and 6 atomic % Al. The composition of the beta phase is 51 atomic % Co, 20 atomic % Cr, and 29 atomic % Al.

Using these assumptions and facts:

- For the 20Cr CoCrAlY the probability of getting three adjacent atoms of cobalt is:

in the alpha phase

(% of cobalt in alpha)^3 x % of alpha phase at surface

$$(0.64)^3 \quad x \quad (0.114) = 0.030$$

in the beta phase

(% of Co in CoCr plane in beta)^3 x % of CoCr planes in beta x % of beta phase at the surface

$$(0.8)^3 \quad x \ 0.5 \ x \ 0.886 = 0.227$$

Total probability of getting three adjacent atoms of cobalt is:

$$0.227 + 0.030 = 0.257$$

- For the 35Cr CoCrAlY the probability of getting three adjacent cobalt atoms is:

in the beta phase

(% of Co in the CoCr plane)^3 x % of CoCr planes in beta x % of beta phase at surface

$$(0.72)^3 \quad x \ 0.5 \ x \ 0.593 = 0.11$$

Total probability of getting three adjacent atoms of cobalt = 0.11.

Consequently, the increased likelihood in going from 35Cr to 20Cr CoCrAlY of getting a three-atom cluster of Co=0.257/0.11=2.3.

116

●For the 20Cr CoCrAlY the probability of getting three

adjacent atoms of chromium is:

in the alpha phase

(% of Cr in alpha)^3 x % of alpha phase at the surface =

$(0.3)^3$ x 0.114 = 0.003

in the beta phase

(% of Cr in CoCr phase)^3 x % of CoCr planes in beta x % of beta phase

at the surface =

$(0.2)^3$ x 0.5 x 0.886 = 0.003

Total probability of getting three adjacent chromium atoms =

0.003 + 0.003 = 0.006

●For the 35Cr CoCrAlY the probability of getting three

adjacent atoms of chromium is:

in the beta phase

(% of Cr in the CoCr plane)^3 x % of CoCr planes in beta x % of

beta phase at the surface =

$(0.28)^3$ x 0.5 x 0.593 = 0.0065

Total probability of getting three adjacent chromium atoms =

0.0065

Consequently the increased likelihood in going from 35Cr to 20Cr

CoCrAlY of getting a three-atom cluster of Cr=0.0065/0.006=1.08

REFERENCES

1. Grisik, J.J., R.G. Miner, and D.J. Wortman, "Performance of Second Generation Airfoil Coatings in Marine Service," Thin Solid Films, Vol. 73, pp. 397-406 (1980).

2. Goward, G.W., "Recent Developments in High Temperature Coatings for Gas Turbine Airfoils," Proc., High Temp. Corr. Conf., NACE-6, Nat. Assoc. Corr. Eng., pp. 553-560 (1981).

3. Luthra, K.L. and J.H. Wood, "High Chromium Cobalt-Base Coatings for Low Temperature Hot Corrosion," Thin Solid Films, Vol. 119, pp. 271-280 (1984).

4. Sinfelt, J.H., J.L. Carter, and D.J.C. Yates, "Catalytic Hydrogenolysis and Dehydrogenation over Copper-Nickel Alloys," J. Catal., Vol. 24, pp. 283-296 (1972).

5. Sprague, J.A., V. Provenzano, and F.A. Smidt, Jr., "Initial Stages of Oxide Formation on a CoCrAlY Coating Alloy at 700°C," Thin Solid Films, Vol. 95, pp. 57-64 (1982).

6. Hwang, S.Y., G.H. Meier, F.S. Pettit, G.R. Johnson, V. Provenzano, and F.A. Smidt, Jr., "The Initial Stages of Hot Corrosion Attack of CoCrAlY Alloys at 700°C," High Temperature Protective Coatings, S.C. Singhal, Ed., Metallur. Soc., Am. Inst. Mech. Eng. (AIME) (1982).

7. Luthra, K.L., "Low Temperature Hot Corrosion of Cobalt-Base Alloys Part 1: Morphology of the Reaction Product," _Metallur. Trans.,_ Vol. 13A, pp. 1843-1852 (1982).

8. Luthra, K.L., "Kinetics of Low Temperature Hot Corrosion of CoCrAl Alloys," _J. Electrochem. Soc.,_ Vol.132, No. 6, pp. 1293-1298 (1985).

9. Furuyama, M., K. Kishi, and S. Idoda, "The Adsorption of SO_2 on Iron Surfaces Studied by XPS," _J. Electron Spectros. Rel. Phenom.,_ Vol. 13, pp. 59-67 (1978).

10. Brundle, C.R. and A.F. Carley, "XPS and UPS Studies of the Adsorption of Small Molecules on Polycrystalline Nickel Films," _Chem. Soc. Faraday Disc.,_ Vol. 60, pp. 51-70 (1975).

11. Nebesny, K.W. and N.R. Armstrong, "Reaction of Clean Lithium Surfaces with SO_2: Molecular Auger Line-Shape Analysis and Reaction Kinetics," _Langmuir,_ Vol. 1, pp. 469-477 (1985).

12. Kohler, U. and H.W. Wassmuth, "Surface Reactions of Sulfur with Oxygen on Pt(111)," _Surf. Sci.,_ Vol. 117, pp. 668-675 (1982).

13. Outka, D.A. and R.J. Madix, "Sulfur Dioxide Adsorption
     and Reaction with Atomic Oxygen on Ag(110) Surface,"
     Surf. Sci., Vol. 137, pp. 242-260 (1984).

14. Outka, D.A., R.J. Madix, G. B. Fisher, and C.R. DiMaggio,
     "Oxidation of Sulfur Dioxide on Ag(110): Vibrational Study
     of the Structure of Intermediate Complexes Formed,"
     J.Phys. Chem., Vol. 90, pp. 4051-4057 (1986).

15. Niemczyk, S.J., "SCF-Xα-SW Investigation of Chemisorption
     Bonding of Chalcogens on Nickel (001)," J. Vac. Sci. Technol.,
     Vol. 12, No. 1, pp. 246-248 (1975).

16. Gates,B.C., J.R. Katzer, and G.C.A. Schuit, Chemistry of
     Catalytic Processes, McGraw-Hill, New York (1979).

17. Cotton, F., Chemical Applications of Group Theory, 2nd
     Ed., Wiley-Interscience, New York (1970).

18. Tanaka, K. and K. Tamaru, "A General Rule in Chemisorption
     of Gases on Metals," J. Catal., Vol. 2, pp. 366-370 (1963).

19. Fassaert, D.J.M. and A. van der Avoird, "LCAO Studies of
     Hydrogen Chemisorption on Nickel," Surf. Sci., Vol. 55,
     pp. 291-312 (1976).

20. Messmer, R.P., S.K. Knudson, K.H. Johnson, J.B. Diamond,
     and C.A. Yang, "Molecular Orbital Studies of Transition
     and Noble Metal Clusters by the SCF-Xα-SW Method," Phys.
     Rev. B, Vol. 13, No. 4, pp. 1396-1415 (1976).

21. Salahub, D.R. and R.P. Messmer, "Molecular Orbital Study of Aluminum Clusters Containing up to 43 Atoms," Phys. Review B, Vol. 16, No. 6, pp. 2526-2536 (1977).

22. Deuss, H. and A. van der Avoird, "Model for Dissociative H_2 Chemsorption on Transition Metals," Phys. Rev. B, Vol. 8, pp. 2441-2444 (1973).

23. Harris, J. and G.S. Painter, "Oxygen Chemisorption of a Small Aluminum Cluster," Phys. Rev. Let., Vol. 36., pp. 151-154 (1976).

24. Johnson, K.H., "Spin Orbital Electronegativity, the $X\alpha$ Method and Reactivity of Transition Metal Interfaces," Internat. J. Quant. Chem.: Symp., Vol. 11 S, pp. 39-60 (1977).

25. Sanderson, R.T., Inorganic Chemistry, Reinhold, New York, p. 95 (1975).

26. Mingos, D.M.P., "Sulfur Dioxide Complexes of the Platinum Metals," Transit. Metal Chem., Vol. 3, pp. 1-15 (1978).

27. Anderson, A.B. and N.C. Debnath, "Reaction of NaCl(s) with $SO_2(g)$ and $O_2(g)$ to Form $Na_2SO_4(s)$. A Charge Transfer Reaction," J. Phys. Chem., Vol. 87, pp. 1938-1941 (1983).

28. David, L.E., "Technique Fundementals in AES and XPS,"
In: Modern Surface Analysis," L.E. Davis, Ed., Chap. 1,
pp. 1-12, Metallur. Soc., Am. Inst. Mech. Eng. (AIME), Warrenton,
Pa.(1979).

29. Briggs, D. and M.P. Seah, Eds.,Practical Surface Analysis by
Auger and X-ray Photoelectron Spectroscopy, John Wiley and
Sons, Ltd. (1983).

30. Luthra, K.L. and E.L. Hall, "High Temperature Oxidation
of Ni-20Cr-12.5Al Coatings Containing 1% Dispersed Oxides,"
Oxid. Metals, Vol. 26, No. 5/6, pp. 385-396 (1986).

31. Wagner, C.D., W.M. Riggs, L.E. Davis, J.F. Moulder, and
G.E. Muilenberg, Eds., Handbook of X-ray Photoelectron
Spectroscopy, Perkin-Elmer Corporation: Eden Prairie,
Minn. (1979).

32. Shinn, N.D. and T.E. Madey, "CO Chemisorption on Cr(110):
Evidence for a Precursor to Dissociation," J. Chem. Phys.,
Vol. 83, No. 11, pp. 5928-5944 (1985).

33. Grant, J.T. and T.W. Haas, "Soe Studies of the Cr(100)
and Cr(110) Surfaces," Surf. Sci., Vol. 17, pp. 484-485
(1969). 34. Kratos XSAM 800 Operator's Handbook, Vol 2., Systems
Operation, Kratos Corp.: Manchester, England (1982).

34. Kratos XSAM 800 Operator's Handbook, Vol.2, Systems
Operation, Kratos Corp.: Manchester, England (1982).

35. Lutnra, K.L., 'Low Temperature Hot Corrosion of Cobalt-Base Alloys: Part II. Reaction Mechanism," Metallur. Trans. A, Vol. 13A, pp. 1852-1864 (1982).

36. Doniach, S. and M. Sunjic, "Many-Electron Singularity in X-ray Photoemission and X-ray Line Spectra from Metals," J. Phys. C, Vol. 3, pp. 285-291 (1970).

37. Cook, M. and D.A. Case, "XASW Computer Program: QCPE 465," Quantum Chemistry Exchange Program, Indiana University, Bloomington, Ind. (1985).

38. Ramanarayanan, T.A., "The Characteristics of Alumina Scales Formed on Fe-Based Yttria Dispersed Alloys," J. Electrochem. Soc., Vol. 131, No. 4, pp. 923-931, (1984).

39. Barkalow, R.H. and G.W. Goward, "Microstructural Features of Low Temperature Hot Corrosion in Nickel and Cobalt Base MCrAlY Coating Alloys," Proc. High Temp. Corr. Conf., NACE-6, Nat. Assoc. Corr. Eng., pp. 502-506 (1981).

40. American Society for Metals, Metals Handbook, Vol. 8, 8th ed., Metals Park, Ohio (1973).

41. Gupta, K.P., N.S. Rajan, and P.A. Beck, "Effect of Si and Al on the Stability of Certain Sigma Phases," Trans. Metallur. Soc. AIME, Vol. 218, pp. 617-624 (1960).

42. Henry, N.F.M. and K. Lonsdale, Eds., _International Tables for X-ray Crystallography, Vol. I, Symmetry Groups,_ International Union of Crystallography, Kynoch Press, Birmingham, England (1952).

43. Dickins, G.J., A.M.B. Douglas, and W.H. Taylor, "The Crystal Structure of Co-Cr Sigma Phase," _Acta Crystall., Vol. 9,_ pp. 297-303 (1956).

44. Algie, S.H. and E.O. Hall, "Site Ordering in Some Sigma Phase Structures," _Acta Crystall.,_ Vol. 20, p. 142 (1966).

45. Provenzano, V., G.R. Johnson, and J.A. Sprague, "The Effects of Ion Implantation on The Initial Stages of Hot Corrosion Attack of Cast Co-22Cr-11Al at 700°C," _Thin Solid Films,_ Vol. 107, pp. 277-286 (1983).

46. Cruickshank, D.W.J., "The Role of 3d-Orbitals in π-Bonds Between (a) Silicon, Phosphorus, Sulfur, or Chlorine and (b) Oxygen or Nitrogen," _J. Chem. Soc. London,_ pp. 5486-5504 (1961).

47. Connolly, J.W.D. and K.H. Johnson, "Calculation of Ionization Energies of the SF_4 Molecule by the Multiple Scattering Method," _Chem. Phys. Let.,_ Vol 10., No. 5, pp. 616-622 (1971).

48. Carter, G.F., _Principles of Physical and Chemical Metallurgy,_ American Society for Metals, Metals Park, Ohio (1979).

49. Anderson, J.R., Structure of Metallic Catalysts, Academic Press, New York (1975).

50. Varma. C.M. and A.J. Wilson, "Systematics of the Binding Energy of Oxygen and Hydrogen on Transition-Metal Surfaces. I.," Phys. Rev. B, Vol. 22, No. 8, pp. 3795-3804 (1980).

51. Brick, R.M., R.B. Gordon, and A. Phillips, Structure and Properties of Alloys, 3rd. Ed., McGraw-Hill, New York (1965).

52. Marcus, P.M., J.E. Demuth, and D.W. Jepson, "Determination of the Structure of Ordered Absorbed Layers by Analysis of LEED Spectra," Surf. Sci., Vol. 53, pp. 501-522 (1975).

53. Van Hove, M. and S.Y. Tong, "Chemisorption Bond Lengths of Chalcogen Overlayers at a Low Coverage by Convergent Perturbation Methods," J. Vac. Sci. Technol., Vol. 12, No. 1, pp. 230-233 (1975).

54. Anderson, A.B. and N.C. Debnath, "Reaction of $NaCl(s)$ with $SO_2(g)$ and $O_2(g)$ to Form $Na_2SO_4(s)$. A Charge-Transfer Reaction," J. Phys. Chem., Vol. 87, pp. 1938-1941 (1983).

55. Kubaschewski, O. and C.B. Alock, Metallurgical Thermochemistry, 5th Ed., Pergamon Press (1979).

56.   Slater, J. C., The Self-Consistent Field for Molecules and Solids: Quantum Theory of Molecules and Solids, Vol. I., McGraw Hill, New York (1974).

57.   Johnson, K.H., "The Scattered Wave Theory of the Chemical Bond," In: Advances in Quantum Chemistry, P.O. Loudin, Ed., Vol.7, pp. 143-185, Academic Press, New York (1973).

58.   Slater, J.C., "A Simplification of the Hartree-Fock Method," Phys. Rev., Vol 81, pp. 385-390 (1951).

59.   Hartree, D.R., "The Wave Mechanics of an Atom with Non-Coulomb Central Field Part I. Theory and Methods," Proc., Math. Phys. Sci., Cambridge Philosophical Society, Vol 24., pp. 89-111 (1928).

60.   Herman, F. and S. Skillman, Atomic Structure Calculations, Prentice-Hall, New Jersey (1963).

61.   Daniels, F. and R. A. Alberty, Physical Chemistry, 4th Ed., John Wiley and Sons, New York (1975).

INITIAL DISTRIBUTION

Copies

Copies			
1	CONR		
	1	1131M	J. Sedriks
1	NRL		
	1	6170	R. Jones
16	NAVSEA		
	1	Library	
	1	SEA 05R	(D. Groghan)
	2	SEA 05R33	(D. Wyvill)
	1	SEA 05X	
	5	SEA 56X31	(S. Shepard)
	2	SEA 99612	
	1	SEA 55Y	
	1	SEA 55Y1	
	1	SEA 55Y3	
	1	SEA 55Y31	
2	NAVSSES		
	2	053B	(G. Katz)
12	DTIC		

Copies	Code	Name
1	012.3	Moran
1	28	Wacker
1	2801	Crisci
3	281	
1	2812	
25	2812	Aprigliano
3	2813	Clarke
1	5211	Knox
10	5211.1	
1	522.1	TIC (C)
1	522.2	TIC (A)
1	5231	Office Services

DTNSRDC ISSUES THREE TYPES OF REPORTS:

1. **DTNSRDC reports, a formal series,** contain information of permanent technical value. They carry a consecutive numerical identification regardless of their classification or the originating department.

2. **Departmental reports, a semiformal series,** contain information of a preliminary, temporary, or proprietary nature or of limited interest or significance. They carry a departmental alphanumerical identification.

3. **Technical memoranda, an informal series,** contain technical documentation of limited use and interest. They are primarily working papers intended for internal use. They carry an identifying number which indicates their type and the numerical code of the originating department. Any distribution outside DTNSRDC must be approved by the head of the originating department on a case-by-case basis.

END

DATE
FILMED

DEC.
1987